Adsorptive removal of nitrate and phosphate ions from aqueous solution with nitrogen-doped carbonaceous materials

窒素ドープ炭素材料による水溶液中からの硝酸・リン酸イオンの吸着除去

2025 年 2 月

千葉大学大学院融合理工学府
先進理化学専攻
共生応用化学コース
王　晶

（千葉大学審査学位論文）

Adsorptive removal of nitrate and phosphate ions from aqueous solution with nitrogen-doped carbonaceous materials

窒素ドープ炭素材料による水溶液中からの硝酸・リン酸イオンの吸着除去

2025 年 2 月

千葉大学大学院融合理工学府
先進理化学専攻
共生応用化学コース
王　晶

Ph.D thesis submitted in particle fulfillment of the requirements for the degree of Ph.D. in Graduate School of Science and Engineering, Chiba University, Japan.

Affiliation:
Department of Applied Chemistry and Biotechnology, Division of Advanced Science and Technology, Graduate School of Science and Engineering, Chiba University.
1-33, Yayoi-cho, Inage-ku, Chiba-shi, Chiba, 263-8522, Japan

Supervisor:
Prof. Motoi Machida
Department of Applied Chemistry and Biotechnology, Graduate School of Engineering, Chiba University

Examiners:
Prof. Satoshi Sato
Department of Applied Chemistry and Biotechnology, Graduate School of Engineering, Chiba University

Prof. Masashi Nakamura
Department of Applied Chemistry and Biotechnology, Graduate School of Engineering, Chiba University

Prof. Masumi Yamada
Department of Applied Chemistry and Biotechnology, Graduate School of Engineering, Chiba University

Assoc. Prof. Yoshimasa Amano
Department of Applied Chemistry and Biotechnology, Graduate School of Engineering, Chiba University

DECLARATION

I hereby declare that this submission is my own work and that, to the best of my knowledge and belief, it contains no material which to a substantial extent has been accepted for the award of any degree or diploma of the university or other institute of higher learning, except where due acknowledgement has been made in the text.

Jing Wang, Chiba, Feb. 2025

ACKNOWLEDGEMENTS

I would like to express my sincerest gratitude to Prof. Motoi Machida, who has been my main supervisor during my studies at Chiba University. Due to the COVID-19 pandemic, I was stranded in China for one year, and from that time, Prof. Machida had provided me with continuous academic encouragement and guidance. After I joined the lab, he always kept motivating and guiding me in my research, offering me confidence and valuable advice. His sense of humor helped me quickly adapt to the new environment, and his deep academic insights will continue to have a positive impact on my future career.

I would also like to express my gratitude to Assoc. Prof. Yoshimasa Amano for his guidance on instruments and English writing during my studies at Chiba University. Over the past three years, Amano-sensei always taking the time to patiently revise my manuscripts and generously helped me in daily communication.

I would like to express my gratitude to Prof. Satoshi Sato, Prof. Masashi Nakamura, and Prof. Masumi Yamada for taking the time to read, review, and provide constructive feedback on this thesis.

I would like to express my gratitude to my friends in the laboratory for their assistance with the experimental equipment and characterization tests.

I would like to give special thanks to my family, my father, mother, and sister, for their emotional and financial support over the past three years. It is their support that has allowed me to pursue my dreams with peace of mind. I would also like to thank myself for the hard work I have put in throughout this journey.

ABSTRACT

The issue of water pollution caused by nitrate and phosphate ions is becoming increasingly severe. Developing technologies that can effectively remove such pollutants is essential. Among the various removal technologies, adsorptive removal overcomes the disadvantages of high operation costs, high energy consumption, and poor adaptability found in other methods, making it become a focal point of interest for researchers. To enhance the adsorption performance of the adsorbent, nitrogen-doped surface modification has been applied in the preparation process of traditional adsorbent. This thesis was carried out three aspects of research: (1) The study of the batch adsorption and fixed-bed column adsorption of glucose-based activated carbon adsorbents for the removal of nitrate ions from aqueous solutions. (2) The study of glucose-based activated carbon adsorbents for the removal of phosphate ions from aqueous solutions, using commercially available anion exchange resins as a reference material. (3) The transition of the preparation materials for carbonaceous adsorbents from dual nitrogen sources to a single nitrogen source, using glucose without nitrogen-doped surface modification as a reference material, to study the adsorption performance of the optimized adsorbent for nitrate ions.

In chapter 2, the glucose-based carbonaceous adsorbent was prepared from glucose, melamine and urea by using $ZnCl_2$ activation and heated at 550ºC under N_2 flow. The sample was treated for the 1st, 2nd and 3rd activation process, and they were characterized by N_2 adsorption and desorption isotherms, elemental analysis and X-ray photoelectron spectroscopy (XPS). The results showed that the content of nitrogen increased and that of oxygen decreased with the increasing of the number of activation process. The adsorbent obtained after the 2nd activation showed the best adsorption properties and was used in batch and fixed-bed column adsorption studies. In batch adsorption experiments, we investigated the factors affecting nitrate adsorption such as initial concentration, solution pH, adsorption isotherms and adsorption kinetics. The isotherm data and kinetic data were fitted well to the Langmuir isotherm model and pseudo-second-order model, respectively, and the maximum adsorption capacity calculated by Langmuir model was 1.58 mmol/g at pH 3.0. The adsorption performance of the adsorbent

in industrial application mode was also investigated by fixed-bed column experiments. The breakthrough time of the packed column was 160 min for the initial nitrate concentration of 200 mg/L at pH 3.0. The saturated column could be regenerated by 1 mol/L HCl and reused for at least 5 adsorption-desorption cycles. The column showed good adsorption performance in both coexisting ions solution and real contamination water.

In chapter 3, aiming to address the issue of phosphate contamination in water, a novel activated carbon adsorbent with excellent adsorption performance for phosphate ions was designed and synthesized through the nitrogen-doped surface modification method. The adsorption experiment results revealed that the sample obtained after the second activation at 600°C (MeUrGlu-600Z0.5-2nd) exhibited a high adsorption capacity of up to 0.42 mmol/g for phosphate ions. The surface modification method using nitrogen-doped significantly enhanced the adsorption capacity of the adsorbent for phosphate anions. The surface characteristics of the sample were analyzed by Brunauer-Emmett-Teller method, elemental analysis, and X-ray photoelectron spectroscopy (XPS). The characterization results indicated that the increase in adsorption capacity primarily attributed to the successful introduction of quaternary nitrogen (N-Q) onto the activated carbon surface. Additionally, the adsorbent demonstrated high adsorption capacity for phosphate ions in acidic solution (pH < 4.5), overcoming the limitation of commercial anion exchange resin HP555 which cannot be used effectively in acidic environment. The Langmuir isotherm model was found to accurately describe the adsorption process which is a monolayer adsorption. Finally, the regenerability of MeUrGlu-600Z0.5-2nd and the recovery of phosphate ions were investigated in a continuous flow adsorption mode.

In chapter 4, the transition of the preparation materials for carbonaceous adsorbents from dual nitrogen sources to a single nitrogen source was achieved. A nitrogen-doped glucose-derived carbonaceous adsorbent (UrGlu-450Z0.6-2nd) was prepared to enhance nitrate adsorption from wastewater. The optimization process of the adsorbent revealed the interaction principles among the raw materials, wherein the special brown porous foam-like intermediate formed after pre-treatment plays a decisive role in enhancing the adsorption performance of the adsorbent. In addition to being optimized for using a single nitrogen source, the adsorbent also

reduced the required preparation temperature by 100°C and exhibited an increased adsorption capacity in nitrate solutions with a pH greater than 5.0 (compare with chapter 2). UrGlu-450Z0.6-2nd exhibited a point of zero charge (pH_{pzc}) at the pH of 3.0 and a specific surface area (S_{BET}) of 6.13 m²/g. It was shown that the nitrogen-doped modified adsorbent exhibited a considerable capacity for adsorbing nitrate over a wide pH range of 2.0-10.0. The Langmuir isotherm model and the pseudo-second-order kinetic model can accurately describe the nitrate adsorption process of UrGlu-450Z0.6-2nd, and the maximum adsorption capacity (X_m) predicted by the Langmuir isotherm model was 1.18 mmol/g. Additionally, UrGlu-450Z0.6-2nd demonstrated an excellent adsorption capacity in practical applications using a fixed-bed column adsorption mode, with a breakthrough time of 136 min. The results of nitrate adsorption studies and surface characterization indicate that the introduction of active quaternary nitrogen (N-Q) adsorption sites after nitrogen-doped is the primary mechanism for enhancing the adsorption capacity of nitrate ions.

List of contents

Chapter 1 General introduction

1.1 Water pollution

1.1.1 Current situation of global water pollution

The Earth is the home on which humanity depends for survival. It nurtures all living things, and millions of species thrive and reproduce on it. However, due to the continuous expansion of human activities, the Earth has been subjected to pollution and destruction from various factors in many ways. In order to satisfy the desires, humans have recklessly exploited and expanded land use. To improve their quality of life, people continuously expand industrial and agricultural production, recklessly discharging toxic and harmful wastewater and gases. These selfish actions have severely damaged the ecological environment, leading to the continuous deterioration of habitats for plants and animals. Many species of organisms are on the verge of extinction or have even become extinct. Protecting the environment is a responsibility that everyone should fulfill, and researchers, in particular, should take the lead in this endeavor. Currently, the major environmental issues include water pollution, air pollution, soil pollution, and radioactive contamination. Since the 1990s, the issue of pollution in rivers, lakes, and even groundwater caused by industrial wastewater, agricultural irrigation, and domestic sewage has become increasingly severe and is expected to worsen further [1]. As a result, the threats and negative impacts on human health and the environment will continue to increase. The World Economic Forum has listed freshwater resource degradation as one of the top ten global risks over the past decade [2]. Therefore, it is essential to develop technologies that can effectively address the issue of global water pollution.

According to statistics, the available water resources for humans, animals, and plants account for only 0.02% of the Earth's total water resources [3]. However, water pollution caused by human activities has further exacerbated the already scarce and precious available water resources. Cases of water pollution are common worldwide. In India, 80% of the water resources are classified as sewage, and the Ganges River has been listed as one of the most polluted rivers in the world. A large amount of untreated domestic sewage, industrial wastewater, and waste from religious activities is discharged into this river, which the river supports the lives of 400 million people. Every day, over 40 million liters of wastewater are

released into its water resources, leading to 38 million people contracting waterborne diseases, with more than 2 million deaths annually [4, 5]. In China, with the continuous advancement of industrialization and urbanization, the Yellow River and the Yangtze River are also facing serious pollution problems. The pollution in the Yellow River Basin is particularly severe, with excessive levels of heavy metals and organic pollutants posing significant threats to the health of residents along the river. In some downstream sections, the river has even dried up [6]. In the Yangtze River Basin, the water quality in the Yangtze River Delta has noticeably deteriorated, and algal blooms have broken out in some tributary areas [7]. According to research, from 1990 to 2017, the percentage of disability-adjusted life years (DALY) per 100,000 people due to 14 out of 21 non-communicable diseases increased from 4.4% to 117% [8]. Chen et al. developed a new model system by linking MARINA (Model to Assess River Input of Nutrient to seAs) with NUFER (Nutrient flows in Food chains, Environment, and Resource use) to study the impact of crops and livestock on nitrogen inputs in the Yangtze River. This allows for future regulation of major crop varieties and livestock production to mitigate nitrogen pollution [9, 10]. The results indicated that in 2012, approximately 6,000 Gg of nitrogen entered all rivers in the Yangtze River Basin in the form of dissolved inorganic nitrogen (DIN) from crop production. Half of this nitrogen came from the production of rice, wheat, and vegetables. In the same year, livestock production resulted in a DIN input of 2000 Gg to the Yangtze River. Pig farming accounted for 55-85% of the manure-related DIN input. Additionally, the Danube River, renowned as the second-longest river in Europe, is a major receiving basin for wastewater discharge, with concentrations of various antibiotics currently exceeding safe thresholds [11]. The researchers studied the fecal contamination and antibiotic resistance of different clinically relevant bacteria [12-14]. The results indicate that in the upper Danube River, one-third of the sampled isolates exhibited resistance to one or two antibiotics, while over 10% of the isolates showed resistance to multiple antibiotics [15]. In addition, the Danube River Basin was defined as a "reservoir of antibiotic resistance" in the Joint Danube Survey 3, which is one of the most serious threats to human health [16, 17]. In summary, the issue of water pollution faced by the world today is extremely severe.

The types of pollutants that cause water pollution include organic pollutants (dyes, fats, proteins), inorganic pollutants (heavy metals, acids, bases), microbial contamination, and

nutrient pollution, among others. Their presence disrupts aquatic ecosystems and threatens the health and survival of plants and animals. In addition, the pollution of clean water resources by these sources also affects agricultural productivity and manufacturing productivity, leading to lower water quality, increased pressure on water resources, and potentially serious consequences that could trigger global economic risks [18].

1.1.2 Harmful effects of nitrate and phosphate ions pollution

Among various pollution sources, the issue of water pollution caused by nitrate and phosphate ions is particularly prominent. Since 1920, the nitrogen deposition on land has doubled due to the development of human society and the demands of agricultural production [19]. Fertilizers, pesticides, and other chemicals designed to increase and ensure crop yields are produced and widely applied, thereby artificially interfering with the balance of nitrogen and phosphorus levels in the original ecosystem. These pollutants are also considered the second largest chemical contaminant in surface water and groundwater [20]. The permissible discharge concentrations of nitrate and phosphate ions vary internationally due to differences in countries, regions, and types of water bodies. The World Health Organization (WHO) states that the concentration of nitrate ions in drinking water should not exceed 50 mg NO_3^-/L [21]. The United States Environmental Protection Agency suggested a mean TP concentration of 10 μg P/L in its nutrient criteria guidelines for lakes and reservoirs [22]. It is worth mentioning that in many regions around the world, both in developed and developing countries, the nitrate ions concentration in drinking water has exceeded 50 mg/L. For example, in the southern Campania region of Italy, some cities in Iran, urban areas in Brazil, southeastern Australia, and rural areas in northern Mexico, among others [23-25].

The permissible level was set to prevent further deterioration of the natural environment and its threat to human health. For phosphate ions, excessive intake can affect calcium metabolism in the body, leading to an imbalance between calcium and phosphorus, which can result in osteoporosis. In addition, high phosphorus intake can increase the metabolic burden on the kidneys, accelerating kidney damage [26]. Elevated phosphate levels can also promote vascular calcification, increasing the risk of cardiovascular and cerebrovascular diseases. Excessive phosphorus intake can also interfere with the secretion of thyroid hormones, leading

to endocrine disorders in the body [27]. On the other hand, excessive intake of nitrate has a more significant negative impact on the human body. Nitrate ions enter the human food chain through residues in groundwater and vegetables [28]. Nitrate ions ingested by the human body could convert into nitrite ions, which can easily bind with hemoglobin in the body, impairing its ability to transport oxygen and leading to methemoglobinemia [29]. This symptom is common among infants and is often referred to as "blue baby syndrome," which is characterized by blue-tinged skin and difficulty breathing. In addition, high intake of nitrate ions poses another significant health threat: cancer. Nitrate ions are precursors to N-nitroso compounds, many of which are teratogens and carcinogens in nature [30]. Nitrate ions enter the human body through both exogenous and endogenous pathways. After being reduced to nitrite ions, they can lead to major diseases such as cancers of the nervous system and colon cancer, as well as metabolic dysfunction, thyroid abnormalities, and genotoxic damage, among others [23, 31-33].

Nitrate and phosphate ions pollution, besides being harmful to human health, also pose a serious threat to the global environment. They can lead to eutrophication, causing excessive growth of aquatic plants and even algal blooms. This can harm fish and aquatic organisms and disrupt the balance among species in aquatic environments [34]. A typical algal bloom is a natural occurrence that results from explosive growth of microscopic algae, primarily due to seasonal temperature fluctuations, abundant sunlight, and sufficient nutrients in the water [35]. Certain algal blooms are classified as harmful because they produce toxic metabolites and organic compounds, which can cause various diseases and even death in humans and aquatic creatures [36]. In addition, although many harmful algae do not produce toxic substances, the organic matter from algae (AOM) and algal biomass can accumulate in large quantities on the surface of the water. The bacterial decomposition of these organic components can lead to a sharp decline in dissolved oxygen levels in the water, severely damaging the habitats of aquatic organisms [37]. The series of negative impacts caused by harmful algal blooms will ultimately lead to economic losses in fisheries and aquaculture. In more severe cases, the metabolic byproducts of algal cells can clog some large operational equipment, such as the filters in seawater desalination plants, resulting in membrane fouling and even producing unpleasant odors [38, 39]. The occurrence of algal blooms is often dominated by a specific type or group

of algae. It has been reported that diatoms, dinoflagellates, and cyanobacteria are three major types of algae that frequently produce large amounts of blooms. They all have harmful effects, including toxic blooms and oxygen depletion [40-44].

1.2 Technologies for treating nitrate and phosphate ions pollution

In response to the serious consequences of water pollution caused by nitrate and phosphate ions mentioned above, various methods have been developed to remove such pollutants from water. Techniques such as ion exchange, reverse osmosis, electrodialysis, biological treatment (biological denitrification and biological phosphorus removal), and adsorption methods will be described in the following sections.

1.2.1 Ion exchange

Ion exchange is a water treatment technology based on ion exchange resins. It works by using the functional groups in the resin to reversibly exchange with pollutant ions in the water solution, thereby removing the target pollutants [45]. In general, depending on the type of pollutants, either anion or cation exchange resins can be selectively used. For example, ion exchange resins with trimethylamine functional groups exhibit a specific ion exchange trend during the ion exchange process, with the sequence $CO_3^{2-} < Cl^- < NO_3^- < PO_4^{2-}$ [46]. When the resin becomes saturated, a regenerant solution can be used to elute the pollutants, thereby restoring its ion exchange capacity. The disadvantage of this technology is that it requires post-treatment and the handling of waste brine [47]. At the same time, if the discarded ion exchange resins are not properly treated in a timely manner, they can also pose serious risks to the environment. Therefore, how to properly dispose of the resulting waste resins remains an unresolved issue.

1.2.2 Reverse osmosis

Reverse osmosis is a technology that uses a semi-permeable membrane to separate pollutants from water. Its working principle involves applying pressure to the polluted water, allowing only water molecules to pass through the membrane, while dissolved pollutants such as phosphate and nitrate ions are retained on the concentrated water side, thereby achieving water purification [48]. This method is suitable for treating wastewater with high concentrations

of nitrate and phosphate ions. The advantages of this technology include high-quality effluent, making it suitable for the production of drinking water. However, it has some disadvantages, such as high system costs, significant energy consumption, the need for regular maintenance of the semi-permeable membrane, and the challenge of further treating the concentrated wastewater [49].

1.2.3 Electrodialysis

Electrodialysis is a technology that drives ions through selective ion exchange membranes using an electric field, thereby separating pollutants from water [50]. The main working principle of this technology is that, under the influence of an electric field, positively charged cations move toward the negative electrode, while negatively charged anions move toward the positive electrode. They pass through cation-selective membranes and anion-selective membranes, respectively, allowing the pollutants to be concentrated in the brine stream [51]. This technology allows for the control of the deionization rate of the treated effluent by adjusting the system voltage. However, electrodialysis also has its disadvantages, including additional energy consumption, unsatisfactory treatment efficiency for high-concentration polluted wastewater, susceptibility of the membrane system to blockage by contaminants, and the need for regular maintenance [52].

1.2.4 Biological treatment

The biological treatment methods in nitrogen and phosphorus wastewater treatment mainly include biological denitrification and biological phosphorus removal. They remove nitrogen and phosphorus from the water through microbial metabolic activities. The biological phosphorus removal relies on the metabolic activity of polyphosphate accumulating organisms (PAOs). These microorganisms release phosphate under anoxic and anaerobic conditions and then store large amounts of phosphate under aerobic conditions [53]. Through this mechanism, phosphates are removed from the water and converted into polyphosphates in the sludge [54]. Biological denitrification is the process in which denitrifying bacteria convert nitrate (NO_3^-) or nitrite (NO_2^-) into nitrogen gas (N_2), thereby removing nitrogen from water. This process occurs under anaerobic conditions, where denitrifying bacteria utilize nitrate as an electron acceptor to reduce it to nitrogen gas, which is released into the atmosphere [55]. Their disadvantages lie

in the high operational requirements for technology and poor adaptability. Additionally, biological denitrification is a lengthy process that typically requires a sufficient organic carbon source and needs to be accompanied by appropriate disposal of the generated biological sludge [56].

1.2.5 Adsorption

Adsorptive removal technology has always been regarded as one of the most attractive methods. Adsorptive removal is based on the interaction between the adsorbent and the adsorbate, where the adsorbate transfers from the aqueous solution to the surface of the adsorbent. Adsorption removal has significant advantages, including low operational costs, ease of operation, regenerability, non-toxicity, cost-effectiveness, and wide applicability. It can effectively circumvent the shortcomings of the aforementioned methods. As a result, it has become a research focus for many scholars and is widely used in the treatment of various pollutants [57-59]. To date, there are various kinds of adsorbents, such as molecular sieve [60], metal oxides/hydroxides [61], organic polymers [62] and carbonaceous adsorbent [63], have been prepared and applied for the treatment of wastewater. Among them, carbonaceous adsorbents are valued for their developed pore structure, wide applicability, excellent regeneration ability, and good thermal stability and mechanical strength.

1.3 Properties of carbonaceous materials

Carbonaceous materials refer to materials primarily composed of carbon, characterized by diverse structural forms and performance features. In the field of adsorptive removal, they are commonly referred to as activated carbon. However, as the porous structure and specific surface area of the adsorbents described in chapter 4 of this paper do not meet the standards of activated carbon, they are collectively referred to carbonaceous materials in the introduction section of this chapter. The adsorption performance of the carbonaceous material is determined by its pore size, specific surface area, and surface chemical properties. These characteristics can be optimized by adjusting the structure of the carbonaceous material, which is often determined by the types of raw materials and preparation methods.

1.3.1 Surface pore structure of carbonaceous materials

The pore structure of carbonaceous materials is a key factor in determining their adsorption performance. The pore sizes of carbonaceous materials are uneven and can generally be classified into three types: micropores, mesopores, and macropores by IUPAC classification [64]. In general, pores with a diameter of less than 2 nm are defined as micropores, and their presence allows carbonaceous materials to have a larger specific surface area [65]. Structures with pore diameters ranging from 2 nm to 50 nm are referred to as mesopores [66]. The presence of mesopores helps enhance diffusivity and serves as channels for mass transfer of reactants and products during the adsorption process. Pores diameter larger than 50 nm are classified as macropores [67]. The adsorption of adsorbates in macropores occurs similarly to adsorption on a flat surface, beginning with monolayer adsorption followed by multilayer adsorption. The pore structure of carbonaceous materials can be tailored by controlling the precursor materials and the preparation conditions, such as the activating agents, temperature, and atmosphere. Common preparation methods of carbonaceous materials include physical activation, chemical activation and template method. Physical activation involves heating precursors (raw materials) in an inert gas or gas environment such as CO_2 for activation. Chemical activation uses chemical reagents to react with precursors, followed by carbonization and activation at high temperatures, resulting in a rich microporous structure. Template method involves using hard templates (such as silica particles) or soft templates (such as surfactants) to control the pore structure within the material, commonly used for the construction of mesopores and macropores [68]. The pore structure of carbonaceous materials can be precisely optimized by regulating their preparation process to meet the requirements of specific applications.

1.3.2 Surface chemical structure of carbonaceous materials

In terms of surface modification of carbonaceous materials, performance optimization can be achieved not only by adjusting their pore structure but also by improving their surface chemical structure. The surface chemical properties of carbonaceous materials directly determine their reactivity, functionality, and ability to interact with external substances. Therefore, suitable preparation schemes can be designed for different types of target pollutants by introducing beneficial functional groups or modifying the material's hydrophilicity or

hydrophobicity, thereby enhancing the adsorption performance of carbonaceous materials [69]. The performance of carbonaceous materials in adsorption can be significantly enhanced by doping or modifying the surface with specific functional groups or metals. Surface functional groups or doped heteroatoms (such as nitrogen, sulfur, phosphorus, etc.) often serve as active sites in the reaction process, effectively regulating the electronic structure and adsorption characteristics of the carbonaceous materials [70]. In this thesis, nitrogen atoms are introduced into the lattice of carbonaceous materials through nitrogen-doped surface modification. Due to the high electronegativity of nitrogen, it attracts surrounding electrons, causing a change in the electron distribution of the carbonaceous materials [71]. Therefore, in this study, the surface modification of glucose-based carbon materials differs from the simple synthesis of all raw materials. The introduction of nitrogen reagents is intended to improve or enhance certain specific surface functionalities of the carbon materials, such as hydrophilicity, hydrophobicity, and the increase of surface active sites, rather than synthesizing or grafting them onto the glucose structure. Depending on the different doping processes and temperatures, various nitrogen doping sites can be formed. Common nitrogen configurations include pyridinic nitrogen (N-6), pyrrolic nitrogen (N-5), quaternary nitrogen (N-Q), and pyridine-N-oxide (N-X) [72, 73] (**Fig. 1-1**). Among them, quaternary nitrogen is considered as an active site that facilitates the adsorption of anions such as nitrate and phosphate ions, as it can carry a positive charge. On the other hand, since N-6 and N-5 are difficult to protonate, they carry a slight negative charge, which may result in repulsion against anions. [74, 75]. Therefore, improving the surface chemical properties of carbonaceous materials can be achieved by developing effective preparation methods that facilitate the loading of quaternary nitrogen on the surface of carbonaceous materials.

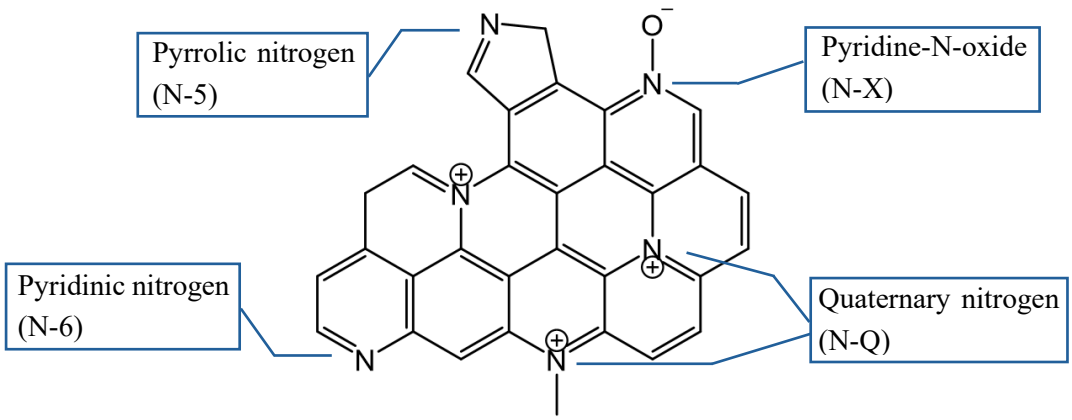

Fig. 1-1. Schematic diagram of the four nitrogen configurations introduced by nitrogen-doped surface modification.

1.4 Evaluation of adsorption performance of carbonaceous materials

The evaluation of the adsorption performance of carbonaceous adsorbents is generally conducted through two modes: batch adsorption and fixed-bed column adsorption.

1.4.1 Batch adsorption

1.4.1.1 Equilibrium adsorption amount

The batch adsorption experiment is usually conducted in a closed reactor, where the adsorbent and adsorbate are mixed in a certain proportion until adsorption equilibrium is reached. The amount of adsorption is measured to evaluate the performance of the adsorbent. The equilibrium adsorption amount is calculated using the following equation:

$$Q_e = \frac{(C_0 - C_e)V}{W} \quad , \qquad (1\text{-}1)$$

where Q_e means the equilibrium adsorption amount (mmol/g). C_0 and C_e represent the initial and the equilibrium concentration of adsorbate (mmol/L), respectively. V signifies the solution volume (L) and W expresses the weight of sample (g).

1.4.1.2 Adsorption isotherm

The Langmuir adsorption isotherm assumes that adsorption occurs as a monolayer, the adsorption sites are homogeneous, and each site can adsorb only one adsorbate molecule. This model is suitable for ideal adsorption systems, where the adsorption capacity gradually saturates as the concentration increases. The Langmuir isotherm equation in liner form:

$$Q_e = \frac{K_e C_e}{1+K_e C_e} X_m \,, \tag{1-2}$$

where Q_e is the adsorption capacity at equilibrium (mmol/g), X_m is the maximum adsorption capacity (mmol/g), K_e is the adsorption equilibrium constant (L/mmol), and C_e is the equilibrium concentration (mmol/L).

Freundlich adsorption isotherm is an empirical formula that applies to multilayer adsorption and adsorption processes on heterogeneous surfaces. The Freundlich isotherm is typically used to describe adsorption behavior at low concentrations. The Freundlich isotherm equation in liner form:

$$lnQ_e = lnK_F + \frac{1}{n} lnC_e \,, \tag{1-3}$$

where K_F means Freundlich isotherm constant [(mmol/g) (L/mmol)$^{1/n}$], and *1/n* is the heterogeneity of the surface.

1.4.1.3 Adsorption kinetic

Pseudo-First-Order Kinetics Model: This model assumes that the adsorption rate is proportional to the amount of adsorbate that has not yet been adsorbed. The pseudo-first-order kinetics equation is:

$$\ln(Q_e - Q_t) = lnQ_e - k_1 t \,, \tag{1-4}$$

where Q_t is the adsorption capacity at time t (mmol/g), Q_e is the equilibrium adsorption capacity (mmol/g), and k_1 is the rate constant (min^{-1}).

Pseudo-Second-Order Kinetics Model: This model assumes that the adsorption rate is proportional to the occupancy of the adsorption sites. The pseudo-second-order kinetic equation:

$$\frac{t}{Q_t} = \frac{1}{k_2 Q_e^2} + \frac{t}{Q_e} \,, \tag{1-5}$$

where k_2 is the pseudo-second-order rate constant (g(mg min)$^{-1}$).

1.4.2 Fixed-bed column adsorption

Fixed-bed column adsorption involves immobilizing an adsorbent in a reactor, while the adsorbate solution flows through the fixed bed. It is commonly used to simulate continuous flow processes, making it more closely aligned with practical applications. This method is particularly suitable for evaluating the performance of adsorbents under continuous operation,

and is of great significance, especially in industrial-scale applications. The amount of nitrate adsorption (Q) in the fixed-bed column adsorption is expressed by the following equation [76]:

$$Q = \frac{R}{Wm}\int_0^t (C_0 - C_t)\, dt\ , \tag{1-6}$$

where R is the flow rate (mL/min), W means the molar mass of nitrate (g/mol), m is the weight of adsorbent (g), t represents the flow time (min), C_0 is the nitrate concentration in the influent (mg/L), C_t is the nitrate concentration in the effluent at time t (mg/L).

1.5 The organization of this thesis

This study focuses on addressing water pollution caused by nitrate and phosphate ions by developing new and effective carbonaceous adsorbents to tackle such environmental issues. The selection of glucose as the primary carbon source material is due to its widespread availability in nature and ease of acquisition, as it can be obtained through simple starch or cellulose hydrolysis. Furthermore, current studies utilizing glucose as the main precursor for material development are mostly focused on applications such as dye adsorption, heavy metal removal, carbon dioxide capture, and the development of supercapacitor materials. However, research on glucose, melamine and urea as the raw material to develop adsorbent for the adsorption of ionic pollutants, which are more challenging to remove from aqueous solutions, has not been reported. Therefore, this thesis takes this aspect as the starting point and conducts in-depth research. Traditional carbonaceous adsorbents have low efficiency in removing ionic pollutants, appropriate modification methods are needed to enhance their pollutant removal capacity. Nitrogen-doped surface modification is applied in the preparation process of the adsorbents to improve their surface physical/chemical properties and adsorption performance. Meanwhile, the thesis also studied and explained the mechanism by which the adsorbent interacts towards pollutant ions.

In chapter 2, a novel glucose-based activated carbon adsorbent (MeUrGlu-550Z0.5-1.0-2nd) with excellent nitrate ions adsorption performance has been designed and synthesized through nitrogen-doped surface modification. The adsorption study was mainly conducted under batch adsorption and fixed-bed column adsorption modes, which helped to thoroughly examining the adsorption performance of the adsorbent. In batch adsorption experiments, the effects of solution pH, initial nitrate ions concentration, adsorption isotherms, and adsorption

kinetics on adsorption capacity were investigated. Through fixed-bed column adsorption to investigate the adsorption breakthrough curve of the adsorbent, the influence of coexisting ions on the removal of nitrate ions, the regeneration performance of the adsorbent, and its ability to remove nitrate ions from real wastewater.

In chapter 3, based on the research on the adsorption of nitrate ions by glucose-based activated carbon adsorbent, this chapter further explores the adsorption performance on phosphate ions (MeUrGlu-600Z0.5-2nd). The commercial anion exchange resin (HP555) was used as a reference material, the effects of different solution pH values on the phosphate ions adsorption capacity of MeUrGlu-600Z0.5-2nd and HP555 were investigated. Their adsorption isotherms were also studied and compared to obtain a more comprehensive analysis of the adsorption principle. At the same time, combined with the characterization results and the findings from adsorption experiments, the adsorption mechanism of phosphate ions by the adsorbent in aqueous solution was elucidated. In addition, the regeneration performance of the adsorbent was evaluated in fixed-bed column adsorption experiments.

In chapter 4, in order to achieve the transition of adsorbent preparation materials to a single nitrogen source, the interaction between the raw materials in the preparation of glucose-based carbonaceous adsorbents is further explored. The principles of the brown porous foam-like intermediate generated during the preparation of the adsorbent in improving adsorption capacity was emphasized, and the preparation scheme was further optimized. The carbonaceous adsorbent without nitrogen doping was used as the reference material. Nitrogen adsorption-desorption isotherm, elemental analysis and X-ray photoelectron spectroscopy (XPS) characterization were carried out on the adsorbents before and after nitrogen-doped modification. The pH_{pzc}, effects of solution pH, adsorption isotherms and adsorption kinetics of the adsorbents were investigated. The breakthrough curves of the adsorbent in a fixed-bed column adsorption were also studied, which further validating the effectiveness of nitrogen-doped surface modification in enhancing the adsorption performance of the adsorbent.

Finally, chapter 5 summarizes the conclusion of this study, and prospects for future research are discussed.

Reference

[1] J. Erisman, M. Sutton, J. Galloway, Z. Klimont, W. Winiwarter, How a century of ammonia synthesis changed the world, Nat. Geosci. 1 (2008) 636-639.

[2] A. Plessis, Persistent degradation: Global water quality challenges and required actions, One Earth 5 (2022) 129-131.

[3] M.Wang, B. L. Bodirsky, R. Rijneveld, F. Beier, M. P. Bak, M. Batool, B. Droppers, A. Popp, M. T. H. van Vliet, M. Strokal, A triple increase in global river basins with water scarcity due to future pollution, Nat. Commun. 15 (2024) 880.

[4] Global Health, How water pollution in india kills millions, (2020). https://www.borgenmagazine.com/water-pollution-in-india/.

[5] Conserve Energy Future, Top 19 most polluted rivers in the world in 2020, (2020). https://www.conserve-energy-future.com/most-polluted-rivers-world.php.

[6] C. Liu, S. Zhang, Drying up of the yellow river: its impacts and counter-measures, Mitigation Adapt. Strategies Global Change 7 (2002) 203-214.

[7] H. Li, H. Tang, X. Shi, C. Zhang, X. Wang, Increased nutrient loads from the Changjiang (Yangtze) River have led to increased Harmful Algal Blooms, Harmful Algae 39 (2014) 92-101.

[8] L. Wu, X. Qiu, T. Wang, K. Tao, L. Bao, E. Y. Zeng, Water quality and organic pollution with health risk assessment in China: A Short Review, ACS ES&T Water 2 (2022) 1279-1288.

[9] X. Chen, M. Strokal, C. Kroeze, I. Supit, M. Wang, L. Ma, X. Chen, X. Shi, Modeling the contribution of crops to nitrogen pollution in the Yangtze River, Environ. Sci. Technol. 54 (2024) 11929-11939.

[10] X. Chen, M. Wang, C. Kroeze, X. Chen, L. Ma, X. Chen, X. Shi, M. Strokal, Nitrogen in the Yangtze River basin: pollution reduction through coupling crop and livestock production, Environ. Sci. Technol. 56 (2022) 17591-17603.

[11] M. Leopold, A. Kabicher, I. Pap, B. Ströbele, G. Zarfel, A. H. Farnleitner, A. K. T. Kirschner, A comparative study on antibiotic resistant Escherichia coli isolates from Austrian patients and wastewater-influenced Danube River water and biofilms, Int. J. Hyg. Environ. Health 258 (2024) 114361.

[12] A. K. T. Kirschner, G. G. Kavka, B. Velimirov, R. L. Mach, R. Sommer, A. H. Farnleitner, Microbiological water quality along the Danube River: integrating data from two whole-river surveys and a transnational monitoring network, Water Res. 43 (2009) 3673-3684.

[13] C. Kittinger, A. Kirschner, M. Lipp, R. Baumert, F. Mascher, A. H. Farnleitner, G. E. Zarfel, Antibiotic Resistance of Acinetobacter spp. Isolates from the River Danube: Susceptibility Stays High, Int. J. Environ. Res. Public Health 15 (2018) 52.

[14] A. K. T. Kirschner, G. H. Reischer, S. Jakwerth, D. Savio, S. Ixenmaier, E. Toth, R. Sommer, R. L. Mach, R. Linke, A. Eiler, S. Kolarevic, A. H. Farnleitner, Multiparametric monitoring of microbial faecal pollution reveals the dominance of human contamination along the whole Danube River, Water Res. 124 (2017) 543-555.

[15] C. Kittinger, M. Lipp, B. Folli, A. Kirschner, R. Baumert, H. Galler, A. J. Grisold, J. Luxner, M. Weissenbacher, A. H. Farnleitner G. Zarfel, Enterobacteriaceae isolated from the River Danube: antibiotic resistances, with a focus on the presence of ESBL and carbapenemases, PLoS ONE 11 (2016) e0165820.

[16] N. A. Alygizakis, H. Besselink, G. K. Paulus, P. Oswald, L. M. Hornstra, M. Oswaldova, G. Medema, N. S. Thomaidis, P. A. Behnisch, J. Slobodnik, Characterization of wastewater effluents in the Danube River Basin with chemical screening, in vitro bioassays and antibiotic resistant genes analysis, Environ. Int. 127 (2019) 420-429.

[17] I. Liska, F. Wagner, M. Sengl, K. Deutsch, J. Slobodnik, Joint Danube Survey 3-a comprehensive analysis of Danube water quality. International commission for the potection of the Danube, 2015, Austriahttp://www.danubesurvey.org/jds-files/nodes/.

[18] J. Yang, J. Li, M. T. H. Vliet, E. R. Jones, Z. Huang, M. Liu, J. Bi, Economic risks hidden in local water pollution and global markets: A retrospective analysis (1995-2010) and future perspectives on sustainable development goal 6, Water Res. 252 (2024) 121216.

[19] M. H. Ward, R. R. Jones, J. D. Brender, T. M. de Kok, P. J. Weyer, B. T. Nolan, C. M. Villanueva, S. G. van Breda, Drinking water nitrate and human health: an updated review, Int. J. Environ. Res. Publ. Health 15 (2018) 1557.

[20] J. O. Back, M. O. Rivett, L. B. Hinz, N. Mackay, G. J. Wanangwa, O. L. Phiri, C. E. Songola, M. A. S. Thomas, S. Kumwenda, M. Nhlema, A. V. M. Miller, R. M. Kalin, Risk assessment to groundwater of pit latrine rural sanitation policy in developing country

settings, Sci. Total Environ. 613-614 (2018) 592-610.

[21] World Health Organization, Nitrate and nitrite in drinking-water, 2023, https://iris.who.int/bitstream/handle/10665/75380/WHO_SDE_WSH_04.03_56_eng.pdf.

[22] P. S. Kumar, L. Korving, M. C. M. van Loosdrecht, G. J. Witkamp, Adsorption as a technology to achieve ultra-low concentrations of phosphate: Research gaps and economic analysis, Water Res. X, 4 (2019) 100029.

[23] E. G. Torres, F. E. R. Rodríguez, Letter to the editor. Additional critical information in regard to "Nitrates in the environment: A critical review of their distribution, sensing techniques, ecological effects and remediation", Chemosphere 309 (2022) 136718.

[24] M. Marhamati, A. Afshari, B. Kiani, B. Jannat, M. Hashemi, Nitrite and nitrate levels in groundwater, water distribution network, bottled water and juices in Iran: A systematic review. Current Pharm. Biotechnol. 22 (2022) 1325-1337.

[25] D. D. Gandarilla-Esparza, E. Y. Calleros-Rinco´n, H. M. Macias, M. F. Gonza´lez-Delgado, G. G. Vargas, J. D. Sustaita, A. Gonza´lez-Zamora, E. Ríos-Sa´nchez, R. P´erez- Morales, FOXE1 polymorphisms and chronic exposure to nitrates in drinking water cause metabolic dysfunction, thyroid abnormalities, and genotoxic damage in women, Genet. Mol. Biol. 44 (2021), e20210020.

[26] A. R. Chang, C. Anderson, Dietary phosphorus intake and the kidney, Annu. Rev. Nutr. 21 (2017) 321-346.

[27] C. A. Wagner, The basics of phosphate metabolism, Nephrology Dial. Transpl. 39 (2024) 190-201.

[28] M. Kundu, P. Krishnan, S. Prasad, A. Vashisth, S. Duhan, K. R. Reddy, Chapter Four - Biosensing technology interventions for the detection of nitrate and nitrite contamination in environment and foods, Adv. Agron. 183 (2024) 193-250.

[29] N. Patel, A. L. Srivastav, A. Patel, A. Singh, S. K. Singh, V. K. Chaudhary, P. K. Singh, B. Bhunia, Nitrate contamination in water resources, human health risks and its remediation through adsorption: a focused review, Environ. Sci. Pollut. Res. 29 (2022) 69137-69152.

[30] Y. Zhai, Y. Lei, J. Wu, Y. Teng, J. Wang, X. Zhao, X. Pan, Does the groundwater nitrate pollution in China pose a risk to human health? A critical review of published data, Environ. Sci. Pollut. Res. 24 (2017) 3640-3653.

[31] S. Singh, A. G. Anil, V. Kumar, D. Kapoor, S. Subramanian, J. Singh, P. C. Ramamurthy, Nitrates in the environment: A critical review of their distribution, sensing techniques, ecological effects and remediation, Chemosphere 287 (2022) 131996.

[32] E. E. Essien, K. S. Abasse, A. Coˆt´e, K. S. Mohamed, M. Baig, M. Habib, M. Naveed, X. Yu, W. Xie, J. Sun, M. Abbas, Drinking-water nitrate and cancer risk: a systematic review and meta-analysis, Arch. Environ. Occup. Health 77 (2022) 51-67.

[33] E. G. Torres, R. P´. Morales, A. G. Zamora, E. Y. Calleros-Rinco´n, Subclinical hypothyroidism in families due to chronic consumption of nitrate- contaminated water in rural areas with intensive livestock and agricultural practices in durango, Mexico, Water 14 (2022) 282.

[34] M. J. Ahmed, B. H. Hameed, M. A. Khan, Recent advances on activated carbon-based materials for nitrate adsorption: A review, J. Anal. Appl. Pyrolysis 169 (2023) 105856.

[35] A. E. Al-Rawajfeh, E. Alzalabieh, G. A. Bazedi, G. M. Al-Mazaideh, M. H. F. Shalayel, A review on harmful algae blooms in Arabian Gulf: causes and impacts on desalination plants, Desalin. Water Treat. 290 (2023) 46-55.

[36] E. Zohdi, M. Abbaspour, Harmful algal blooms (red tide): a review of causes, impacts and approaches to monitoring and prediction, Int. J. Environ. Sci. Technol. 16 (2019) 1789-1806.

[37] Y. Li, X. Chen, O. Wai, B. King, Study on the dynamics of algal bloom and its influence factors in Tolo Harbour, Hong Kong, Water Environ. Res. 76 (2004) 2643-2654.

[38] R. M. Kudela, A. Bickel, M. L. Carter, M. D. A. Howard, L. Rosenfeld, Chapter 5-The monitoring of harmful algal blooms through ocean observing: The development of the California harmful algal bloom monitoring and alert program, coastal ocean observing systems, Elsevier Inc. (2015) 58-75.

[39] D. A. Caron, M. Garneau, E. Seubert, M. D. A. Howard, L. Darjany, A. Schnetzer, I. Cetinić, G. Filteau, P. Lauri, B. Jones, S. Trussell, Harmful algae and their potential impacts on desalination operations off southern California, Water Res. 44 (2010) 385-416.

[40] R. Yu, S. Lü, Y. Liang, Harmful algal blooms in the coastal waters of China, Global Ecology and Oceanography of Harmful Algal Blooms 232 (2018) 309-316.

[41] A. Kremp, T. Tamminen, K. Spilling, Dinoflagellate bloom formation in natural

assemblages with diatoms: nutrient competition and growth strategies in Baltic spring phytoplankton, Aquat. Microb. Ecol. 50 (2008) 181-196.

[42] N. Kashulin, T. Kashulina, A. Bekkelund, Long-term eutrophication and dynamics of bloom-forming microbial communities during summer HAB in large arctic lake, Environments 8 (2021) 82.

[43] B. Durán-Vinet, K. Araya-Castro, T. C. Chao, S. A. Wood, V. Gallardo, K. Godoy, M. Abanto, Potential applications of CRISPR/Cas for next-generation biomonitoring of harmful algae blooms: a review, Harmful Algae 103 (2021) 102027.

[44] S. E. Papoulis, S. W. Wilhelm, D. Talmy, E. R. Zinser, Nutrient loading and viral memory drive accumulation of restriction modification systems in bloom-forming cyanobacteria, mBio 12 (2021) e0087321.

[45] A. M. Bergquist, J. K. Choe, T. J. Strathmann, C. J. Werth, Evaluation of a hybrid ion exchange-catalyst treatment technology for nitrate removal from drinking water, Water Res. 96 (2016) 177-187.

[46] S. Samatya, N. Kabay, Ü. Yüksel, M. Arda, M. Yüksel, Removal of nitrate from aqueous solution by nitrate selective ion exchange resins, React. Funct. Polym. 66 (2006) 1206-1214.

[47] S. Duan, T. Tong, S. Zheng, X. Zhang, S. Li, Achieving low-cost, highly selective nitrate removal with standard anion exchange resin by tuning recycled brine composition, Water Res. 173 (2020) 115571.

[48] F. Zirrahi, M. Hadi, R. N. Nodehi, E. G. Milan, P. Bashardoust, S. Abolli, M. Alimohammadi, A systematic review on the investigation of optimal operating conditions of the reverse osmosis process in nitrate removal from drinking water, Results Eng. 21 (2024) 101947.

[49] A. Shrivastava, S. Rosenberg, M. Peery, Energy efficiency breakdown of reverse osmosis and its implications on future innovation roadmap for desalination, Desalination 368 (2015) 181-192.

[50] R. K. Nagarale, G. S. Gohil, V. K. Shahi, Recent developments on ion-exchange membranes and electro-membrane processes, Adv. Colloid Interface Sci. 119 (2006) 97-130.

[51] P. Bhatt, G. Bhandari, M. Bilal, Occurrence, toxicity impacts and mitigation of emerging micropollutants in the aquatic environments: Recent tendencies and perspectives, J. Environ. Chem. Eng. 10 (2022) 107598.

[52] S. Al-Amshawee, M. Y. B. M. Yunus, A. A. M. Azoddein, D. G. Hassell, I. H. Dakhil, H. A. Hasan, Electrodialysis desalination for water and wastewater: A review, Chem. Eng. J. 380 (2020) 122231.

[53] S. M. Saia, H. J. Carrick, A. R. Buda, J. M. Regan, M. T. Walter, Critical review of polyphosphate and polyphosphate accumulating organisms for agricultural water quality management, Environ. Sci. Technol. 55 (2021) 2722-2742.

[54] M. Wu, R. Zhu, H. Zhu, X. Dai, J. Yang, Phosphorus removal and simultaneous sludge reduction in humus soil sequencing batch reactor treating domestic wastewater, Chem. Eng. J. 215-216 (2013) 136-143.

[55] L. Zhang, H. Zhao, S. Qin, C. Hu, Y. Shen, B. Qu, Y. Bai, B. Liu, Genome-resolved metagenomics and denitrifying strain isolation reveal new insights into microbial denitrification in the deep vadose zone, Environ. Sci. Technol. 58 (2024) 2323-2334.

[56] H. Cui, Y. Feng, Z. Yin, K. Qu, L. Wang, J. Li, T. Jin, Y. Bai, Z. Cui, Organic carbon release, denitrification performance and microbial community of solid-phase denitrification reactors using the blends of agricultural wastes and artificial polymers for the treatment of mariculture wastewater, Ecotox. Environ. Safe. 255 (2023) 114791.

[57] D. Zhang, B. Wang, X. Gong, Z. Yang, Y. Liu, Selective reduction of nitrate to nitrogen gas by novel Cu_2O-Cu^0@Fe^0 composite combined with HCOOH under UV radiation, Chem. Eng. J. 359 (2019) 1195-1204.

[58] J. Wang, S. Zhuang, Y. Liu, Metal hexacyanoferrates-based adsorbents for cesium removal, Coord. Chem. Rev. 374 (2018) 430-438.

[59] A. Shahat, H. M. A. Hassan, M. F. El-Shahat, O. E. Shahawy, M. R. Awual, Visual nickel(II) ions treatment in petroleum samples using a mesoporous composite adsorbent, Chem. Eng. J. 334 (2018) 957-967.

[60] Y. Gao, Y. Ru, L. Zhou, X. Wang, J. Wang, Preparation and characterization of chitosan-zeolite molecular sieve composite for ammonia and nitrate removal, Adv. Compos. Lett. 27 (2018) 185-192.

[61] S. Mahdavi, P. Molodi, M. Zarabi, Functionalized MgO, CeO_2 and ZnO nanoparticles with humic acid for the study of nitrate adsorption efficiency from water. Res. Chem. Intermed. 44 (2018) 5043-5062.

[62] P. Karthikeyan, S. SD. Elanchezhiyan, S. Meenakshi, C. M. Park, Magnesium ferrite-reinforced polypyrrole hybrids as an effective adsorbent for the removal of toxic ions from aqueous solutions: Preparation, characterization, and adsorption experiments, J. Hazard. Mater. 408 (2021) 124892.

[63] P. Karthikeyan, S. Vigneshwaran, S. Meenakshi, Removal of phosphate and nitrate ions from water by amine crosslinked magnetic banana bract activated carbon and its physicochemical performance, Environ. Nanotechnol. Monit. Manag. 13 (2020) 100294.

[64] K. S. W. Sing, D. H. Everett, R. A. W. Haul, L. Moscou, R. A. Pierotti, J. Rouauerol, T. Siemieniewska, Reporting physisorption data for gas/solid systems with special reference to the determination of surface area and porosity, Pure Appl. Chem. 57 (1985) 603-619.

[65] Z. Ryu, J. Zheng, M. Wang, B. Zhang, Characterization of pore size distributions on carbonaceous adsorbents by DFT, Carbon 37 (1999) 1257-1264.

[66] M. Thommes, K. Kaneko, A. V. Neimark, J. P. Olivier, F. Rodriguez-Reinoso, J. Rouquerol, K. S. W. Sing, Physisorption of gases, with special reference to the evaluation of surface area and pore size distribution (IUPAC Technical Report), Pure Appl. Chem. 87 (2015) 1051-1069.

[67] L. Wu, Y. Li, Z. Fu, B. L. Su, Hierarchically structured porous materials: synthesis strategies and applications in energy storage, Natl. Sci. Rev. 7 (2020) 1667-1701.

[68] S. S. Hoseini, A. Seyedkanani, G. Najafi, A. P. Sasmito, A. Akbarzadeh, Multiscale architected porous materials for renewable energy conversion and storage, Energy Storage Mater. 59 (2023) 102768.

[69] T. Cheng, Y. Bian, J. Li, X. Ma, L. Yang, L. Zhou, H. Wu, Nitrogen-doped porous biochar for selective adsorption of toluene under humid conditions, Fuel 334 (2023) 126452.

[70] M. Machida, Y. Amano, F. Imazeki, Water purification with activated carbons (ACs): A short review -Influence of the textural and surface properties of ACs on the adsorptive removal of pollutants -, Tanso 270 (2015) 241-249.

[71] S. Cheng, T. Wang, L. Chu, J. Li, L. Zhang, Preparation of nitrogen-doped activated carbon

used for catalytic oxidation removal of H_2S, Sci. Total Environ. 915 (2024) 170073.

[72] K. Stańczyk, Temperature -time sieve- A case of nitrogen in coal, Energy Fuels 18 (2004) 405-409.

[73] J. R. Pels, F. Kapteijn, J. A. Moulijn, Q. Zhu, K. M. Thomas, Evolution of nitrogen functionalities in carbonaceous materials during pyrolysis, Carbon 33 (1995) 1641-1653.

[74] M. Machida, Y. Tsuchiya, J. Yuan, Y. Amano, Efficient nitrate adsorbent applicable to wide pH range derived from polyacrylonitrile (PAN) fiber, Results Eng. 11 (2021) 100276.

[75] Y. Tsuchiya, Y. Yamaya, Y. Amano, M. Machida, Effect of two types of adsorption sites of activated carbon fibers on nitrate ion adsorption, J. Environ. Manage. 289 (2021) 112484.

[76] J. T. Oliveira, A. B. L. Arsufi, D. C. Estumano, L. A. Féris, Bayesian computational technique for modeling caffeine adsorption in a fixed-bed column: Use of the maximum adsorption capacity deterministically and experimental design, Ind. Eng. Chem. Res. 62 (2023) 7127-7137.

Chapter 2 Nitrate removal from aqueous solution by glucose-based carbonaceous adsorbent: batch and fixed-bed column adsorption studies

2.1 Introduction

The contamination of nitrate ion (NO_3^-) due to the excessive use of agricultural fertilizers and the discharge of municipal and industrial wastewater has become a significant global environmental concern [1]. The World Health Organization (WHO) has established a maximum allowable nitrate concentration of 10 mg N/L (or 50 mg NO_3^-/L) in public drinking water [2]. However, numerous studies have reported groundwater nitrate levels exceeding these limits across the globe. For instance, Singh et al. [3] highlighted that in India, approximately 108.2 million individuals consume water with nitrate concentrations surpassing 100 mg/L, while 117.93 million rely on drinking water containing 45-100 mg/L of nitrate. Similarly, a study conducted in the United States found that nitrate concentrations in 20% of 1414 wells located in agricultural areas exceeded 10 mg N/L [4]. Excessive nitrate levels pose serious risks to both human health and the environment. On the one hand, NO_3^- serves as a precursor to carcinogenic nitrite and nitrosamine [5], compromising the immune system and increasing the risk of cancer [6] as well as methemoglobinemia (commonly known as blue-baby syndrome). On the other hand, NO_3^- contributes to eutrophication in aquatic ecosystems, leading to phenomena like algal blooms and red tides, which threaten biodiversity and disrupt ecological balance [7,8]. Therefore, developing efficient methods to mitigate nitrate contamination in water and wastewater is crucial.

Adsorption is recognized as an effective method for removing soluble substances from water due to the advantages of being simple to operate, requiring no auxiliary equipment and flexible to remove pollutants [9,10]. Over the past decades, significant attention has been given to nitrate adsorption using biomass waste-based and carbonaceous adsorbents [11-13]. However, biomass waste-derived adsorbents often exhibit limited nitrate adsorption capacity. For instance, date palm-based biochar [14] and olive solid waste-based activated carbon [15] demonstrated adsorption capacities of only 0.07 mmol/g and 0.09 mmol/g, respectively. In contrast, the modification of carbonaceous adsorbents with quaternary nitrogen (N-Q) through

thermochemical deposition has shown promise. Yuan et al. [16] reported that N-Q modified adsorbent achieved a maximum nitrate adsorption capacity of 0.74 mmol/g, which is 10 times higher than that of the biomass-based adsorbents mentioned above. This indicates that incorporating N-Q onto the carbon surface is an efficient strategy for improving nitrate adsorption [17]. According to the literature, incorporating suitable functional groups to target specific ions is more effective for adsorption than merely increasing the surface area [18]. Since nitrate is a negatively charged monovalent anion, introducing positively charged adsorption sites onto the adsorbent's surface is more favorable to the adsorption of nitrate. Nitrogen doping on carbonaceous adsorbent surface can generate Lewis acid, which facilitate nitrate ion adsorption [19]. Specifically, nitrogen doping promotes the formation of N-Q, a functional group that improves nitrate uptake through electrostatic interactions, as it retains a positive charge across a broad pH range [20]. Our previous research has demonstrated that thermochemical deposition is an effective technique for introducing N-Q functional groups [16,21]. However, this method typically requires high temperatures of approximately 1000°C, making it less practical for industrial applications. Therefore, exploring alternative methods to prepare N-Q-enriched adsorbents under milder conditions is necessary. In addition, glucose is a widely available monosaccharide derived from starch hydrolysis, which offers a sustainable raw material for developing adsorbents. To the best of our knowledge, there is no glucose-based carbonaceous adsorbent that has been reported for the applications of nitrate adsorption. Melamine and urea are rich in nitrogen which are often used as the nitrogen source in the nitrogen-doped surface modification process. The adsorbent developed in this chapter combines these two nitrogen-containing reagents to introduce more beneficial nitrogen-containing functional groups onto the adsorbent's surface. As far as we know, there have been no reports on the preparation of an adsorbent using glucose as a carbon source, activated by zinc chloride, with melamine and urea as nitrogen sources, and its application in the adsorption of nitrate ions from aqueous solutions. Therefore, considering these insights, it can be believed that incorporating N-Q functional groups onto glucose matrix could obtain a novel and effective adsorbent for the removal of nitrate ions in aqueous solution.

This study aims to develop a novel N-Q containing glucose-based carbonaceous adsorbent with efficient adsorption performance for nitrate. The adsorbent was prepared from glucose,

melamine and urea through pyrolysis at 550ºC, with zinc chloride serving as an activating agent. The nitrate adsorption performance was evaluated using both batch and fixed-bed column experiments. Batch adsorption experiments examined the influence of factors such as solution pH and initial nitrate concentration on adsorption efficiency. To gain deeper insights, adsorption isotherms and adsorption kinetics were studied to elucidate the underlying adsorption mechanism. Fixed-bed column adsorption was performed to study the practical applicability of the adsorbent.

2.2 Materials and methods

2.2.1 Materials

All the reagents were obtained from Kanto Chemical Co., Inc Japan, and were used as received without additional purification. Pure water, processed through ion-exchange and distillation system, was utilized in all experiments.

2.2.2 Preparation of carbonaceous adsorbent

The preparation process of the adsorbent is shown in **Fig. 2-1**. A mass of 20 g of glucose, 10 g of melamine and 10 g of urea were mixed in the stainless vessel and 20 g of zinc chloride was added as activator. During the preparation of the adsorbent, $ZnCl_2$ as a strong dehydrating agent, can break the bonding structure of organic molecules at high temperatures, generating volatile substances that are released, thereby contributing to the formation of more porous structures. Then, they were placed in an oven at 110ºC overnight for the pre-treatment process. Subsequently, 10 g of the resulting polymer was transferred to a horizontal tubular furnace for heat treatment. The temperature was increased to 550°C within 45 min at an N_2 flow rate of 20 mL/min and maintained for Y h (Y = 0.5, 1.0, 1.5). During this process, the polymer underwent carbonization and activation. Afterward, the sample was cooled down and removed from the furnace under a continuous N_2 flow. The activated material was then washed with 3 mol/L HCl, followed by rinsing with hot deionized water until the pH of the rinse water was no longer changed. Finally, the washed sample was dried in an oven at 110ºC for 2 h. The prepared adsorbent was designated as MeUrGlu-550Z0.5-Y-1st, where MeUrGlu represents melamine (Me), urea (Ur) and glucose (Glu), respectively. The notation of 550Z0.5 indicates heating at

550ºC with $ZnCl_2$ at 0.5 times the total weight of the reagents. Y corresponds to the maintaining time during the first activation, and 1st signifies the sample was obtained after the first activation process.

We compared the effect of different numbers of reaction times on the adsorption performance. Here, the preparation process employed repeated activation instead of simply extending the duration of the activation time. This is because the activation of the raw materials in the horizontal tubular furnace causes their volume to expand, leading to irregular lateral expansion of the sample, which results in uneven heating. To avoid the negative impact of this uncontrollable factor, a stepwise activation approach was adopted. The samples obtained were ground uniformly before undergoing reactivation. The sample obtained after the first activation (before washing) was pulverized for uniformity and subjected to further activation in the tubular furnace for second and third cycles. Each activation involved heating to 550ºC within 45 min under an N_2 flow of 20 mL/min, and the heating process was maintained for 30 min. The samples were then washed and dried using the same procedures described earlier. The final sample was labeled as MeUrGlu-550Z0.5-Y-2nd and MeUrGlu-550Z0.5-Y-3rd, where 2nd and 3rd indicate the second and third activation processes, respectively.

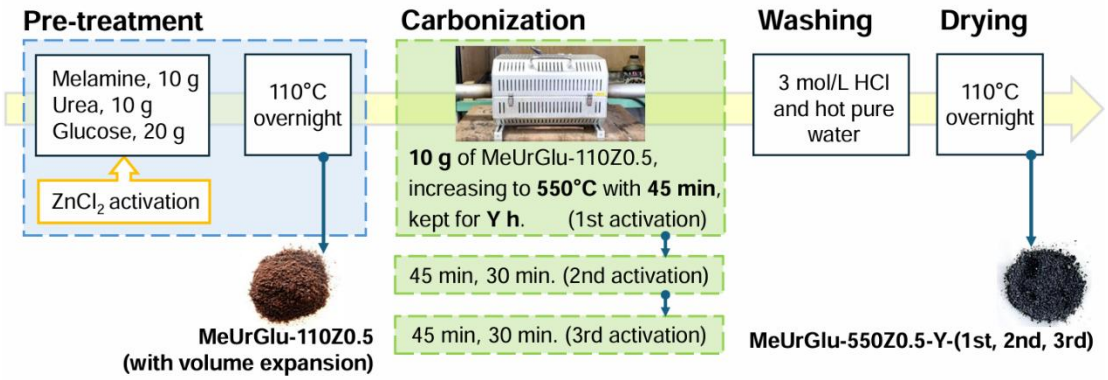

Fig. 2-1. Preparation process of the adsorbent.

2.2.3 Characterization of prepared samples

The prepared samples were characterized by N_2 adsorption and desorption isotherms, elemental analysis and X-ray photoelectron spectroscopy (XPS). The specific surface area and

pore structure of the prepared carbonaceous adsorbents were determined through nitrogen adsorption-desorption measurements at -196ºC using BELSORP-mini II surface analyzer (MicrotracBEL Corporation, Japan). Prior to measurement, samples were dried in an oven at 110ºC overnight and then degassed under vacuum at 300ºC for 1 h. The specific surface area S_{BET} (m^2/g), average pore diameter D_{avg} (nm) and pore volume V_{total} (cm^3/g) will be calculated using the Brunauer-Emmer-Teller (BET) method. The micropore volume V_{micro} was estimated via α_s plots, while the mesopore volume V_{meso} was determined by subtracting V_{micro} from V_{total}. The elemental compositions of C, H and N of the samples were determined by PerkinElmer CHN analyzer model PE2400II, and O content was calculated by difference. X-ray photoelectron spectroscopy (XPS) (JPS-9030, JEOL Ltd., Japan) was used to investigate the configurations of the nitrogen species on the surface of the prepared samples. Surface nitrogen species such as pyridinic nitrogen (N-6), pyrrolic nitrogen (N-5), quaternary nitrogen (N-Q) and pyridine-N-oxide (N-X) on the carbonaceous adsorbent were measured with XPS N1s signal [22]. Boehm titration [23] was also applied to estimate the amount of positively charged quaternary nitrogen.

The pH of point of zero charge (pH_{pzc}) for adsorbent is a crucial parameter for evaluating the effect of pH on adsorption performance [24]. The determination method followed our previous study [17]. Briefly, the pH of 15 mL of 200 mg/L NO_3^- solution was adjusted within the range of 2.0 to 12.0, and 30 mg of prepared sample was added to the above solution. The pH_{pzc} was identified as the pH at which the equilibrium pH (pH_e) equaled to the initial pH (pH_0).

2.2.4 Batch adsorption experiments

Batch adsorption experiments were performed to evaluate the adsorption capacity of the prepared sample. Sodium nitrate was dissolved in deionized water to prepare the nitrate solution. Prior to starting the experiment, the adsorbent was dried at 110ºC for at least 30 min. Then, 30 mg of the dried sample was added into a 30 mL Erlenmeyer flask containing 15 mL of 200 mg/L nitrate solution. The mixture was stirred at 100 rpm for a minimum of 24 h at room temperature to reach adsorption equilibrium. During the process, the pH of the solution was adjusted using 0.1 mol/L HCl and 0.1 mol/L NaOH. A portable pH meter (D-71, Horiba, Japan) was employed to monitor the solution pH. Once equilibrium was achieved, the nitrate

concentrations (both residual and initial) were analyzed using ion chromatography (ICS-1100, Nippon Dionex KK, Japan). The equilibrium adsorption capacity was calculated using the following equation:

$$Q_e = \frac{(C_0 - C_e)V}{W}, \quad (2\text{-}1)$$

where Q_e means the equilibrium adsorption amount (mmol/g). C_0 and C_e represent the initial and the equilibrium concentration of nitrate (mmol/L), respectively. V signifies the solution volume (L) and W expresses the weight of sample (g).

2.2.4.1 Effect of solution pH and initial nitrate concentration

The experiments were carried out by varying the solution pH and initial nitrate concentrations. The pH of the nitrate solution was adjusted between 2.0-12.0, and the adsorption performance was evaluated at initial nitrate concentrations of 40 mg/L and 200 mg/L. The experiments were conducted using a constant adsorbent dosage of 2 g/L, as described previously.

2.2.4.2 Adsorption isotherms

Adsorption isotherm experiments were carried out by varying the initial nitrate concentration between 10 and 600 mg/L at pH values of 3.0 and 5.0. A constant adsorbent dosage of 2 g/L was used. The experimental data were analyzed and fitted to both Langmuir and Freundlich isotherm models.

The linear form of Langmuir isotherm model is described as follows:

$$\frac{C_e}{Q_e} = \frac{1}{X_m} C_e + \frac{1}{X_m K_e}, \quad (2\text{-}2)$$

where Q_e is the equilibrium adsorption amount of nitrate (mmol/g). C_e is the equilibrium solution concentration (mmol/L) and X_m is the maximum adsorption capacity (mmol/g). K_e represents the Langmuir isotherm constant (L/mmol).

The linear form of Freundlich isotherm model is:

$$lnQ_e = lnK_F + \frac{1}{n} lnC_e, \quad (2\text{-}3)$$

where K_F means Freundlich isotherm constant [(mmol/g) (L/mmol)1/n], and 1/n is the heterogeneity of the surface.

2.2.4.3 Adsorption kinetics

The adsorption kinetics were examined by adding 400 mg of prepared sample into 200 mL of 200 mg/L nitrate solution at solution pH 3.0 and 5.0. The concentration of nitrate solution was measured at time *t* min (*t* = 2.5, 5, 7.5, 10, 12.5, 15, 17.5, 20, 25, 30, 40, 50, 60, 70, 80, 90, 100 and 120). The experimental data were fitted and analyzed by pseudo-first-order and pseudo-second-order models. They are respectively described as follows:

$$\ln(Q_e - Q_t) = lnQ_e - k_1 t\,, \tag{2-4}$$

$$\frac{t}{Q_t} = \frac{1}{k_2 Q_e^2} + \frac{t}{Q_e}\,, \tag{2-5}$$

where Q_e is the adsorption capacity at equilibrium (mmol/g). Q_t is the adsorption amount at time *t* (mmol/g). k_1 and k_2 are the kinetic constant for pseudo-first-order (min^{-1}) and pseudo-second-order model ($g(mg\ min)^{-1}$), respectively.

2.2.5 Fixed-bed column adsorption experiments

For experimental purposes, a laboratory-scale flow adsorption device (**Fig. 2-2**) was designed using a peristaltic pump (MP-3, Tokyo Rikakikai Co., Ltd., Japan) and a glass column (internal diameter of 0.7 cm, outer diameter of 0.9 cm, and length of 16 cm). Firstly, 0.8 g of MeUrGlu-550Z0.5-1.0-2nd was packed into the column, creating a bed with a 100 mm length. The glass wool was placed at both top and bottom of the bed to prevent the adsorbent from washing out and to ensure even distribution of the influent solution. The peristaltic pump was connected to the top of the column to deliver the nitrate solution upward at a controlled and steady flow rate. Prior to introducing the nitrate solution, deionized water was pumped through the column for 2 h to stabilize the flow rate and eliminate air bubbles. Then, 200 mg/L of nitrate solution was introduced into the column at a flow rate of 1.25 mL/min at room temperature. The pH of the nitrate solutions was 3.0 and 5.0. Finally, effluent was collected at predefined time intervals using a graduated cylinder, and nitrate concentrations in both the influent and effluent were analyzed via ion chromatography.

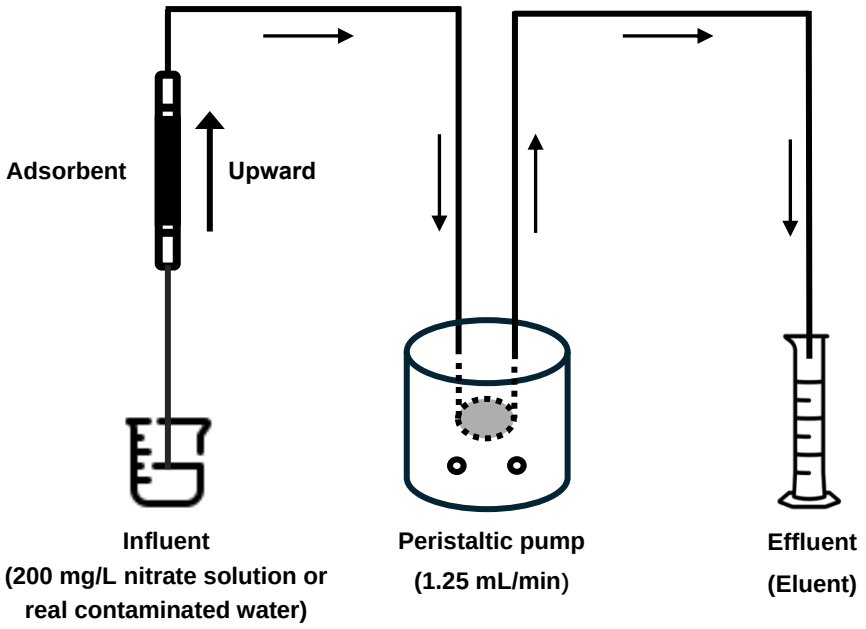

Fig. 2-2. Systemic diagram of up-flow fixed-bed column adsorption set up.

2.2.5.1. Fixed-bed column adsorption characteristics analysis

The adsorption performance of MeUrGlu-550Z0.5-1.0-2nd as packing material in the fixed-bed column adsorption for the removal nitrate can be evaluated by the parameters of the breakthrough curve [25]. The breakthrough curve is usually expressed by plotting C_t/C_0 (the ratio of nitrate concentration in the effluent at time t to the initial nitrate concentration) versus time t. The amount of nitrate adsorption (Q) in the fixed-bed column adsorption is expressed by the following equation [26]:

$$Q = \frac{R}{Wm}\int_0^t (C_0 - C_t)\, dt\,, \tag{2-6}$$

where R is the flow rate (mL/min), W means the molar mass of nitrate (g/mol), m is the weight of adsorbent (g), t represents the flow time (min), C_0 is the nitrate concentration in the influent (mg/L), C_t is the nitrate concentration in the effluent at time t (mg/L).

The total effluent volumes for reaching the breakthrough point and saturation point are expressed by the following equations [27]:

$$V_b = Rt_b\,, \tag{2-7}$$

$$V_s = Rt_s\,, \tag{2-8}$$

where V_b is the total effluent volume up to the breakthrough point (mL), V_s is the total effluent volume up to the saturation point (mL). t_b is breakthrough time when $C_t/C_0 \geq 5\%$. t_s is the saturation time when $C_t/C_0 \geq 95\%$.

Nitrate removal rate R% can be determined by:

$$R\% = \frac{Q_t}{RC_0t} \ , \tag{2-9}$$

where Q_t expresses the adsorption amount of nitrate (mmol/g) at time t.

Commonly used mathematical models to describe adsorption kinetics in fixed-bed column include Thomas model (Eq. 2-10) and Yoon-Nelson model (Eq. 2-11). The parameters obtained by fitting the experimental data with the models allow a better assessment of the performance for the fixed-bed column and help us to scale up for industrial applications. It is clearly demonstrated in the study of Ansari et al. [28] that, since both models have a similar mathematical form [29,30], the relevant kinetic parameters can be calculated more conveniently by a standard logistic equation (Eq. 2-12).

$$\ln\left(\frac{C_0}{C_t} - 1\right) = \frac{K_{Th}Q_m m}{R} - K_{Th}C_0 t \ , \tag{2-10}$$

$$\ln\left(\frac{C_t}{C_0 - C_t}\right) = K_{YN}t - \tau K_{YN} \ , \tag{2-11}$$

$$\frac{C_t}{C_0} = \frac{1}{1+\exp\left(a-bt\right)} \ , \tag{2-12}$$

where K_{Th} is the Thomas rate constant (L/min · mg), Q_m is the model adsorption capacity (mg/g), m is the amount of adsorbent (g), R is the flow rate (mL/min), K_{YN} is the Yoon-Nelson rate constant (min^{-1}), τ is the time when the adsorbate reaches half of the breakthrough (min). a and b are the parameters of the standard logistic equation.

2.2.5.2 Effect of coexisting ions on nitrate removal

The fixed-bed column adsorption performance of nitrate in the presence of coexisting ions, including chloride (Cl^-), sulfate (SO_4^{2-}), and phosphate (PO_4^{3-}), was evaluated. Each coexisting ion was introduced at a concentration of 200 mg/L, making the total ion concentration four times higher than the nitrate concentration. A mass of 0.8 g of adsorbent was packed into the column, resulting in a bed length of 100 mm. The flow rate was set to 1.25 mL/min, and the pH of the solution was maintained at 3.0. The experimental procedure followed the methods described previously. These ions were selected due to their common occurrence in surface and

groundwater [31]. The stock solution was prepared using sodium nitrate ($NaNO_3$), sodium chloride (NaCl), sodium sulfate (Na_2SO_4) and potassium dihydrogen phosphate (KH_2PO_4). Ion concentrations in both influent and effluent solutions were determined using ion chromatography.

2.2.5.3 Regeneration of the column

The regeneration capability of the column is crucial for evaluating its practical application. A column was prepared by packing 1.0 g of MeUrGlu-550Z0.5-1.0-2nd, resulting in a bed length of 130 mm. It was loaded with a 200 mg/L nitrate solution at pH 3.0 until saturation. After the adsorption process, the saturated column was regenerated in siu by introducing 1 mol/L HCl at a flow rate of 1.25 mL/min for 3 h, followed by rinsing with deionized water for 2 h to prepare it for reuse. The adsorption-desorption process was repeated for 5 cycles to evaluate the column's performance.

2.2.5.4 Nitrate removal from real contaminated water

Given the complexity of real contaminated water, it is essential to evaluate the performance of the MeUrGlu-550Z0.5-1.0-2nd packed column for nitrate adsorption in such systems. A sample solution from eutrophic Lake Tega (Chiba Prefecture, Japan) was filtered using a 0.45 μm membrane. The initial nitrate concentration was adjusted from 23.5 mg/L to 100 mg/L (by concentration), with the solution pH set at 5.7. The column was packed as detailed in **Section 2.2.5.2** and the contaminated water was introduced at a flow rate of 1.25 mL/ min at room temperature. Nitrate concentrations in the influent and effluent were measured to obtain the adsorption breakthrough curve for nitrate ions in the real contaminated water system.

2.3 Results and discussion

2.3.1 Characterization of the adsorbents

The physical properties and adsorption capacities of the carbonaceous adsorbents after the 1st, 2nd and 3rd activation processes are summarized in **Table 2-1**. With each successive activation, the hydrogen and oxygen content decreased progressively. This trend can be attributed to the decomposition of acidic oxygen-containing functional groups, such as carboxyl groups, which release CO/CO_2 and H_2O from the carbon surface during the prolonged heating

[32]. Conversely, the nitrogen content consistently increased, exceeding 19% in all products. These findings confirm the successful incorporation of nitrogen on the adsorbent surface.

Apparently, the specific surface area (S_{BET}) of the adsorbents increased with the number of the activation processes, while the average pore size (D_{avg}) was gradually decreased. The S_{BET} of MeUrGlu-550Z0.5-1.0-3rd increased by 91% and the average pore size decreased by 68% compared to MeUrGlu-550Z0.5-1.0-1st. With the increase in the number of activations, the activation time of the raw material was correspondingly extended, allowing further etching of the adsorbent's surface. This process generated more mesopores and micropores, resulting in a significant increase in the specific surface area of the adsorbent after the third activation. The results indicate that the continuous activation process would be favored to the expansion of S_{BET} and the establishment of microporous structure. However, it is notable that the adsorption capacity did not always increase with S_{BET} and V_{total}. For instance, while the S_{BET} of MeUrGlu-550Z0.5-1.0-3rd was nearly 10 times greater than that of MeUrGlu-550Z0.5-1.0-2nd, the latter exhibited the highest nitrate adsorption among the three adsorbents. This suggests that an adsorbent's adsorption capacity is influenced not only by its physical characteristics but also by the chemical composition of its surface structure.

Table 2-1 Elemental composition and textural properties of carbonaceous adsorbents.

Sample	Q_e (mmol/g)	Elemental analysis (wt%)				Textural properties				
		C	H	N	O	S_{BET} (m^2/g)	V_{total} (cm^3/g)	V_{micro} (cm^3/g)	V_{meso} (cm^3/g)	D_{avg} (nm)
MeUrGlu-550Z0.5-1.0-1st	0.61	53.3	2.47	19.9	24.3	11.3	0.02	0.01	0.01	6.80
MeUrGlu-550Z0.5-1.0-2nd	0.79	53.5	2.38	22.4	21.7	16.6	0.01	0.01	0.00	3.60
MeUrGlu-550Z0.5-1.0-3rd	0.69	56.0	2.04	22.3	19.7	130	0.07	0.07	0.00	2.20

XPS N1s spectra were used to analyze the configuration of specific nitrogen-containing groups on the adsorbent surface. As shown in **Fig. 2-2 (a)-(c)**, the peak areas of each nitrogen species within the binding energy range of 394–406 eV were examined. The dotted line represents the original N1s intensity, while the smooth solid line indicates the peak sum. The high-resolution of N1s spectra for the prepared sample were deconvoluted into four peaks, corresponding to pyridinic nitrogen (N-6), pyrrolic nitrogen (N-5), quaternary nitrogen (N-Q) and pyridine-N-oxide (N-X), located at 398.7 ± 0.3 eV, 400.4 ± 0.3 eV, 401.3 ± 0.3 eV and 402-403 eV, respectively [32]. The corresponding peak for each individual nitrogen species configuration has been identified on the graph. Combining the results of elemental analysis and XPS deconvolution, the content of each nitrogen species configuration was quantified. N-6 and N-5, being poor at accommodating protons (H^+), do not contribute to anionic pollutant adsorption [17]. Conversely, N-Q is always positively charged, so it will play an important role in removing nitrate ions. Table 2-2 shows that the samples after the first activation had the highest N-Q content, but their nitrate adsorption capacity was not the greatest. This is attributed to the reduced oxygen content of the carbonaceous adsorbent after the 2nd activation, which favors the reduction of some oxygen-containing functional groups such as carboxyl groups. The 3rd activation resulted in the lowest N-Q content, weakening the nitrate adsorption performance of MeUrGlu-550Z0.5-1.0-3rd. This explains why MeUrGlu-550Z0.5-1.0-2nd, despite a much smaller S_{BET} compared to MeUrGlu-550Z0.5-1.0-3rd, exhibited superior nitrate adsorption. The results of Boehm titration are shown in **Table 2-3**. The trend of the N-Q content measured by Boehm titration was in good agreement with the XPS analysis. Thus, these fundings are fully demonstrate the successful introduction of N-Q onto the carbonaceous adsorbent surface.

Table 2-2 Results of XPS N1s analysis of carbonaceous adsorbents.

Sample	Configuration of nitrogen-containing groups (wt%)			
	N-6	N-5	N-Q	N-X
MeUrGlu-550Z0.5-1.0-1st	0.71	11.5	6.51	1.23
MeUrGlu-550Z0.5-1.0-2nd	6.08	11.0	4.28	1.08
MeUrGlu-550Z0.5-1.0-3rd	12.9	8.04	0.88	0.47

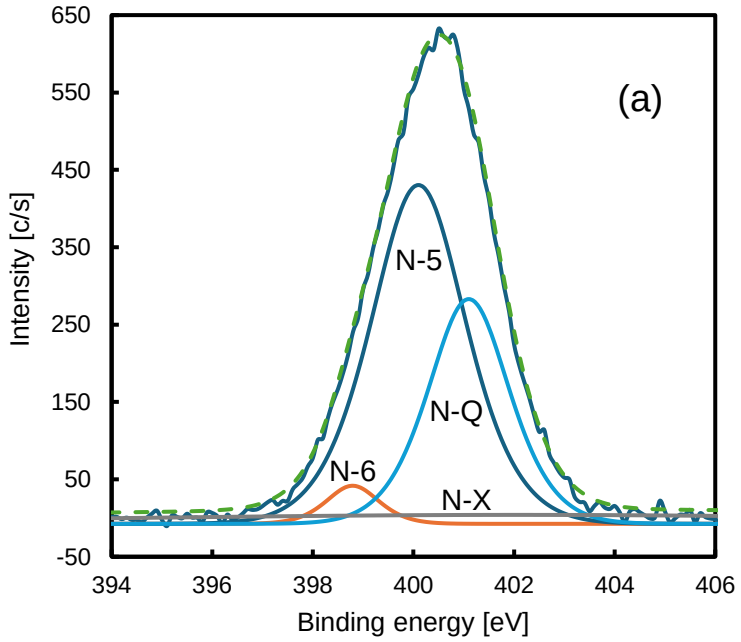

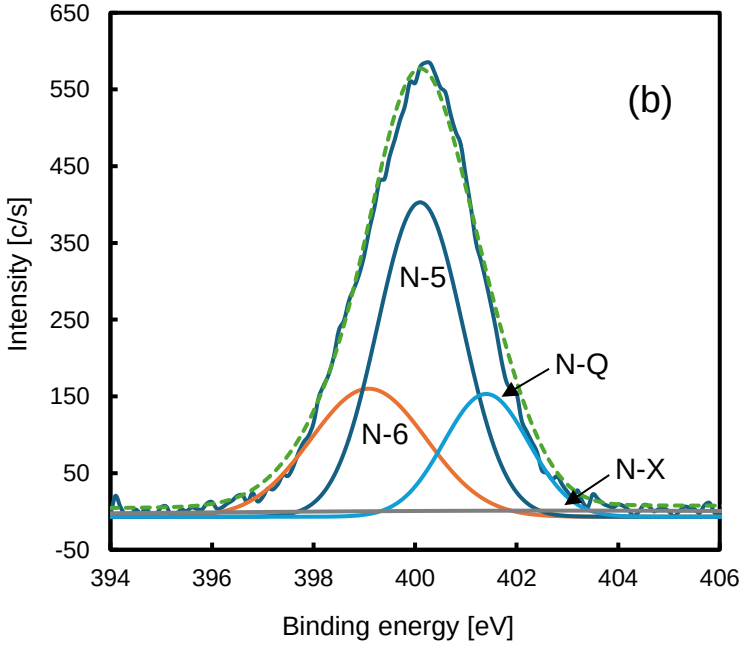

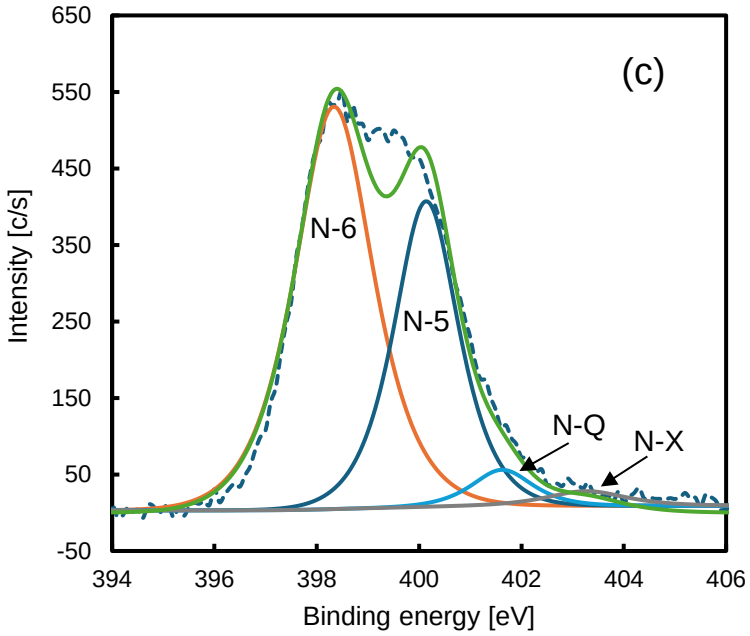

Fig. 2-3. XPS N1s spectra of (a) MeUrGlu-550Z0.5-1.0-1st, (b) MeUrGlu-550Z0.5-1.0-2nd, (c) MeUrGlu-550Z0.5-1.0-3rd.

Table 2-3 Surface functional groups on carbonaceous adsorbents measured by Boehm titration.

Sample	Carboxy and/or N-Q (mmol/g)	Lactonic (mmol/g)	Phnolic (mmol/g)	Basic sites (mmol/g)
MeUrGlu-550Z0.5-1.0-1st	1.07	0.17	3.25	0.05
MeUrGlu-550Z0.5-1.0-2nd	0.60	0.27	3.28	0.05
MeUrGlu-550Z0.5-1.0-3rd	0.53	0.70	3.22	0.05

The results in **Fig. 2-4** showed that the pH_{pzc} of MeUrGlu-550Z0.5-1.0-2nd was around 4.0. This indicates that the adsorbent performs better adsorption performance at the solution pH below 4.0, where the adsorbent surface will be positively charged at this pH range. Additionally, the final solution pH decreased to 4.0 even when the initial pH was 10.0, confirming the retention of carboxy groups on the sample surface. Therefore, it seems more reasonable to utilize this adsorbent under acidic conditions for nitrate adsorption.

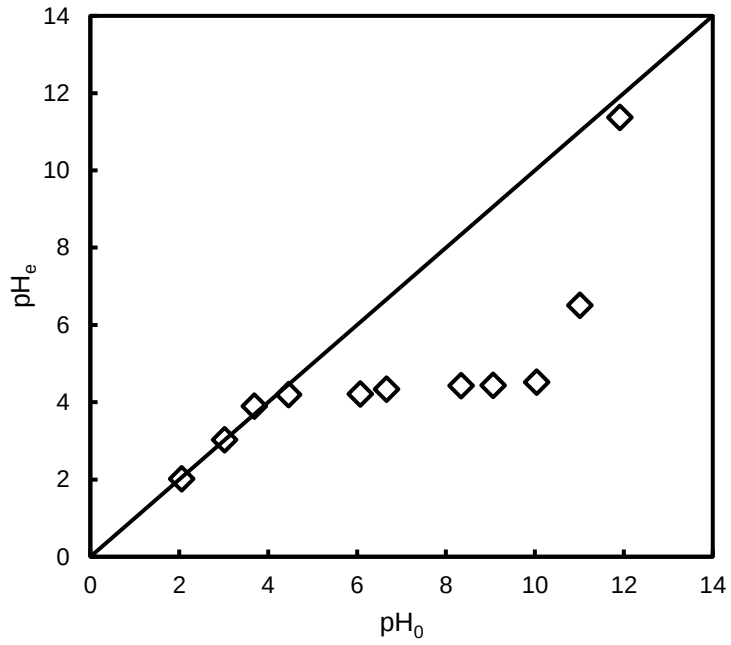

Fig. 2-4. The pH of the point of zero charge (pH_{pzc}) for MeUrGlu-550Z0.5-1.0-2nd.

2.3.2 The effect of activation maintaining time and the number of activation processes

As shown in **Fig. 2-5**, increasing the activation maintaining time from 1.0 h to 1.5 h resulted in a decrease in adsorption capacity. This would be due to the reduction of active functional groups on the surface of the adsorbent after extending the activation time. On the contrary, reducing the time to 0.5 h also resulted in lower performance compared to 1.0 h, suggesting that a 1.0 h activation time facilitated more effective reactions among the four reagents during the 1st activation process. Regardless of the activation time in the 1st process, **Fig. 2-5** reveals that the highest adsorption capacity was consistently achieved after the 2nd activation. This would be explained as the 2nd activation process could realize the removal of some functional groups that were unfavorable for nitrate adsorption. This improvement is attributed to the removal of functional groups unfavorable for nitrate adsorption, such as negatively charged carboxyl groups that repel anions. In summary, the optimal adsorption performance of the prepared adsorbent was obtained after the 2nd activation process, with a 1.0 h activation time in the 1st process. Therefore, MeUrGlu-550Z0.5-1.0-2nd was selected for further adsorption studies.

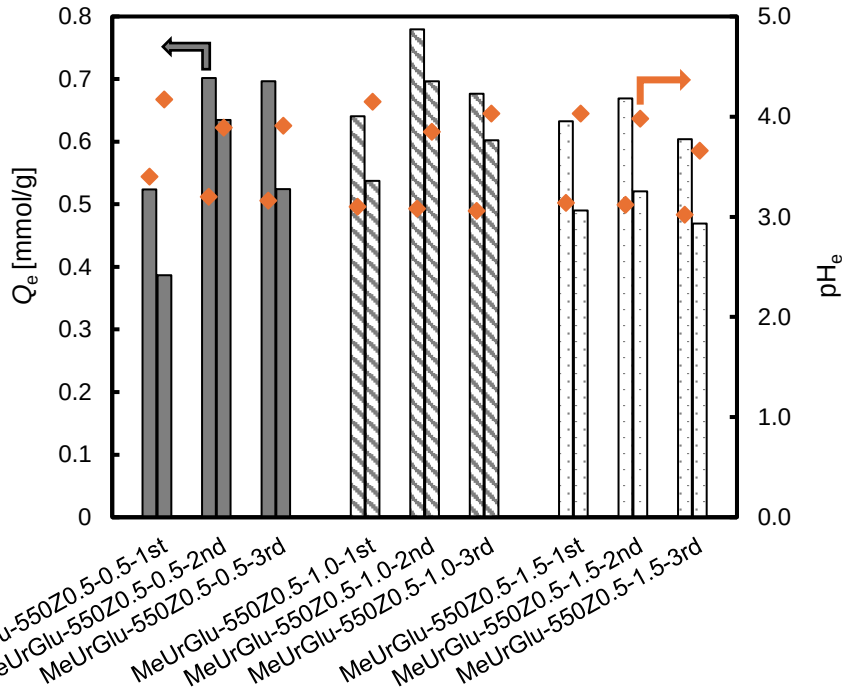

Fig. 2-5. Effect of activation maintaining time and the number of activation processes. (■; 0.5 h, ▩ 1.0 h, □; 1.5 h, ◆; Solution pH)

2.3.3 Batch adsorption

2.3.3.1 Effect of solution pH and initial nitrate concentration

To further investigate nitrate adsorption performance, experiments were conducted by varying the solution pH and initial NO_3^- concentrations. As shown in **Fig. 2-6**, it can be observed that the effect of solution pH on the adsorption capacity of MeUrGlu-550Z0.5-1.0-2nd differed notably between high initial concentrations and low initial concentrations. At a higher concentration of 200 mg/L, the adsorbent achieved maximum adsorption capacity at pH 3.0. This is consistent with the conclusion of the pH_{pzc} analysis that acidic conditions enhance adsorption. Beyond pH 3.0, Q_e decreased sharply with the rise in solution pH. In contrast, in case of low initial concentration of 40 mg/L, instead of the sharply decrease with the ascendant solution pH, Q_e remained relatively stable. This phenomenon can clarify the existence of N-Q, as supported by the results of XPS and Boehm titration in the previous section. Because N-Q is always positively charged, maintains a steady adsorption capacity despite pH changes [20]. However, in the case of 200 mg/L, the sharp decrease in adsorption capacity after the pH greater

than 3.0 can be explained by the role of C-π sites. C-π site is also a key adsorption site in the adsorption process of carbon materials. These sites accommodate protons to form positively charged surfaces that attract nitrate anions [23]. Therefore, as the pH of the solution approaches neutrality, the protonation ability of C-π sites diminishes, leading to a significant drop in Q_e as the solution pH increased. These results indicate that at high nitrate concentrations, both protonated C-π and N-Q sites contribute to nitrate adsorption while at lower concentrations, N-Q primarily governs the process. This highlights that N-Q exhibits a stronger adsorption affinity for nitrate ions compared to C-π sites.

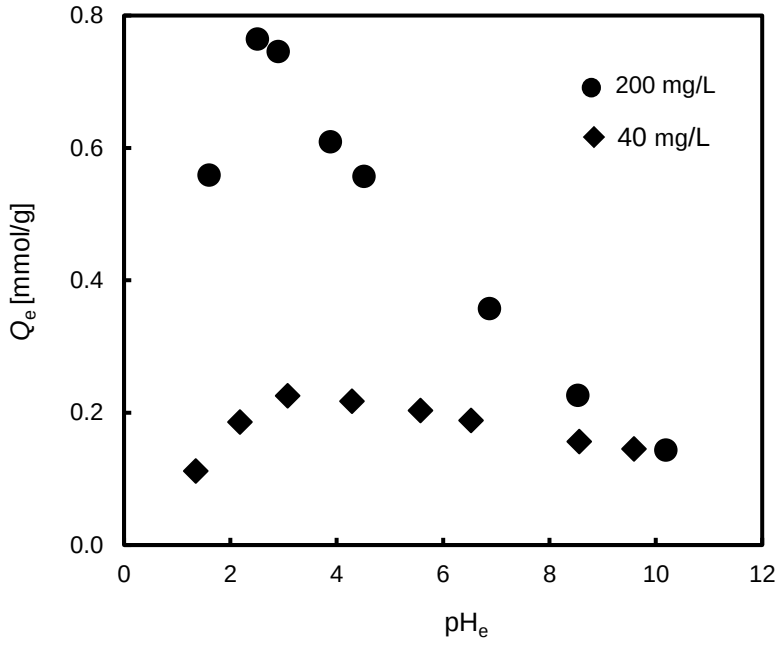

Fig. 2-6. Effect of solution equilibrium pH and initial concentration on nitrate adsorption amount of MeUrGlu-550Z0.5-1.0-2nd.

2.3.3.2 Adsorption isotherms

Adsorption isotherms provide insight into the interactions between adsorbent and adsorbate and allow for the prediction of adsorption behavior without additional experiments. The Langmuir model described that the adsorbate was adsorbed on the uniform surface in a monolayer, also determined the maximum equilibrium adsorption capacity (X_m). Freundlich model is an empirical equation representing multilayer adsorption on heterogeneous surfaces

[33]. **Fig. 2-7** presents adsorption isotherms fitted using the Langmuir and Freundlich models at pH 3.0 and 5.0. The experiments were conducted at two different pH levels to facilitate a more comprehensive understanding of the adsorption mechanisms of the adsorbent under different conditions. The results indicate that at both pH 3.0 or pH 5.0, the Q_e of MeUrGlu-550Z0.5-1.0-2nd exhibited a non-linear increase with rising initial nitrate concentrations. Furthermore, the adsorption capacity of the adsorbent at pH 3.0 was consistently higher than that at pH 5.0. **Table 2-4** summarizes the corresponding parameters of Langmuir and Freundlich model. At both pH levels, the Langmuir model exhibited higher coefficients of determination (R^2) and lower Sum of Squared Errors (*SSE*) and Mean Squared Error (*MSE*) compared to the Freundlich model. Furthermore, regardless of the solution pH, the values of *SSE* (Sum of Squared Errors) and *MSE* (Mean Squared Error) in the Langmuir adsorption isotherm model are smaller than those in the Freundlich model. These findings suggest that the Langmuir model more accurately describes the adsorption behavior, indicating that nitrate ions uniformly cover the surface of MeUrGlu-550Z0.5-1.0-2nd.

The maximum adsorption amount (X_m) was 1.58 mmol/g at pH 3.0, which was larger than 1.03 mmol/g at pH 5.0. However, the K_e at pH 3.0 was smaller than that at pH 5.0. The K_e parameter of the Langmuir isotherm is related to the affinity between the adsorbate and the adsorbent. This can be explained by the assumption, based on the findings of this study, that the K_e of the developed adsorbent was mainly influenced by the N-Q and C-π sites. Among them, in comparison to the C-π site, N-Q exhibited stronger adsorption affinity for nitrate ions (as discussed in **Section 2.3.3.1**). Due to the less contribution of C-π sites in the removal of nitrate ions in the solution of pH 5.0, N-Q served as the primary adsorption site, resulting in a higher K_e. Conversely, in the nitrate solution at pH 3.0, in addition to the role of N-Q, the C-π sites on the adsorbent surface can also attract nitrate ions as they accept protons from the aqueous solution. While the involvement of C-π sites increases X_m , their lower adsorption affinity reduces the overall K_e value of the Langmuir isotherm. Consequently, this explains why the value of K_e at pH 3.0 is lower than that at pH 5.0.

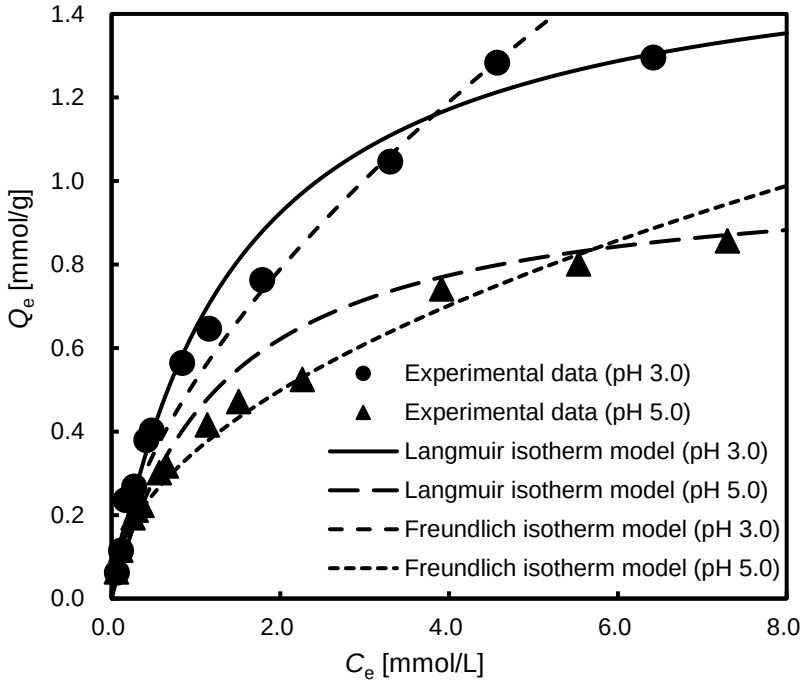

Fig. 2-7. Nitrate adsorption isotherms of MeUrGlu-550Z0.5-1.0-2nd at solution pH 3.0 and 5.0.

2.3.3.3 Adsorption kinetics

The adsorption kinetics study focused on evaluating the nitrate removal rate by the adsorbent. The experiments were conducted using nitrate solutions at pH 3.0 and pH 5.0, with the experimental data analyzed using both the pseudo-first-order and pseudo-second-order models. As illustrated in **Fig. 2-8**, MeUrGlu-550Z0.5-1.0-2nd demonstrated a rapid increase in Q_e within the first 5 min of the adsorption process due to its extremely fast adsorption rate. Equilibrium was subsequently achieved in just 10 min. The adsorption capacity stabilized after reaching equilibrium, indicating that MeUrGlu-550Z0.5-1.0-2nd is an adsorbent with a fast adsorption rate and high efficiency. **Table 2-5** presents the corresponding parameters derived from the pseudo-first-order and pseudo-second-order model. Regardless of the solution pH, the R^2 value for the pseudo-second-order model consistently exceeded that of the pseudo-first-order model. Furthermore, at both pH levels of the solution, the pseudo-second-order model exhibited smaller *SSE* and *MSE* compared to those of the pseudo-first-order model. This indicates that MeUrGlu-550Z0.5-1.0-2nd aligns more closely with the pseudo-second-order model, suggesting a diffusion-controlled adsorption process [34,35]. The high removal efficiency of

nitrate by the adsorbent also could be explained by the presence of positively charged nitrate acceptors on its surface. Although the S_{BET} of MeUrGlu-550Z0.5-1.0-2nd was only 16.6 m^2/g (Q_e = 0.79 mmol/g, C_0 = 200 mg/L), it significantly outperformed the olive solid waste-based activated carbon reported by Heba et al. [15], which had a much higher specific surface area of 1489 m^2/g (Q_e = 0.09 mmol/g, C_0 = 300 mg/L). Despite having an S_{BET} approximately 87 times smaller, MeUrGlu-550Z0.5-1.0-2nd achieved an adsorption capacity 8 times greater than the olive solid waste-based activated carbon. This comparison highlights that incorporating appropriate functional groups is more effective than merely increasing specific surface area in the modification of adsorbent materials.

The parameters calculated from the pseudo-second-order kinetic model revealed that at pH 3.0, Q_e was greater than that at pH 5.0. However, the kinetic constant (k_2) was lower at pH 3.0 compared to pH 5.0. The more favorable adsorption kinetics at pH 5.0 can be attributed to the fact that the adsorption of nitrate ions by the adsorbent is primarily controlled by the N-Q adsorption sites. It showed a greater affinity for nitrate ions, which consequently led to a higher value of the k_2 in the pseudo-second-order kinetic model. While at pH 3.0, both protonated C-π sites and N-Q sites contribute to the adsorption of nitrate ions. The C-π sites, however, are more deeply and evenly distributed in micropores and have a lower affinity for nitrate ions compared to N-Q sites, leading to a lower k_2 at pH 3.0.

Table 2-4 Langmuir and Freundlich isotherm parameters of MeUrGlu-550Z0.5-1.0-2nd for nitrate adsorption at solution pH 3.0 and 5.0.

Solution	Langmuir isotherm model					Freundlich isotherm model				
pH	X_m (mmol/g)	K_e (L/mmol)	R^2	SSE	MSE	$1/n$	K_F ((mmol/g) (L/mmol)$^{1/n}$)	R^2	SSE	MSE
3.0	1.58	0.68	0.993	0.01	0.03	0.59	0.52	0.950	0.24	0.13
5.0	1.03	0.77	0.986	0.02	0.04	0.49	0.35	0.974	0.06	0.06

Table 2-5 Kinetic parameters of MeUrGlu-550Z0.5-1.0-2nd for nitrate adsorption at solution pH 3.0 and 5.0.

Solution	Experime-	Pseudo-first-order model					Pseudo-second-order model				
pH	ntal Q_e (mmol/g)	Q_e (mmol/g)	k_1 (min^{-1})	R^2	SSE $\times 10^{-3}$	MSE$\times$ 10^{-3}	Q_e (mmol/g)	k_2 (g/mmol min)	R^2	SSE $\times 10^{-3}$	MSE$\times$ 10^{-3}
3.0	0.79	0.69	0.70	0.614	43.98	2.43	0.74	7.37	0.999	0.64	0.04
5.0	0.69	0.57	0.20	0.014	303.86	16.88	0.68	15.41	0.991	2.16	1.20

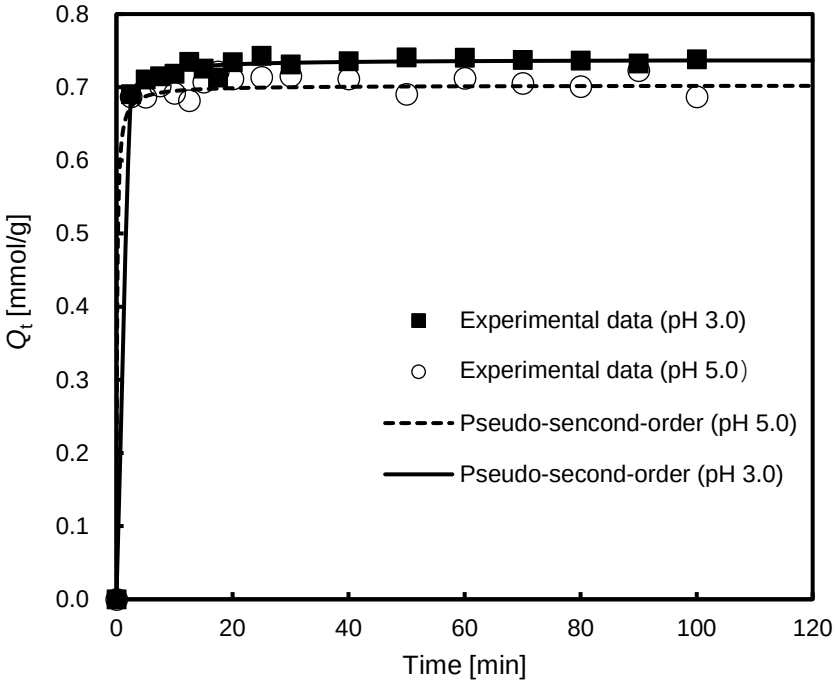

Fig. 2-8. Nitrate adsorption kinetics of MeUrGlu-550Z0.5-1.0-2nd at solution pH 3.0 and 5.0 fitted by pseudo-second-order model. (C_0 = 200 mg/L)

2.3.4 Fixed-bed column adsorption

2.3.4.1 Fixed-bed column adsorption of nitrate

Studies on nitrate adsorption in fixed-bed columns were also conducted using nitrate solutions at pH 3.0 and 5.0. In studying breakthrough curves for fixed-bed column adsorption, we introduced a key parameter known as the breakthrough point. It refers to the point where the ratio of nitrate ion concentration in the effluent to that in the influent (200 mg/L nitrate solution) exceeds 5%, as illustrated in **Fig. 2-9**. The maximum permissible nitrate ion concentration in the effluent before reaching the breakthrough point is 10 mg/L, in accordance with WHO standards. Once the adsorption process exceeds the breakthrough point, the column becomes progressively saturated, causing the nitrate ion concentration to rise continuously. As a result, the nitrate ion removal efficiency gradually declines. In **Fig. 2-9**, the nitrate concentration in the effluent decreased to nearly zero before the breakthrough point, then rose rapidly to the saturation point. This indicates effective adsorption, which is beneficial for achieving purer treated water in industrial applications. **Tables 2-6** and **2-7** illustrate the

influence of solution pH on the column parameters and model parameters, respectively. The breakthrough point remained unchanged with increasing solution pH, resulting in the same values for t_b, V_b and R_b%. At both pH 3.0 and pH 5.0, the purified volume of nitrate solution obtained (V_b) was 200 mL, and the nitrate removal rate (R_b%) was 100%. The rise in solution pH shifted the saturation point of the breakthrough curve earlier, resulting in a shorter t_s. However, the R_s% at pH 5.0 was higher than that of pH 3.0 at this time due to the total volume of nitrate solution passing through the column being reduced due to the advancement of the saturation point. As listed in **Table 2-7**, both K_{Th} and K_{YN} were observed to increase with the solution pH. It was indicated that a higher pH accelerated the nitrate adsorption process in the fixed-bed column, which also decreased τ [36]. This finding was consistent with the pseudo-second-order kinetic model results from batch adsorption, where k_2 at pH 5.0 was higher than that at pH 3.0. From these observations, it can be inferred that the breakthrough curve reached to the saturation point in fixed-bed column adsorption at pH 5.0 was faster than that at pH 3.0, possibly related to its larger kinetic constant k_2 during the batch adsorption process.

Interestingly, the adsorption capacity in the batch adsorption study differed significantly between pH 3.0 (0.79 mmol/g) and pH 5.0 (0.69 mmol/g). However, the adsorption capacity before the breakthrough point in fixed-bed column adsorption was nearly identical at pH 3.0 and pH 5.0. This result suggested that, in practical applications, the fixed-bed column may perform better than predicted by theoretical batch studies. In the batch adsorption experiments, a fixed amount of adsorbent and excess nitrate solution was used to reach adsorption equilibrium. The pH of the solution was strictly controlled at 3.0 and 5.0 by adding 0.1 mol/L of HCl and NaOH. In contrast, in the fixed-bed column adsorption studies, excess adsorbent was packed into the column, so that there were sufficient active adsorption sites to adsorb nitrate ions before reaching the breakthrough point [37]. As a result, the nitrate removal percentage before the breakthrough point was not significantly influenced by the solution pH. After the breakthrough point, the breakthrough curve reached saturation earlier at pH 5.0 due to the higher Thomas and Yoon-Nelson rate constants, leading to a reduced adsorption capacity at pH 5.0.

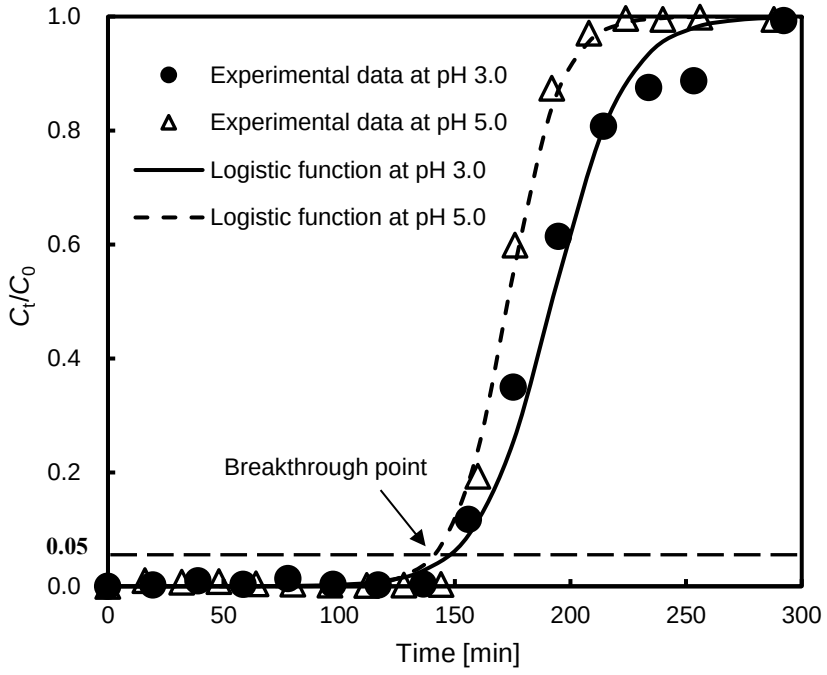

Fig. 2-9. Breakthrough curve of nitrate adsorption on MeUrGlu-550Z0.5-1.0-2nd packed column at solution pH of 3.0 and 5.0. (m = 0.8 g, R = 1.25 mL/min, C_0 = 200 mg/L)

Table 2-6 Parameters of column experiments.

Solution pH	t_b (min)	V_b (mL)	Q_b (mmol/g)	R_b%	t_s (min)	V_s (mL)	Q_s (mmol/g)	R_s%
3.0	160	200	0.95	100	272	350	1.10	74
5.0	160	200	0.90	100	220	275	1.02	90

Table 2-7 Parameters of Thomas model and Yoon-Nelson model.

Solution pH	R^2	Thomas		Yoon-Nelson	
		$K_{Th}\times10^{-3}$ (L/mg.min)	Q_m (mmol/g)	$K_{YN}\times10^{-2}$ (min^{-1})	τ (min)
3.0	0.935	0.31	0.99	6.38	192.20
5.0	0.862	0.43	0.89	8.81	173.11

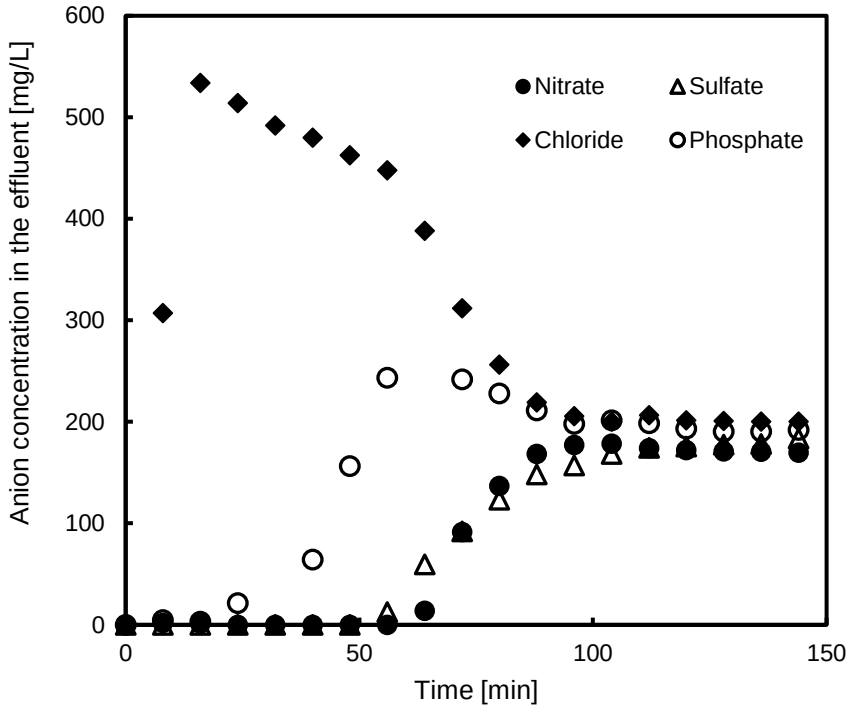

Fig. 2-10. Competitive breakthrough curves for nitrate, chloride, sulfate and phosphate on fixed-bed column adsorption. (m = 0.8 g, R = 1.25 mL/min, C_0 = 200 mg/L)

2.3.4.2 Effect of coexisting ions on nitrate removal

Fig. 2-10 illustrates the competitive breakthrough curve for nitrate, chloride, sulfate, and phosphate ions in fixed-bed column adsorption. The results indicate that sulfate was the least favorable ion for nitrate adsorption, followed by phosphate and chloride. The high concentration of chloride appeared at the beginning of adsorption was due to its release from the carbon surface. Similar findings were reported by Kang et al. [38]. When the adsorbent no longer adsorbed the other three ions, the chloride ion concentration returned to its original level in the solution. Phosphate was detected in the effluent at 24 min, while nitrate and sulfate were not present at that time. Sulfate and nitrate ions appeared almost simultaneously because sulfate ions have higher hydration energy (Sulfate ions carry two negative charges, while nitrate ions carry one negative charge.), which reduced the nitrate adsorption capacity. Although the breakthrough time of nitrate in the presence of coexisting ions was reduced by half compared to that in **Section 2.3.4.1**. However, it is important to note that the adsorbent still maintained some capacity for nitrate removal under these challenging conditions.

2.3.4.3 Regeneration of the column

Table 2-8 presents the parameters of the breakthrough curves for the adsorbent after each adsorption-desorption cycle. The volume of effluent obtained before the breakthrough point (V_b) directly reflects the effectiveness of the column's adsorption performance. The results showed that the V_b of effluent obtained before the breakthrough point in the five adsorption-desorption cycles were 230 mL, 165 mL, 195 mL, 195 mL and 180 mL, respectively. After the 5th regeneration, V_b decreased by 50 mL compared to the initial value. This decrease may be attributed to the incomplete desorption of nitrate ions from deeper or stronger adsorption sites during regeneration. Despite the reduction in V_b, the regenerated column still retained a certain degree of nitrate ion adsorption capacity. **Fig. 2-11** presents the breakthrough curve and adsorption capacity of the column after each adsorption-desorption cycle. Over five adsorption-desorption cycles, there was no significant decrease in adsorption capacity, except for some fluctuation during the second cycle. Repeated experiments confirmed that the amount of adsorption always decreased in the second cycle then rose to a similar value to the initial adsorption amount in the third cycle. This could be explained by the N-Q sites contained on the adsorbent surface is one of the strong adsorption sites. As a result, nitrate was not easily desorbed during the first regeneration. After completing a new adsorption-desorption cycle, the regeneration process weakened some of the exposed N-Q sites, allowing nitrate to detach. Consequently, after the 5th cycle, the adsorption capacity remained nearly the same as the initial value. This result clearly demonstrates the reusability of MeUrGlu-550Z0.5-1.0-2nd in practical applications [39].

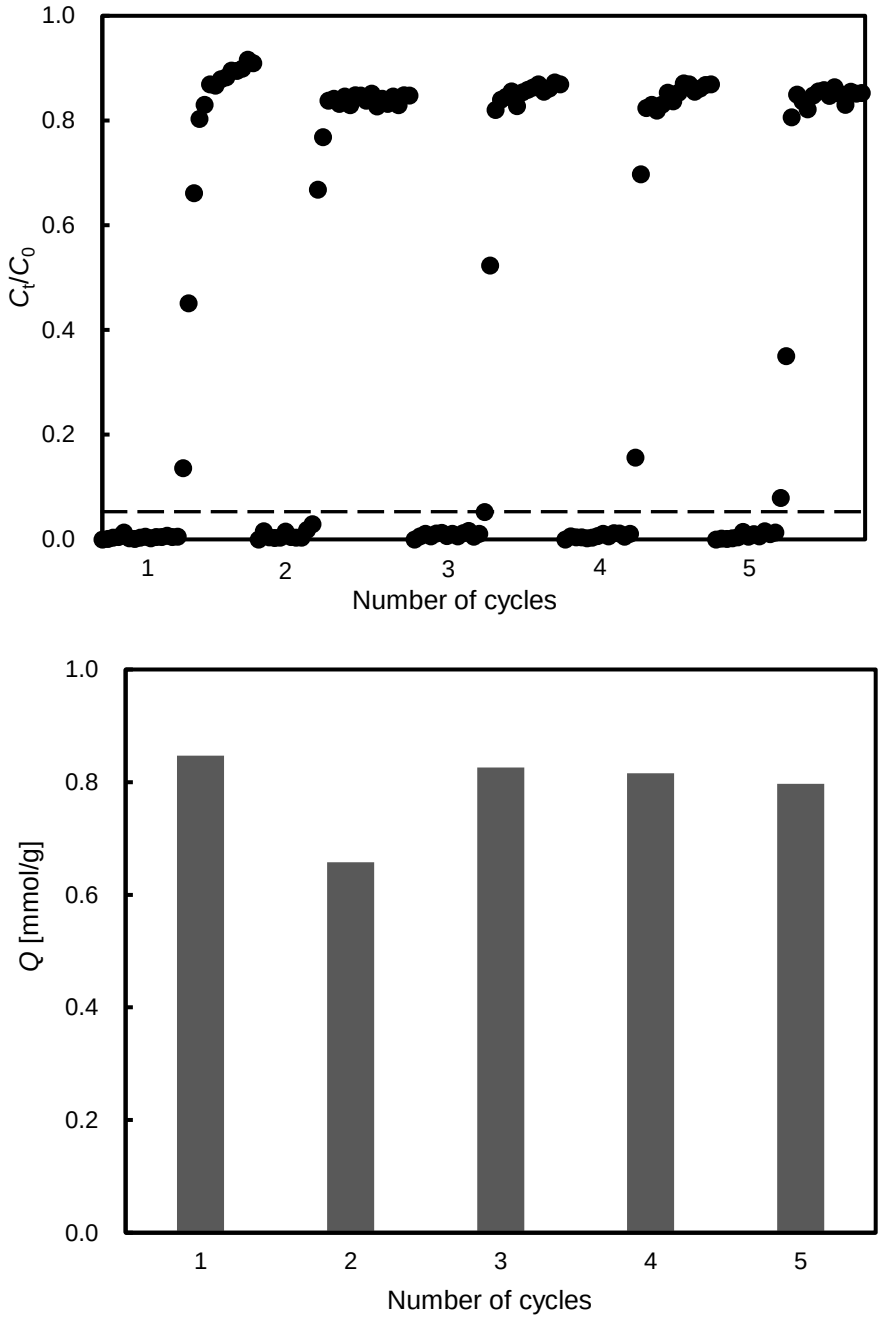

Fig. 2-11. The breakthrough curves and adsorption capacities of the column for five adsorption-desorption cycles. (m = 1.0 g, R = 1.25 mL/min, C_0 = 200 mg/L)

Table 2-8 The parameters after each adsorption-desorption cycle.

Number of cycles	t_b (min)	V_b (mL)	Q_b (mmol/g)	R_b%	t_s (min)	V_s (mL)	Q_s (mmol/g)	R_s%
1	180	230	0.77	100	320	400	0.85	66
2	132	165	0.54	100	324	405	0.68	52
3	156	195	0.67	100	324	405	0.83	63
4	156	195	0.67	100	324	405	0.82	62
5	160	200	0.90	100	324	405	0.80	61

2.3.4.4 Nitrate removal from real contaminated water

The adsorption performance of MeUrGlu-550Z0.5-1.0-2nd as packing material for nitrate removal was further evaluated using real contaminated water. The nitrate concentration in the sample solution was adjusted to 100 mg/L, which is twice the WHO safety limit. As seen in

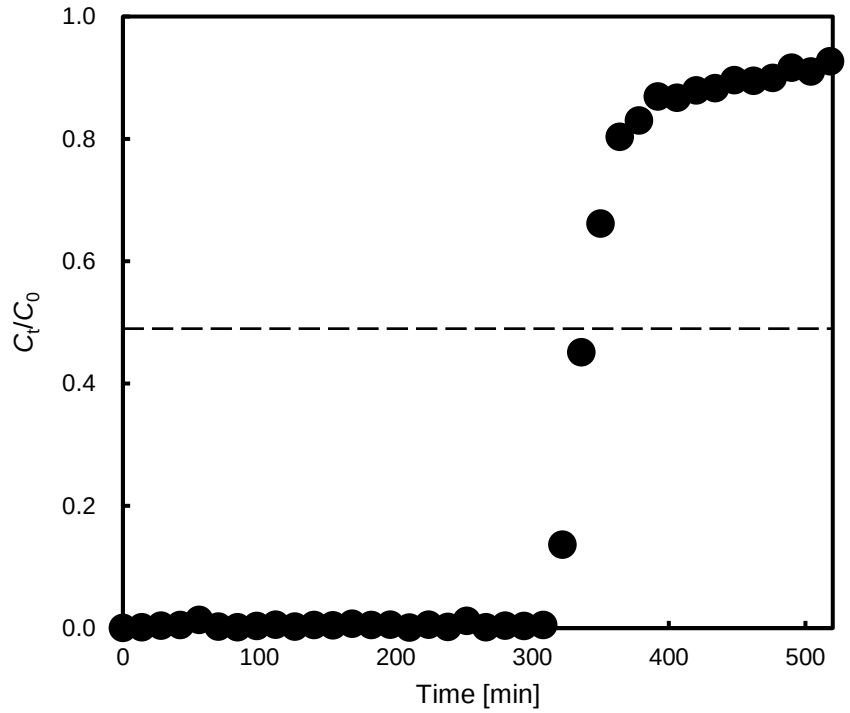

Fig. 2-12. The breakthrough curves for nitrate removal from real contaminated water. (m = 0.8 g, R = 1.25 mL/min, C_0 = 100 mg/L)

Fig. 2-12, the dotted line represents the WHO standard of 50 mg/L for the allowed nitrate concentration. The MeUrGlu-550Z0.5-1.0-2nd packed column could effectively remove nitrate for up to 308 min from the start of adsorption. The nitrate concentration in the sample solution was half that of **Section 2.3.4.1**, resulting in a delayed breakthrough point. The t_b required to reach the WHO standard of 50 mg/L for nitrate concentration was 350 min. While the composition of real contaminated water is more complex, nitrate adsorption may be influenced by certain substances that could hinder the adsorbent's effectiveness. Nevertheless, the findings demonstrated that MeUrGlu-550Z0.5-1.0-2nd is capable of effectively removing nitrate ions from real contaminated water, making it a promising candidate for future practical applications.

2.3.5 Adsorption mechanism

The proposed mechanism that controls the adsorption of nitrate on the carbonaceous adsorbent is illustrated in **Scheme 1**. Initially, the active adsorption sites on the surface of MeUrGlu-550Z0.5-1.0-2nd are occupied by chloride ions (Cl^-). Upon the introduction of nitrate solution, the conjugation effect and polyatomic structure of nitrate ions allow them to exhibit higher affinity in chemical reactions. As a result, nitrate ions can effectively displace chloride ions through competitive adsorption, thereby reoccupying the surface adsorption sites. Based on the adsorption characteristics of nitrate, it can be inferred that the adsorption may be controlled by the active N-Q and C-π sites. On the one hand, nitrate adsorption is influenced by electrostatic attraction between negatively charged nitrate ions and the positively charged N-Q sites on carbonaceous adsorbents. On the other hand, at low pH, C-π sites attract protons, becoming positively charged and capable of adsorbing nitrate ions. However, as the pH of the solution increases, the ability of C-π sites to bind protons diminishes, resulting in a reduced adsorption capacity. Based on the surface functional group content of MeUrGlu-550Z0.5-1.0-2nd obtained through Boehm titration listed in **Table 2-3** of this chapter, a quantitative analysis of nitrate ion adsorption on N-Q active sites can be conducted. Boehm titration determines the types and amounts of surface acidic or basic functional groups by measuring the reaction of the sample surface with different acid or base solutions. According to **Table 2-3**, the maximum content of N-Q on the surface of MeUrGlu-550Z0.5-1.0-2nd is 0.60 mmol/g, with an adsorption capacity of 0.79 mmol/g. Therefore, it can be calculated that each N-Q active site can adsorb up to 1.31 nitrate ions. Additionally, in the adsorption kinetics study, the Q_e value from the

pseudo-second-order kinetic model in **Table 2-5** represented the theoretical saturation adsorption capacity, which was 0.74 mmol/g for the 200 mg/L nitrate solution at pH 3.0. Meanwhile, in the adsorption isotherm studies showed a maximum adsorption capacity (X_m) of 1.58 mmol/g with increasing the initial nitrate concentration. It is reasonable to assume that the higher initial concentration of the nitrate solution provides a greater mass transfer driving force, facilitating the diffusion of adsorbate into the narrow pores of the adsorbent. N-5 and N-6 are poor at accommodating protons (H^+), so they could not contribute to the adsorption of nitrate ions. Oxygen-containing functional groups, such as carboxyl and hydroxyl groups, dissociate in aqueous solutions to form negative charges, which hinder the adsorption of nitrate ions on the surface of MeUrGlu-550Z0.5-1.0-2nd.

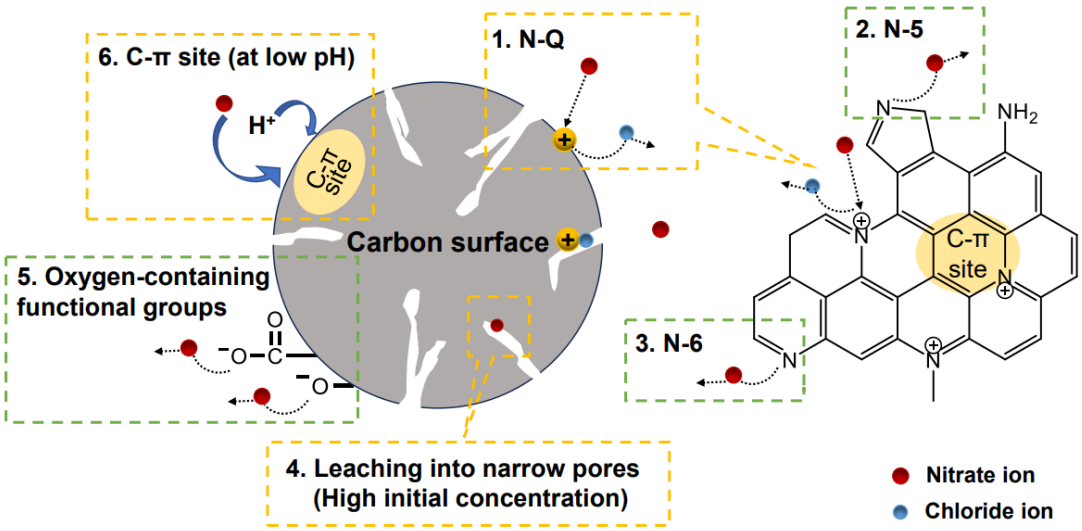

Scheme 1. The proposed mechanism that controls the adsorption of nitrate onto MeUrGlu-550Z0.5-1.0-2nd.

2.3.6 Comparison of adsorption capacity of MeUrGlu-550Z0.5-1.0-2nd with other adsorbents

The prepared adsorbent was compared with other previously reported adsorbents in terms of nitrate removal through batch and fixed-bed column adsorption. **Table 2-9** lists some adsorbents obtained with different precursors and prepared by different modification methods.

MeUrGlu-550Z0.5-1.0-2nd had an excellent adsorption performance. It could be deduced that MeUrGlu-550Z0.5-1.0-2nd will be an efficient adsorbent for the removal of nitrate in the future.

2.4 Conclusion

In conclusion, a novel glucose-based carbonaceous adsorbent with high nitrate adsorption capacity was successfully developed. MeUrGlu-550Z0.5-1.0-2nd demonstrated excellent adsorption performance in terms of both batch adsorption and fixed-bed column adsorption. Batch adsorption experiments revealed that in case of low initial NO_3^- concentration, quaternary nitrogen (N-Q) served as a strong adsorption site that kept the Q_e without significant reduction. As the pH of the solution increased, the ability of C-π sites to accommodate protons weakened, leading to a decline in adsorption capacity. The isotherm and kinetic data were fitted well to the Langmuir model and pseudo-second-order model, respectively, with the Langmuir model estimating a maximum adsorption capacity of 1.58 mmol/g. The results of fixed-bed column adsorption studies further validated the potential of the adsorbent in industrial applications. Effective removal of nitrate could be achieved even in solutions containing high concentrations of coexisting ions. The adsorbent was also regenerable using 1 mol/L HCl and maintained efficiency for at least five adsorption-desorption cycles. These findings highlight MeUrGlu-550Z0.5-1.0-2nd as a promising candidate for practical nitrate removal applications.

Table 2-9 Comparison of different reported adsorbents for the nitrate adsorption.

Adsorbent	Batch adsorption			Fixed-bed column adsorption				Reference
	Concentration range (mg/L)	pH	X_m (mmol/g)	C_0 (mg/L)	Bed heigh (cm)	Adsorbent amount (g)	Q_m (mmol/g)	
Date palm-based biochar	10	6	0.07	-	-	-	-	[14]
Olive solid waste-based activated carbon	100-300	4	0.09	-	-	-	-	[15]
Amine-grafted agricultural waste	20	6.5	0.95	20	20	15	0.30	[31]
Surface-modified red mud	300	5.5	0.69	400	-	15	0.56	[40]
Amino-functionalized MCM-41 silica	30-250	7	0.63	110	-	4	0.38	[41]
Modified activated carbon fiber	200	3	0.74	-	-	-	-	[16]
MeUrGlu-550Z0.5-1.0-2nd	10-600	3	1.58	200	0.8	10	0.99	This study

Reference

[1] A. Dioum, S. Hamoudi, Mono- and quaternary-ammonium functionalized mesoporous silica materials for nitrate adsorptive removal from water and wastewaters, J. Porous Mater. 21 (2014) 685-690.

[2] W. L. Yang, J. C. Wang, X. X. Shi, H. Tang, X. Z. Wang, S. S. Wang, W. M. Zhang, J. L. Lu, Preferential nitrate removal from water using a new recyclable polystyrene adsorbent functionalized with triethylamine groups, Ind. Eng. Chem. Res. 59 (2020) 5194-5201.

[3] S. Singh, A.G. Anil, V. Kumar, D. Kapoor, S. Subramanian, J. Singh, P. C. Ramamurthy, Nitrates in the environment: a critical review of their distribution, sensing techniques, ecological effects and remediation, Chemosphere 287 (2022) 131996.

[4] K. R. Burow, B. T. Nolan, M. G. Rupert, N. M. Dubrovsky, Nitrate in groundwater of the United States, 1991-2003, Environ. Sci. Technol. 44 (2010) 4988-4997.

[5] T. Kalble, A. R. Tricker, K. Mohring, M. R. Berger, H. Geiss, G. Staehler, Ureterosigmoidostomy: long-term results, risk of carcinoma and etiological factors for carcinogenesis, J. Urol. 18 (1990) 1110-1114.

[6] P. J. Weyer, J. R. Cerhan, B. C. Kross, G. R. Hallberg, J. Kantamneni, G. Breuer, M. P. Jones, W. Zheng, C. F. Lynch, Municipal drinking water nitrate level and cancer risk in older women: the Iowa women's health study, Epidemiology 12 (2001) 327-338.

[7] Y. Liu, J. Wang, Reduction of nitrate by zero valent iron (ZVI)-based materials: a review, Sci. Total Environ. 671 (2019) 388-403.

[8] Y. Liu, X. Zhang, J. Wang, A critical review of various adsorbents for selective removal of nitrate from water: structure, performance and mechanism, Chemosphere 291 (2022) 132-728.

[9] S. He, Q. Chen, G. Chen, G. Shi, C. Ruan, M. Feng, Y. Ma, X. Jin, X. Liu, C. Du, C. He, H. Dai, C. Cao, N-doped activated carbon for high-efficiency ofloxacin adsorption, Microporous Mesoporous Mater. 335 (2022) 111-848.

[10] M. Inagaki, M. Toyoda, Y. Soneda, T. Morishita, Nitrogen-doped carbon materials, Carbon 132 (2018) 104-140.

[11] S. Hokkanen, A. Bhatnagar, M. Sillanpaa, A review on modification methods to cellulose-based adsorbents to improve adsorption capacity, Water Res. 91 (2016) 156-173.

[12] A. Nayak, B. Bhushan, V. Gupta, S. Kotnala, Fabrication of microwave-assisted biogenic magnetite-biochar nanocomposite: a green adsorbent from jackfruit peel for removal and recovery of nutrients in a water sample, J. Ind. Eng. Chem. 100 (2021) 134-148.

[13] H. Samaraweera, J. Edwards, C. Reid, S. S. Perera, R. V. K. G. Thirumalai, C. U. Pittman, T. Mlsna, Pyrolyzed Ca-impregnated lignite for aqueous phosphate removal: batch and column studies, J. Environ. Chem. Eng. 9 (2021) 106077.

[14] H. F. Yohanna, S. Banu, Y. Ibrahim, Manganese and nitrate removal from groundwater using date palm biochar: Application for drinking water, Environ. Adv. 8 (2022) 100-237.

[15] N. Heba, Z. Ahed, El-H. Amer, T. Rafeeq, H. Nour, S.H. Hikmat, Aqueous nitrate ion adsorption/desorption by olive solid waste-based carbon activated using $ZnCl_2$, Sustain. Chem. Pharm. 18 (2020) 100335.

[16] J. Yuan, Y. Amano, M. Machida, Surface modified mechanism of activated carbon fibers by thermal chemical vapor deposition and nitrate adsorption characteristics in aqueous solution, Colloids Surf. A Physicochem. Eng. Asp. 580 (2019) 123-710.

[17] Y. Tsuchiya, Y. Yamaya, Y. Amano, M. Machida, Effect of two types of adsorption sites of activated carbon fibers on nitrate ion adsorption, J. Environ. Manag. 289 (2021) 112-484.

[18] S. Wong, N. Ngadi, N. Inuwa, O. Hassan, Recent advances in applications of activated carbon from biowaste for wastewater treatment: A short review, J. Clean. Prod. 175 (2018) 361-375.

[19] M. Machida, Y. Amano, F. Imazeki, Water purification with activated carbons (ACs): a short review-Influence of the textural and surface properties of ACs on the adsorptive removal of pollutants, Tanso (270) (2015) 241-249.

[20] J. Yuan, Y. Amano, M. Machida, Study on the characteristics of nitrogen-doped activated carbon fibers to remove nitrate ions by multi-factor analysis, Int. J. Environ. Sci. Technol. 17 (2020) 2563-2570.

[21] M. Machida, Y. Tsuchiya, J.H. Yuan, Y. Amano, Efficient nitrate adsorbent applicable to wide pH range derived from polyacrylonitrile (PAN) fiber, Results Eng. 11 (2021) 100-276.

[22] M. Machida, P. Yoo, Y. Amano, Adsorption of nitrate from aqueous phase onto nitrogen-doped activated carbon fibers (ACFs), SN Appl. Sci. 1 (2019) 323.

[23] K. Kino, T. Sakamoto, J. Yuan, Y. Amano, M. Machida, Quaternary nitrogen functionalized carbonaceous adsorbents to remove nitrate from aqueous phase, Catal. Today 388-389 (2022) 269-273.

[24] Y. Xue, P. Xiang, H. Wang, Y. Jiang, Y. Long, H. Lian, W. Shi, Mechanistic insights into selective adsorption and separation of multi-component anionic dyes using magnetic zeolite imidazolate framework-67 composites, J. Mol. Liq. 296 (2019) 111-990.

[25] G. Alemu, Z. Feleke, C. Yonas, M. Andualem, T. Melakuu, Simultaneous nitrate and phosphate abatement using calcium silicate hydrate adsorbent: fixed bed column adsorption study, Surf. Interfaces 30 (2022) 101961.

[26] J. Cruz-Olivares, C. Pérez-Alonso, C. Barrera-Díaz, F. Ureña-Nuñez, M. Chaparro-Mercado, B. Bilyeu, Modeling of lead (II) biosorption by residue of allspice in a fixed-bed column, Chem. Eng. J. 228 (2013) 21-27.

[27] S. V. Manjunath, M. Kumar, Simultaneous removal of antibiotic and nutrients via Prosopis juliflora activated carbon column: performance evaluation, the effect of operational parameters and breakthrough modeling, Chemosphere 262 (2021) 127820.

[28] A. Ansari, E. T. Nadres, M. Đoˆ, D. F. Rodrigues, Investigation of the removal and recovery of nitrate by an amine-enriched composite under different fixed-bed column conditions, Process. Saf. Environ. Prot. 150 (2021) 365-372.

[29] Q. Hu, Y. Xie, C. Feng, Z. Zhang, Fractal-like kinetics of adsorption on heterogeneous surfaces in the fixed-bed column, Chem. Eng. J. 358 (2019) 1471-1478.

[30] K. H. Chu, Breakthrough curve analysis by simplistic models of fixed bed adsorption: In defense of the century-old Bohart-Adams model, Chem. Eng. J. 380 (2020) 122513.

[31] M. Kalaruban, P. Loganathan, W. G. Shim, J. Kandasamy, H. H. Ngo, S. Vigneswaran, Enhanced removal of nitrate from water using amine-grafted agricultural wastes, Sci. Total Environ. 565 (2016) 503-510.

[32] J. R. Pels, F. Kapteijn, J. A. Moulijn, Q. Zhu, K. M. Thomas, Evolution of nitrogen functionalities in carbonaceous materials during pyrolysis, Carbon 33 (1995) 1641-1653.

[33] L. C. Santos, A. Silva, P. Lins, J. Duarte, L. Meili, Mg-Fe layered double hydroxide with chloride intercalated: synthesis, characterization and application for efficient nitrate removal, Environ. Sci. Pollut. Res. 27 (2019) 5890-5900.

[34] M. A. Hubbe, S. Azizian, S. Douven, Implications of apparent pseudo-second-order adsorption kinetics onto cellulosic materials: A review, BioRes. 14 (2019) 7582-7626.

[35] K. L. Tan, B. H. Hameed, Insight into the adsorption kinetics models for the removal of contaminants from aqueous solutions, J. Taiwan Inst. Chem. Eng. 74 (2017) 25-48.

[36] A. Nuryadin, T. Imai, Application of amorphous zirconium (hydr)oxide/MgFe layered double hydroxides composite in fixed-bed column for phosphate removal from water, Glob. J. Environ. Sci. Manag. 7 (2021) 485-502.

[37] Y. He, H. Lin, Y. Dong, Q. Liu, L. Wang, Simultaneous removal of phosphate and ammonium using salt-thermal-activated and lanthanum-doped zeolite: fixed-bed column and mechanism study, Desalin. Water Treat. 57 (2016) 27279-27293.

[38] J. K. Kang, S. C. Lee, H. Y. Jang, C. G. Lee, S. B. Kim, Nitrate removal by quaternized mesoporous silica gel in ternary anion solutions: flow-through column experiments and artificial neural network modeling, J. Water Process. Eng. 41 (2021) 102067.

[39] A. Gizaw, F. Zewge, A. Kumar, A. Mekonnen, M. Tesfaye, A comprehensive review on nitrate and phosphate removal and recovery from aqueous solutions by adsorption, J. Water Supply Res. Technol. 70 (2021) 921-947, https://doi.org/ 10.2166/aqua.2021.146.

[40] E. Allahkarami, A. Azadmehr, F. Noroozi, S. Farrokhi, M. Sillanpaa,Nitrate adsorption onto surface-modified red mud in batch and fixed-bed column systems: equilibrium, kinetic, and thermodynamic studies, Environ. Sci. Pollut. Res. 29 (2022) 48438-48452.

[41] M. Ebrahimi-Gatkash, H. Younesi, A. Shahbazi, A. Heidari, Amino-functionalized mesoporous MCM-41 silica as an efficient adsorbent for water treatment: batch and fixed-bed column adsorption of the nitrate anion, Appl. Water Sci. 7 (2017) 1887-1901.

Chapter 3 Preparation of nitrogen-doped glucose-derived activated carbon and its application for the efficient removal of phosphate ions from aqueous solution

3.1 Introduction

Phosphorus is an essential nutrient for living organisms and plays a key role in modern agriculture. However, the excessive use of fertilizers has led to an accumulation of phosphate ions in rivers and lakes. According to the United States Environmental Protection Agency (US-EPA), phosphate concentrations in streams entering lakes or reservoirs should not exceed 0.05 mg/L [1]. Elevated phosphate levels in natural water bodies can trigger eutrophication, causing rapid algal growth, reducing oxygen availability for aquatic life, and resulting in the death of various species due to oxygen depletion [2]. Moreover, excessive phosphate ions in drinking water pose a health risk due to their toxic effects. Phosphate deposition in human tissues can cause cardiovascular calcification, a potentially life-threatening condition [3]. Moreover, phosphate mainly comes from phosphate rock, a finite and non-renewable resource. Therefore, developing effective methods to remove and recover phosphate ions is essential.

Generally, compared to methods like electrodialysis, biological denitrification, and reverse osmosis, etc., adsorption [4,5] is not only an effective method for removing phosphate, but also has the advantages such as simple operation and cost-saving. Moreover, adsorbents are easy to regenerate, and the adsorbates can be easily recovered, making adsorption particularly suitable for treating phosphate pollution. During adsorption, the functional groups on the activated carbon surface govern various interfacial reactions, and the number of active functional groups influences the adsorption capacity for the target pollutants [6]. Therefore, effective functional groups can be introduced to the surface of activated carbon through suitable surface modification methods. To remove positively charged cationic pollutants, it can be achieved by introducing carboxy and sulfonic groups onto the carbon surface to create a negatively charged surface. For the adsorption of anionic pollutants, attractive sites such as quaternary nitrogen (N-Q) can be created by introducing nitrogen heteroatoms. HP555 is a well-established commercial anion exchange resin known for its excellent performance in removing anions like phosphate. Its excellent adsorption capacity is due to its functionalized with only quaternary

amine groups ($-N^+(CH_3)_3$). Based on the above findings, it is anticipated that activated carbon adsorbents rich in N-Q could also exhibit improved adsorption performance. Introducing nitrogen could facilitate the formation of N-Q. Generally, the types of nitrogen typically introduced onto the carbon surface include pyridinic nitrogen (N-6), pyrrolic nitrogen and pyridone-N (N-5), quaternary nitrogen (N-Q), and pyridine-N-oxide (N-X) [7]. N-6 and N-5 are inefficient at accommodating protons (H^+), so they do not contribute to the adsorption of anionic pollutant [8]. However, N-Q remains positively charged across a wide pH range [9], making it an effective exchange site for anionic pollutants like phosphate ions. Therefore, exploring effective methods for introducing N-Q is essential. It is well documented that some surface nitrogen can be gradually converted into N-Q at temperatures of 500°C or higher [10]. Sakamoto et al. successfully enhanced the N-Q content of activated carbon fiber (ACF) from 0.47% to 1.58% using thermal chemical vapor deposition (CVD) method at 950°C [11]. The modified ACF exhibited over five times higher phosphate ion adsorption capacity, increasing from 0.05 mmol/g to 0.27 mmol/g, compared to the unmodified ACF. Sun et al. reported a quaternary nitrogen-grafted granular activated carbon for removing trifluoroacetate (CF_3COO^-), which was prepared through a four-step modification process which took at least 7 days [12]. The adsorption capacity of the modified activated carbon for CF_3COO^- significantly increased from 11.1 mg/g to 32.9 mg/g, marking a substantial improvement. However, these methods have the shortcomings of complexity, time-consuming, and required high temperature around 1000℃, which limits their practical applications. Therefore, it is essential to develope simpler and milder methods for preparing efficient N-Q-containing adsorbents to remove phosphate ions.

In this study, taking the advantages of N-Q, new preparation conditions were explored to introduce N-Q adsorption sites onto the activated carbon derived from glucose for the removal of phosphate ions in aqueous solution. The carbonaceous adsorbent developed in this study demonstrated excellent performance in removing phosphate ions, with its adsorption capacity surpassing that of the commercially available anion exchange resin HP555 under low solution pH and initial concentration conditions. The impact of temperature gradients on the formation of N-Q adsorption sites on the carbon surface was thoroughly discussed. A series of experimental results clearly demonstrate that N-Q is crucial for phosphate adsorption on the

activated carbon surface. Additionally, since the adsorption of ionic pollutants like phosphate ions is strongly influenced by solution pH, the adsorption performance of the prepared activated carbon was evaluated in phosphate solutions at different pH levels. The adsorption isotherm was studied to estimate the maximum adsorption capacity and adsorption affinity of the prepared adsorbent. Additionally, the adsorbent's regeneration ability and phosphate ion recovery were assessed through continuous flow adsorption experiments.

3.2 Materials and methods

3.2.1 Preparation of glucose-derived activated carbon

In this chapter, the preparation method of activated carbon is generally similar to that described in chapter 2. In chapter 2, we determined the optimal activation maintaining time (1st time) and the number of activation process of the adsorbent. Based on the conclusion, this chapter further investigates the effects of different activation temperatures on the performance of the adsorbent. The preparation procedures of the adsorbent are shown in **Fig. 3-1**. In the process of preparing activated carbon, using zinc chloride as the activator can effectively promote the carbonization process and improve the structure and properties of activated carbon. In this study, a mass of 10 g of melamine, 10 g of urea, 20 g of glucose, and 20 g of zinc chloride (equivalent to 0.5 times of the total mass of the three reagents) were mixed and pre-treated in an oven at 110℃ for 12 h to obtain the sample MeUrGlu-110Z0.5. Then, 10 g of MeUrGlu-110Z0.5 was taken into a horizontal tubular furnace for the heat treatment of raising temperature from room temperature to Y℃ (Y = 500, 550, 600, 650, 750) within 45 min at the N_2 flow rate of 20 mL/min and maintained for 60 min. After cooling down, the obtained sample was designated as MeUrGlu-YZ0.5-1st. Subsequently, the obtained MeUrGlu-YZ0.5-1st was thoroughly ground in a mortar to make it more uniform and prepared for the second activation process. The sample was heated in a tubular furnace to Y℃ within 45 min and kept at Y℃ for 30 min for the second activation process. The resulting sample was designated as MeUrGlu-YZ0.5-2nd. Similarly, MeUrGlu-YZ0.5-2nd was further activated for the third activation process by heating it in a tubular furnace from room temperature to Y℃ in 45 min and maintained for 30 min to obtain the sample which was designated as MeUrGlu-YZ0.5-3rd. The samples obtained after each activation were thoroughly washed with 1 mol/L HCl for three

times to remove the residual zinc in the samples. Then, boiled pure water was added to wash off the HCl until the pH of the filtration was neutral. Finally, the washed samples were dried in an oven at 110℃ overnight and prepared for the adsorption experiments.

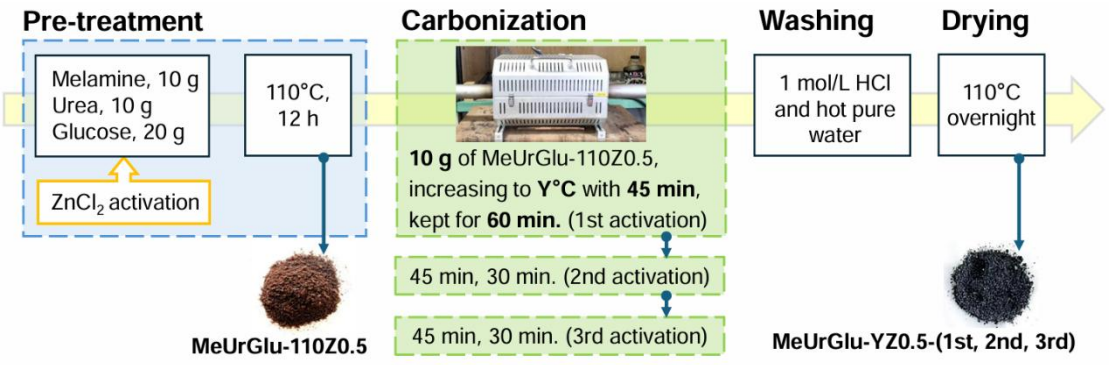

Fig. 3-1. Preparation procedures of the adsorbent.

3.2.2 Characterization of glucose-derived activated carbon

The textual and surface properties of the prepared activated carbon were further examined. The specific surface area and pore distribution of the activated carbon were obtained by N_2 adsorption-desorption isotherms at -196°C in liquid nitrogen using BELSORP-mini II surface analyzer (MicrotracBEL Corporation, Japan). The specific surface area S_{BET} (m^2/g), average pore diameter D_{avg} (nm) and pore volume V_{total} (cm^3/g) were calculated by Brunauer-Emmer-Teller (BET) method. The micropore volume V_{micro} was obtained by α_s plots. The mesopore volume V_{meso} was calculated from the difference between V_{total} and V_{micro}. The elemental compositions of carbon, hydrogen and nitrogen of the samples were determined by PE2400II CHN analyzer (PerkinElmer, Inc., US-MA), and the content of oxygen was calculated as the difference between 100% and the sum of C, H and N carbon. The configurations of the nitrogen species on the surface of the prepared samples were investigated by X-ray photoelectron spectroscopy (XPS, JPS-9030, JEOL Ltd., Japan). C1s and O1s XPS spectra were also obtained through XPS analysis.

3.2.3 Phosphate ions adsorption and determination

The adsorption of phosphate ions on the surface of activated carbon was mainly studied in batch systems, and a slightly extended continuous flow adsorption experiment was carried out

to investigate the reusability of the adsorbent. Before use, the sample was dried in an oven at 110°C for 2 h. Phosphate solution was obtained by dissolving potassium dihydrogen phosphate in pure water.

In batch adsorption experiments, 30 mg of dried sample was added into 15 mL phosphate solution with an initial concentration of 3.0 mmol/L and initial solution pH of 4.5 at room temperature, and then stirred for at least 24 h to establish adsorption equilibrium. In this process, an appropriate amount of 0.1 mol/L hydrochloric acid was added to adjust the pH of the solution to maintain it at 4.5 ± 0.2. Subsequently, the solution was filtered and diluted. The concentrations of phosphate ions before and after adsorption can be measured by molybdenum blue absorption spectrophotometry using a UV-visible spectrophotometer (UV-2550, Shimadzu Corporation, Japan) at the wavelength of 710 nm [13,14]. The equilibrium adsorption amount (Q_e, mmol/g) of phosphate ions was calculated using the following formula:

$$Q_e = \frac{(C_0 - C_e)V}{W} \quad , \tag{3-1}$$

where Q_e means the equilibrium adsorption amount (mmol/g). C_0 and C_e represent the initial and the equilibrium concentration of phosphate (mmol/L), respectively. V signifies the solution volume (L) and W expresses the weight of sample (g).

In continuous flow adsorption experiments, a phosphate solution with a concentration of 3.0 mmol/L and a pH of 4.5 was introduced into a glass column (inner diameter of 0.7 cm, length of 16 cm) at a flow rate of 1.25 mL/min, and 1.0 g of the optimal sample was packed into the column. The effluent at the outlet of the device was collected at pre-set time intervals. The time when the ratio of the phosphate ions concentration in the effluent to that in the influent exceeded 5% was defined as the breakthrough time (t_b), and the corresponding effluent volume (V_b) and adsorption amount (Q_b) at the breakthrough point can be obtained. In addition, the moment when the ratio of the concentration of phosphate ions in the effluent to that in the influent exceeded 95% was defined as the saturation time (t_s), and the corresponding effluent volume (V_s) and adsorption amount (Q_s) at the saturation point can be obtained. The amount of phosphate adsorption (Q) in the continuous flow adsorption is expressed by the following equation [15]:

$$Q = \frac{R}{Wm} \int_0^t (C_0 - C_t)\, dt \quad , \tag{3-2}$$

where R is the flow rate (mL/min), W means the molar mass of phosphate (g/mol), m is the weight of adsorbent (g), t represents the flow time (min), C_0 is the phosphate concentration in the influent (mg/L), and C_t is the phosphate concentration in the effluent at time t (mg/L).

The total effluent volumes for reaching the breakthrough point and saturation point are expressed by the following equations [16]:

$$V_b = Rt_b \quad , \tag{3-3}$$

$$V_s = Rt_s \quad , \tag{3-4}$$

where V_b is the total effluent volume up to the breakthrough point (mL), V_s is the total effluent volume up to the saturation point (mL). t_b is breakthrough time when $C_t/C_0 \geq 5\%$, and t_s is the saturation time when $C_t/C_0 \geq 95\%$.

Phosphate removal rate $R\%$ can be determined by:

$$R\% = Q_t R C_0 t \quad , \tag{3-5}$$

where Q_t expresses the adsorption amount of phosphate (mmol/g) at time t.

3.2.4 Effect of solution pH

In the experiment to investigate the effect of different solution pH on phosphate ions adsorption, an initial concentration of 3.0 mmol/L was selected, and the pH range of the solution was adjusted from 2.0 to 12.0. The other adsorption conditions in batch system were performed as described in **Section 3.2.3**. During the adsorption process, 0.1 mol/L HCl and NaOH were used to maintain the initial pH of the phosphate solution for each gradient. Depending on the solution pH and ionic strength, phosphorus presents in aqueous solution as one of the orthophosphate anions (PO_4^{3-}, HPO_4^{2-} or H_2PO^{4-}) [17]. This distinction will be made in the latter section. Furthermore, for comparison purpose, the effect of solution pH on the adsorption of phosphate ions by the commercial anion exchange resin HP555 was also studied.

3.2.5 Adsorption isotherms

In the study of the adsorption isotherms, the initial phosphate ions concentration was in the range of 0.1-10 mmol/L with a constant solution pH at 4.5. The other adsorption conditions in batch system were also conducted according to the description in **Section 3.2.3**. The equilibrium concentration (C_e) and equilibrium adsorption amount (Q_e) was determined after the adsorption was completed. The resultant equilibrium data were fitted by both Langmuir and

Freundlich isotherms to evaluate the adsorption parameters. In this section, the commercial HP555 was also used as a reference material.

The linear Langmuir isotherm model is described by the following equation:

$$\frac{C_e}{Q_e} = \frac{1}{X_m} C_e + \frac{1}{X_m K_e} \quad , \tag{3-6}$$

where Q_e is the equilibrium adsorption amount of phosphate ion (mmol/g). C_e is the equilibrium solution concentration (mmol/L) and X_m is the maximum adsorption capacity (mmol/g). K_e represents the Langmuir isotherm constant representing adsorption affinity (L/mmol).

The linear form of Freundlich isotherm model is:

$$lnQ_e = lnK_F + \frac{1}{n} lnC_e \quad , \tag{3-7}$$

where K_F means Freundlich isotherm constant [(mmol/g) (L/mmol)$^{1/n}$], and *1/n* is the heterogeneity of the surface.

3.2.6 The regeneration and reusability of adsorbent

The regeneration performance of the prepared adsorbent was evaluated using 7 desorption reagents in batch adsorption experiments, and the optimal reagent was selected for continuous flow adsorption to assess reusability in practical applications. A phosphate solution of 3.0 mmol/L at pH 4.5 was prepared for the experiment. A mass of 200 mg sample was added into 100 mL of the phosphate solution and stirred at 100 rpm for at least 24 h at room temperature to ensure full phosphate loading. During this time, 0.1 mol/L HCl was used to maintain the initial pH of the phosphate solution. Once adsorption equilibrium was reached, the sample was filtered, and then filter paper was used to remove any remaining solution from the sample. Subsequently, the sample was subjected to desorbed in 200 mL of 0.1 mol/L and 1 mol/L hydrochloric acid, sodium hydroxide, sodium chloride solutions, and 200 mL of pure water with stirring at 100 rpm for 24 h at room temperature. After the desorption process was completed, the desorbed sample was filtered and then washed with 500 mL of pure water multiple times. The washed sample was dried with N_2 gas at atmospheric pressure and then further dried to a constant weight under vacuum. The dried sample was reused for phosphate ion adsorption in the batch system, following the procedure outlined in **Section 3.2.3**. The optimal regenerant was selected based on the difference in phosphate adsorption by the sample before and after desorption in batch adsorption experiments. The optimal regenerant was then

applied in the continuous flow adsorption experiment, which was conducted as described in **Section 3.2.3**. After the first flow adsorption process, the optimal regenerant was introduced into the column at a rate of 1.0 mL/min for 3 h for the purpose of column regeneration. Pure water was then passed through the column at the same rate for 5 h to remove any residual regenerant and prepare the column for the next adsorption cycle. The optimal regenerant was used for 3 cycles of adsorption-desorption process.

3.3 Results and Discussion

3.3.1 Characterization of activated carbon

The surface properties and elemental composition of activated carbon are closely related to its adsorption performance. Therefore, the physicochemical properties of the adsorbents under different preparation conditions were thoroughly examined to understand how the surface properties of activated carbon change under varying conditions. **Table 3-1** shows the surface characteristics and elemental composition of the samples prepared under varying temperature gradients and activation cycles, while **Fig. 3-2** illustrates the adsorption capacity of the samples for phosphate ions in batch systems. The effect of activation temperature on the adsorption performance of activated carbon showed that as the temperature increased, the S_{BET}, V_{total} and V_{micro} of the adsorbents showed an upward trend with the increase of temperature. This suggests that higher activation temperatures enhance the dehydrating ability of zinc chloride, leading to the formation of more developed pore structures and larger specific surface areas [18]. When the activation temperature rose from 500℃ to 750℃, the S_{BET} of increased by 28.1 times, and the V_{total} and V_{micro} grew by 10 times and 13 times, respectively. The decrease in D_{avg} could be attributed to the expansion of the microporous structure on the surface of the activated carbon. When investigating the effect of activation cycles on the performance of the adsorbent, it was observed that at a constant activation temperature of 600℃, the S_{BET}, V_{total}, and V_{micro} of the adsorbents were proportional to the activation cycles. The S_{BET} of MeUrGlu-600Z0.5-3rd was 35.6 and 1.2 times higher than that of MeUrGlu-600Z0.5-1st and MeUrGlu-600Z0.5-2nd, respectively. Therefore, increasing the activation temperature and activation cycles during the preparation of glucose-derived adsorbents enhances the expansion of their specific surface area and the development of pore structures. Typically, a more developed porous structure in an

adsorbent is conducive to increasing its adsorption capacity [19]. However, as shown in **Fig. 3-2**, the adsorption capacity (Q_e) of each adsorbent did not strictly follow this trend. The adsorption capacity of the adsorbents from the first, second, and third activation cycles initially increased with temperature but decreased when the activation temperature surpassed 600°C. Specifically, the adsorption capacity of MeUrGlu-600Z0.5-2nd was 50% higher than that of MeUrGlu-500Z0.5-2nd, and 100% higher than that of MeUrGlu-750Z0.5-2nd after two activation cycles. From **Fig. 3-2**, it can also be observed that the adsorption capacity of the products consistently peaked during the second activation cycle, regardless of activation temperature. For instance, MeUrGlu-600Z0.5-2nd always exhibited the highest adsorption capacity, which was 14% and 5% greater than MeUrGlu-600Z0.5-1st and MeUrGlu-600Z0.5-3rd, respectively. In conclusion, MeUrGlu-600Z0.5-2nd demonstrates the best adsorption performance, despite its specific surface area not being the largest. This indicates that the adsorption mechanism cannot be fully explained solely by examining the textural properties of the adsorbent.

The elemental compositions of each sample, shown in **Table 3-1** , reveal that MeUrGlu-600Z0.5-2nd consistently exhibited the highest nitrogen content and the lowest oxygen content, regardless of activation temperature or cycle number. Notably, this sample also achieved the highest phosphate adsorption capacity. The elevated nitrogen content indicates that these preparation conditions are optimal for effectively incorporating nitrogen into the carbon framework. It can be inferred that certain nitrogen-containing functional groups primarily influence the adsorbent's capacity for phosphate ion adsorption, while some oxygen-containing functional groups hinder the process. The reduction in oxygen and hydrogen contents at temperatures below 600℃ is likely due to the decomposition of hydroxyl (-OH) and carboxyl (-COOH) groups on the carbon surface [20]. In particular, the decline in acidic oxygen-containing functional groups, such as carboxyl groups, is beneficial for the adsorption of anions on the carbon surface. Studies have shown that carboxyl groups on activated carbon decompose within the temperature range of 100-700℃ [21]. Carboxyl groups will hinder the accessibility and affinity of activated carbon by forming water clusters through hydrogen bonding, which generates a repulsive force against anions. As the temperature increased, the carboxyl group

Table 3-1. Textural properties and elemental analysis of prepared adsorbents.

Sample	Textural properties					Elemental analysis			
	S_{BET} [m^2/g]	V_{total} [cm^3/g]	V_{micro} [cm^3/g]	V_{meso} [cm^3/g]	D_{avg} [nm]	C [wt%]	H [wt%]	N [wt%]	O* [wt%]
MeUrGlu-500Z0.5-2nd	21.6	0.03	0.02	0.01	4.49	59.0	2.44	15.9	23.1
MeUrGlu-550Z0.5-2nd	314	0.17	0.15	0.02	2.10	52.7	2.23	21.3	23.7
MeUrGlu-600Z0.5-1st	13.9	0.02	0.01	0.01	4.61	54.2	1.96	21.5	22.3
MeUrGlu-600Z0.5-2nd	423	0.19	0.18	0.01	1.89	53.6	1.74	25.4	19.3
MeUrGlu-600Z0.5-3rd	495	0.21	0.19	0.02	1.87	52.9	1.52	22.6	23.0
MeUrGlu-650Z0.5-2nd	591	0.28	0.25	0.03	1.86	51.6	1.27	13.5	33.6
MeUrGlu-750Z0.5-2nd	606	0.30	0.26	0.04	1.72	52.4	0.89	12.1	34.6

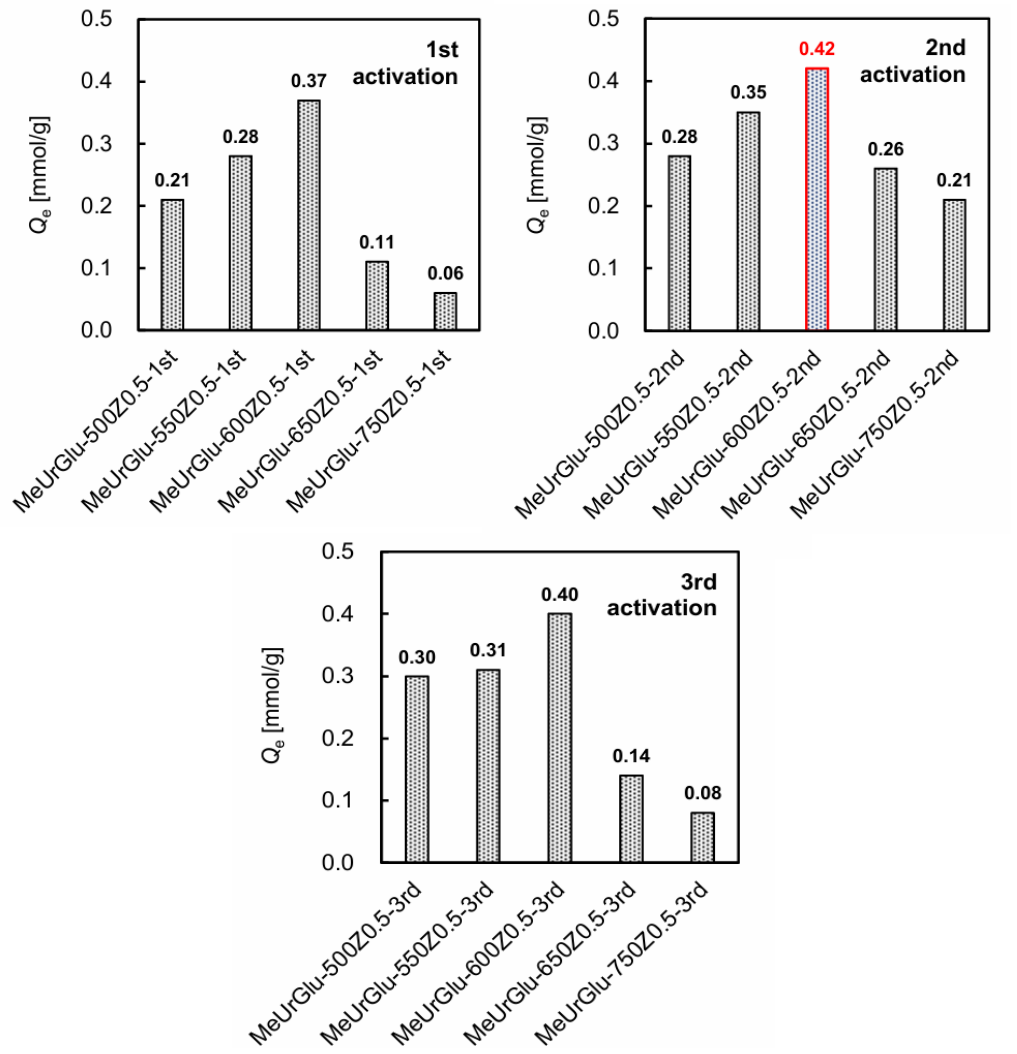

Fig. 3-2. The equilibrium adsorption capacity (Q_e) of each sample at different activation temperature and activation cycles.

content continued to decrease, while the oxygen content increased by 1.79 times. This phenomenon can be attributed to the formation of more non-hydrogen-containing groups of lactone (-COO-) on the carbon surface at elevated temperatures. Although lactone groups exhibit weak adsorption properties, the overall adsorption capacity did not improve with their increased presence. This is primarily due to the decline in nitrogen content of the sample, which reduced the availability of effective adsorption sites. Consequently, it can be concluded that the superior adsorption performance of MeUrGlu-600Z0.5-2nd is a result of achieving an optimal balance between functional groups that favor or inhibit adsorption.

XPS analyses were conducted on the prepared activated carbon to further investigate the chemical composition. The N1s, C1s and O1s XPS spectra of the samples prepared under

varying conditions are presented in **Fig. 3-3.** The N1s signal obtained by XPS measurements was deconvoluted into four peaks corresponding to different nitrogen species: N-6 (pyridinic-N, 398.6 ± 0.3 eV), N-5 (pyrrolic-N and pyridone-N, 400.5 ± 0.3 eV), N-Q (quaternary nitrogen, 401.3 ± 0.3 eV) and N-X (pyridine-N-oxide, 402-405 eV). These peak assignments and binding energies align well with previously reported values in the literature [10, 23-25]. As explained by Pels et al., the term quaternary nitrogen does not correspond to a classical quaternary nitrogen structure, such as the ammonium ion (NH_4^+). Instead, it refers to nitrogen atoms with a relatively higher positive charge compared to pyridinic-N, including protonated pyridinic-N ammonium ions and nitrogen atoms replacing carbon atoms in the graphene structure [10]. Consequently, N-Q is distinct from the tertiary nitrogen reported in some literature, which typically occupies similar positions. The term N-Q more accurately describes nitrogen-containing functional groups located within the basal plane of graphene layers in carbonaceous materials during pyrolysis processes. Moreover, in the XPS N1s spectrum, the N-5 peak appears broader, with a full width at half maximum (FWHM) of approximately 3.0 eV, compared to the peaks of N-6, N-Q, and N-X. This broadness arises because N-5 encompasses both pyrrolic-N and pyridone-N [10], which have very similar peak positions (pyrrolic-N at 400.4 eV and pyridone-N at 400.6 eV). Additionally, pyridone-N exists in two tautomeric forms, further complicating its distinction from pyrrolic-N, contributing to the broader FWHM of N-5. By integrating XPS results with the total nitrogen content from elemental analysis, the distribution of different nitrogen species in each sample can be determined. The results, as summarized in Table 3-2, demonstrate a clear positive correlation between the content of N-Q active sites and the adsorption capacity of the adsorbent. Among all the samples prepared, MeUrGlu-600Z0.5-2nd exhibited the highest N-Q content, reaching 7.10%. Despite not having the largest S_{BET}, it achieved the highest equilibrium adsorption capacity (Q_e = 0.42 mmol/g). The finding highlights that during the surface modification of adsorbents, the introduction of effective active adsorption sites plays a more critical role than merely increasing the specific surface area [26]. With the significant increase in N-Q content, the adsorption capacity of MeUrGlu-600Z0.5-2nd surpassed all other samples, being 1.5 times higher than that of MeUrGlu-500Z0.5-2nd, which contained only 0.72% N-Q. This clearly establishes a positive correlation between the adsorption capacity and the N-Q content.

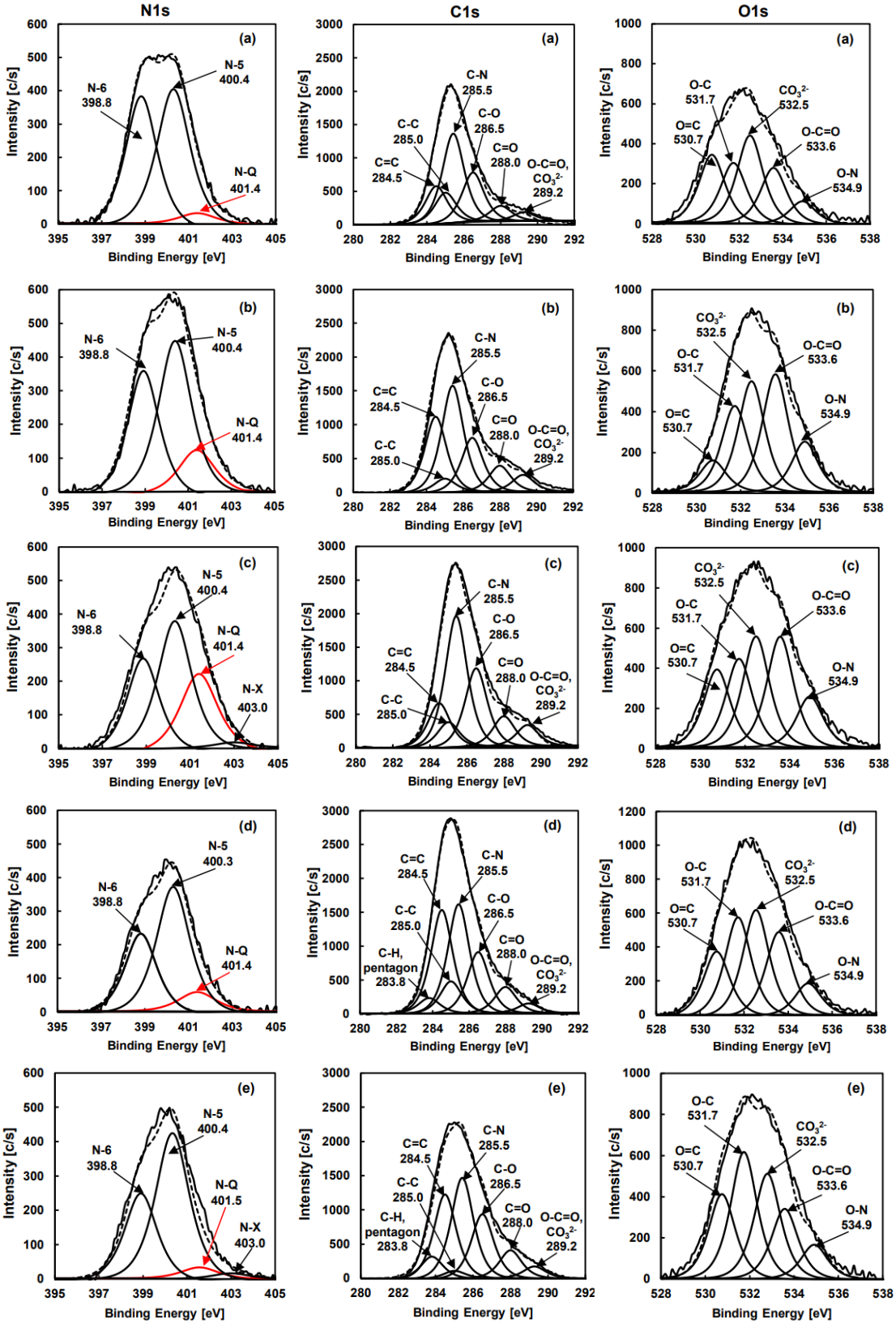

Fig. 3-3. N1s, C1s and O1s XPS spectrum of the samples obtained at different activation temperatures, (a) MeUrGlu-500Z0.5-2nd, (b) MeUrGlu-550Z0.5-2nd, (c) MeUrGlu-600Z0.5-2nd, (d) MeUrGlu-650Z0.5-2nd, (e) MeUrGlu-750Z0.5-2nd, peak sum was drawn in dotted line and N1s original intensity was described in solid line.

Table 3-2 Results of XPS N1S analysis and adsorption amount of prepared adsorbents.

Sample	Configuration of nitrogen-containing groups [wt%]					N-Q ratio [%]	Q_e [mmol/g]
	N_{total}	N-Q	N-6	N-5	N-X		
MeUrGlu-500Z0.5-2nd	15.9	0.72	7.28	7.90	0.00	4.54	0.28
MeUrGlu-550Z0.5-2nd	21.3	3.29	7.94	10.08	0.00	15.4	0.35
MeUrGlu-600Z0.5-1st	21.5	3.40	6.59	11.23	0.28	16.0	0.37
MeUrGlu-600Z0.5-2nd	25.4	7.10	7.36	10.46	0.48	27.9	0.42
MeUrGlu-600Z0.5-3rd	22.6	0.31	13.46	8.68	0.15	1.37	0.40
MeUrGlu-650Z0.5-2nd	13.5	1.30	4.62	7.58	0.00	9.63	0.26
MeUrGlu-750Z0.5-2nd	12.1	0.63	4.04	7.12	0.32	5.21	0.21

Moreover, although MeUrGlu-750Z0.5-2nd exhibited the highest specific surface area, the N-Q content accounted for only 5.21% of its total nitrogen, which is approximately one-eleventh of that in MeUrGlu-600Z0.5-2nd. Consequently, its adsorption capacity was reduced by 50% compared to MeUrGlu-600Z0.5-2nd. A similar trend was observed in the products obtained by increasing the activation cycles at a constant activation temperature. These findings clearly demonstrate that N-Q present in the basal plane of graphene layers serves as the primary active site for phosphate ion adsorption. Thus, even though a substantial amount of nitrogen was incorporated into all the samples, some of them lacked effective binding sites, leading to a deficiency in adsorption capacity. No clear correlation was found between the content of N-6 and N-5 with temperature, suggesting that N-Q is not derived from N-6 or N-5 during the formation process, but is more likely directly doped onto the carbon framework. Additionally, it could be observed that the content of pyridine N-oxide (N-X) was minimal in all samples obtained after pyrolysis. It could be explained in terms of the nitrogen heteroatoms of N-X located at the periphery of the graphite structure that can be easily eliminated in the form of ammonia (NH_3). The C1s signal obtained from XPS measurements was deconvoluted into five peaks with binding energies centered at 283.8 eV (C-H, pentagon), 284.5 eV (C=C), 285.0 eV (C-C), 285.5 eV (C-N), 286.5 eV (C-O), 288.0 eV (C=O) and 289.2 eV (O-C=O, CO_3^{2-}). The assignment of these characteristic peaks is consistent with the results reported in the literature [27-29]. It is important to note that the peak position of C-N varies based on the bonding state of C-N, as explained by Yamada et al. [28]. It was consistently observed that for all samples

synthesized at different temperatures, the best-fitting C-N bond in the C1s XPS spectrum appeared at 285.5 eV. Therefore, we propose that the predominant bonding state of C-N in the samples was likely to be the quaternary-tertiary (Q-T2). The C-N peak in the C1s XPS spectrum of the sample further confirms the successful nitrogen incorporation on the surface of the activated carbon (**Fig. 3-3, Table 3-3**). The O1s XPS spectrum for the samples was deconvoluted into five peaks that can be assigned to 530.7 eV (O=C), 531.7 eV (O-C), 532.5 eV (CO_3^{2-}), 533.6 eV (O=C-O) and 534.9 eV (O-N). The results are in good agreement with the findings reported in the literature [30,31]. Although high-temperature decarboxylation typically reduces carboxyl group content, some carboxyl groups may remain in the samples, possibly due to ester group hydrolysis during HCl washing. Despite the presence of these unfavorable groups, the sample treated at 600°C demonstrated the highest adsorption capacity. This can be attributed to the balance between the favorable and unfavorable functional groups on the surface of adsorbent, further emphasis the crucial role played by N-Q in the process of anionic adsorption. In general, the series of characterization results highlighted how the modification steps of heating at 600°C for twice activation effectively preserved the N-Q adsorption sites and indeed enhanced the adsorption capacity of the activated carbon.

Table 3-3 C1s and O1s XPS data for the prepared sample.

Peaks		MeUrGlu-500Z0.5-2nd	MeUrGlu-550Z0.5-2nd	MeUrGlu-600Z0.5-2nd	MeUrGlu-650Z0.5-2nd	MeUrGlu-750Z0.5-2nd
C1s	C-C	17.9	12.7	8.12	22.3	22.0
	C=C	22.4	27.1	25.2	25.0	22.9
	C-N, C-O	29.2	38.0	40.2	31.4	30.5
	C=O	20.2	14.1	15.4	13.5	16.3
	O-C=O, CO_3^{2-}	10.2	8.14	11.0	7.71	8.35
O1s	O=C	23.1	7.96	17.7	16.8	20.0
	O-C	20.4	21.7	20.2	25.6	30.1
	CO_3^{2-}	29.9	27.9	25.3	27.5	25.0
	O-C=O	19.0	29.8	25.3	21.7	16.7
	O-N	7.75	12.6	11.6	8.33	8.18

3.3.2 Influence of equilibrium solution pH on phosphate adsorption

Solution pH is a key factor influencing the adsorption of ionic pollutants. Therefore, this section examines the effect of solution pH on the adsorption of phosphate ions. **Fig. 3-4** presents the results showing how solution pH affects phosphate adsorption using the representative prepared adsorbent (MeUrGlu-600Z0.5-2nd) and commercial anion exchange resin (HP555). The initial concentration of phosphate solution was kept constant 3.0 mmol/L. MeUrGlu-600Z0.5-2nd exhibited its highest phosphate adsorption capacity of 0.42 mmol/g at pH 4.5. This adsorption capacity was the best result for phosphate adsorption in the present studies, which is higher than that of the modified activated carbon fiber-based adsorbent by 0.15 mmol/g [11]. Additionally, there was a fluctuation in the adsorption amount below pH 4.5, with a gradual increase. However, when the solution pH surpassed 4.5, the phosphate adsorption on MeUrGlu-600Z0.5-2nd was significantly influenced by pH changes, with a sharp decrease in adsorption as the pH rose from 4.5 to 12.0. The peak adsorption at pH 4.5 may be due to the ionization state of phosphate in the solution, as the pH determines the form of phosphate species. Considering the acid dissociation constants (pK_a) of the triprotic phosphoric acid (2.12, 7.21, and 12.67), it can be inferred that as the pH of the solution reaches to 4.5, the presence of phosphorus gradually changes from H_3PO_4 to $H_2PO_4^-$, which carries a negative charge. This transition enhanced its adsorption on adsorbents with positively charged adsorption sites (N-Q). As the pH continues to rise, the dominant species in the solution will change from $H_2PO_4^-$ to HPO_4^{2-}, which has a lower negative charge density and a weaker affinity for the adsorbent. The decrease in adsorption at higher pH values can be attributed to the shift of phosphate species to HPO_4^{2-}, which has a lower affinity for the adsorbent. Moreover, the fluctuation in adsorption amount before pH 4.5 could also be explained by the competition between phosphate anions and excess chloride ions. This is due to the fact that more 0.1 mol/L HCl needs to be added to adjust the solution pH within the acidic range, which causes the adsorption capacity of phosphate anions to fluctuate within the pH range of 2.0-4.5. Similarly, in more alkaline solutions, the increasing concentration of OH^- also leads to a reduction in the adsorption of phosphate ions.

The adsorption capacity of the commercial anion exchange resin HP555, which is functionalized with only N-Q (trimethylammonium, $-N^+(CH_3)_3$) site, also followed a trend of

increase and then decrease as the pH of the solution changed. HP555 is commonly used as a reference material to evaluate the performance of adsorbents due to its strong anion removal performance [8]. In **Fig. 3-4**, it is evident that Q_e of HP555 is always greater than MeUrGlu-600Z0.5-2nd above pH 4.5. However, surprisingly, below pH 4.5, the adsorption capacity of MeUrGlu-600Z0.5-2nd is consistently higher than that of HP555. This difference in adsorption behavior is attributed to the structural variations between the two materials. MeUrGlu-600Z0.5-2nd has N-Q groups embedded within the carbon framework, while HP555 has N-Q groups located outside the carbon framework (as shown in **Fig. 3-5**). Below pH 4.5, HP555's performance drops significantly, but MeUrGlu-600Z0.5-2nd can still exhibit a high adsorption capacity of 0.34-0.41 mmol/g. Therefore, it can be anticipated that MeUrGlu-600Z0.5-2nd is a practical activated carbon adsorbent in low pH range solutions, and sufficient performance can be expected. HP555 maintained a certain adsorption capacity in solutions with a pH greater than 7.0 because, in addition to ion exchange, it might exhibit strong electrostatic attraction and van der Waals interactions with nitrate ions. These interactions enable HP555 to retain its adsorption capacity for nitrate ions, which is not entirely diminished by the competitive adsorption of OH^- ions.

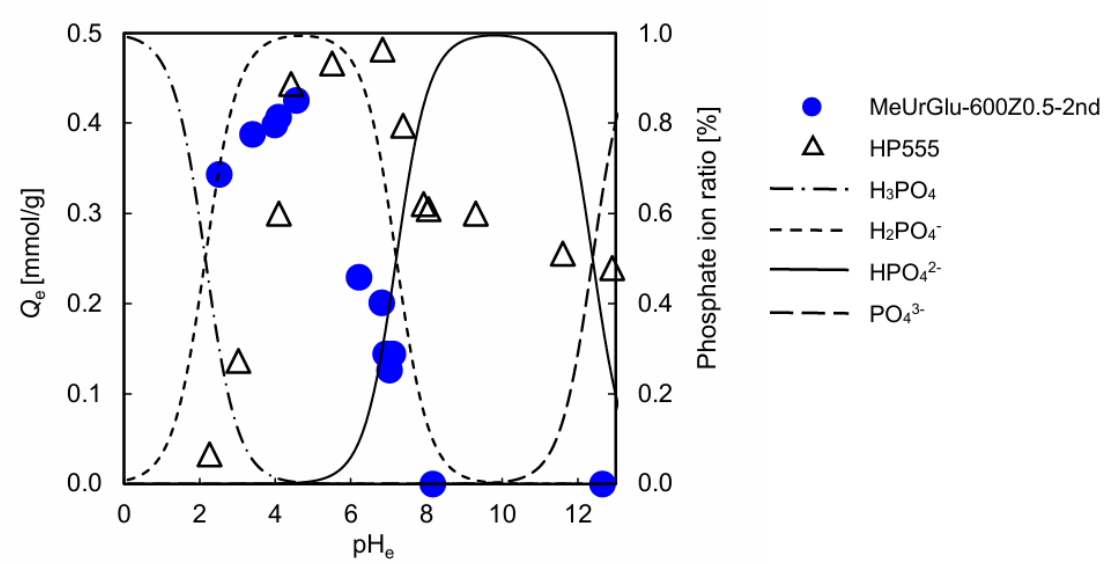

Fig. 3-4. Influence of equilibrium solution pH on the phosphate adsorption of MeUrGlu-600Z0.5-2nd and HP555. Solid and dotted lines; speciation diagram of H_3PO_4. (Initial phosphate concentration of 3.0 mmol/L, dosage of 2 g/L, room temperature)

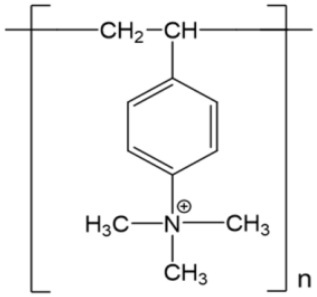

Fig. 3-5. Chemical structure of commercial anion exchange resin HP555.

3.3.3 Adsorption isotherms

Fig. 3-6 shows the phosphate adsorption isotherms for MeUrGlu-600Z0.5-2nd and HP555 at room temperature. HP555, known for its high anion adsorption capacity, was also used for comparison purposes. The equilibrium concentration (C_e) of phosphate solution varied between 0.1-10.0 mmol/L, and the pH of the equilibrium solution was 4.5. The experimental data obtained were analyzed using Langmuir and Freundlich adsorption isotherm models. The parameters obtained from fitting the experimental data reflect adsorbent's affinity and surface properties under specific pH and temperature conditions, as shown in **Table 3-4**. The Langmuir equation is used for monolayer adsorption on surfaces with a limited number of uniform sites [32]. The Freundlich isotherm model describes the adsorption on heterogeneous surfaces, where stronger binding sites are occupied first, with binding strength decreasing as more sites are occupied [33]. The experimental data for MeUrGlu-600Z0.5-2nd indicated that phosphate adsorption initially increased with the rising equilibrium concentration. However, the rate of increase gradually slowed until the adsorption capacity reached a plateau. This behavior can be attributed to the strengthening electrostatic forces as phosphate concentration rises, which enhances phosphate adsorption on the adsorbent surface. As the limited active adsorption sites become increasingly occupied, the adsorption capacity gradually stabilizes. Similarly, the adsorption capacity of HP555 for phosphate showed a similar trend as MeUrGlu-600Z0.5-2nd, with an initial increase followed by gradual stabilization. Both Langmuir and Freundlich models seem to fit the experimental data well based on their fitting curves (**Fig. 3-6**). However, based on the parameters in **Table 3-4**, the Langmuir isotherm model for MeUrGlu-600Z0.5-2nd had a regression coefficient (R^2) of 0.992, while the Freundlich isotherm model had an R^2

of 0.984. The Langmuir model provided the best fit for the phosphate adsorption equilibrium data, with a correlation coefficient $R^2 > 0.99$. For HP555, the Langmuir model also had a higher R^2 value of 0.993, compared to 0.925 for the Freundlich model. In conclusion, the Langmuir isotherm model better describes the adsorption characteristics of the two phosphate removal materials, suggesting that their adsorption of phosphate ions is a monolayer adsorption. Additionally, the basic characteristics of Langmuir isotherm can be expressed by the dimensionless separation factor R_L, which is given by Eq. (3-8).

$$R_L = \frac{1}{1+C_0 K_e} \quad , \tag{3-8}$$

where C_0 and K_e were obtained from the experimental data and Langmuir isotherm parameter. When $0 < R_L < 1$, the adsorption process between phosphate and adsorbent is favorable. Based on experimental data and calculated parameters, R_L values for HP555 ranged from 0.05 to 0.46, while those for MeUrGlu-600Z0.5-2nd ranged from 0.05 to 0.45. These results confirm the suitability of the prepared samples for achieving equilibrium adsorption of phosphate ions.

Additionally, from **Fig. 3-6**, at a phosphate ion concentration of 0.42 mmol/L, the adsorption capacity of MeUrGlu-600Z0.5-2nd reached 0.28 mmol/g. However, when the phosphate ion concentration increased to 0.48 mmol/L, the adsorption capacity of HP555 was limited to 0.23 mmol/g. Furthermore, in the phosphate ion concentration range below 0.48 mmol/L, the Q_e value of HP555 consistently remained slightly lower than that of MeUrGlu-600Z0.5-2nd. This indicates that the prepared adsorbent would exhibit excellent adsorption performance when phosphate ions in contaminated water sources are present at extremely low concentrations (less than 0.48 mmol/L).

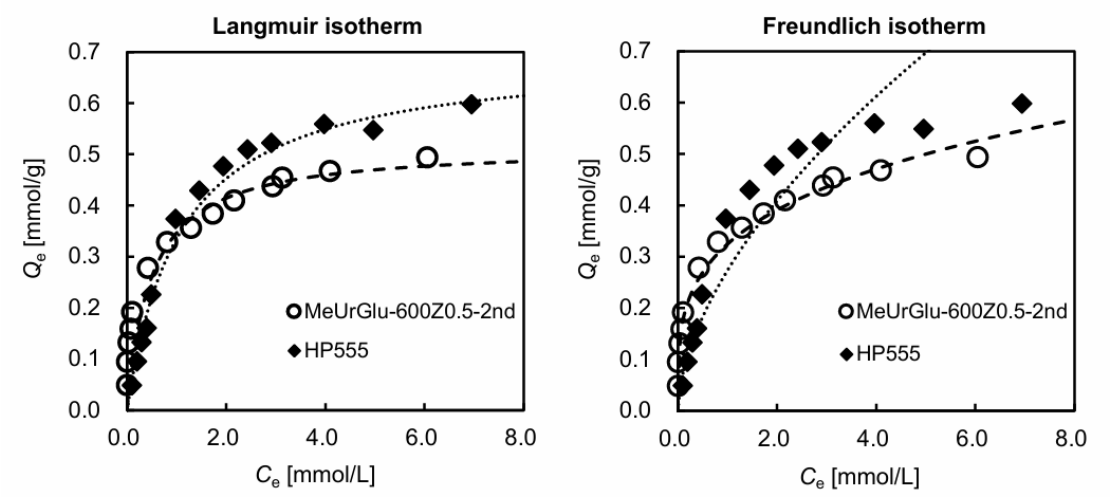

Fig. 3-6. Phosphate ions adsorption isotherms of MeUrGlu-600Z0.5-2nd and HP555 fitted by (a) Langmuir isotherm and (b) Freundlich isotherm. (Solution pH at 4.5, dosage of 2 g/L, room temperature)

Table 3-4 Langmuir and Freundlich isotherm parameters for phosphate adsorption onto MeUrGlu-600Z0.5-2nd and HP555.

Sample	Langmuir isotherm model			Freundlich isotherm model		
	X_m [mmol/g]	K_e [L/mmol]	R^2	$1/n$	K_F [[mmol/g] [L/mmol]$^{1/n}$]	R^2
MeUrGlu-600Z0.5-2nd	0.52	2.03	0.992	0.27	0.32	0.984
HP555	0.69	0.92	0.993	0.58	0.27	0.925

3.3.4 Regeneration of the adsorbent and recovery of phosphate

The ability of regeneration is a crucial factor in assessing the properties of adsorbents. Moreover, recovering phosphate ions removed from wastewater could significantly promote the recycling and sustainable use of this finite resource. In this study, 1 mol/L and 0.1 mol/L solutions of hydrochloric acid, sodium chloride, and sodium hydroxide were employed as regenerants to evaluate the adsorbent's regeneration efficiency. The desorption in pure water was also used as a reference to assess the effectiveness of the regenerants. The regenerant

demonstrating the highest regeneration efficiency was subsequently employed in a continuous flow adsorption experiment, followed by 3 cycles of adsorption-desorption experiments. As illustrated in **Fig. 3-7**, HCl and NaCl exhibited superior regeneration performance compared to NaOH. While 0.1 mol/L HCl and NaCl can achieve similar regeneration effects as those at 1 mol/L, the standard deviations of the adsorbent after three parallel experiments were generally higher, leading to inconsistent regeneration performance. Therefore, it is recommended to avoid using regenerants with a concentration of 0.1 mol/L. Moreover, after regeneration with 1 mol/L NaCl, the adsorbent's phosphate ion adsorption capacity was 0.03 mmol/g higher than that achieved with 1 mol/L HCl. Additionally, NaCl exhibited more attractive features than HCl, such as being environmental-friendly and more suitable for the desorption of adsorbent. Hence, 1 mol/L NaCl is identified as the optimal regenerant for MeUrGlu-600Z0.5-2nd. The regeneration performance of MeUrGlu-600Z0.5-2nd using NaOH was poor, even less effective than desorption in pure water. This could be attributed to changes in the adsorbent's surface properties, such as its pore structure, caused by NaOH during the desorption process [34]. The good regeneration performance exhibited by NaCl may be attributed to the to the abundance of chloride ions in the solution, which displace phosphate ions from the N-Q adsorption sites, facilitating the phosphate ions to be desorbed. Furthermore, the NaCl solution used for regeneration contains desorbed phosphate ions that can be used as fertilizer to support plant growth [35].

Fig. 3-8 presents the outcomes of the 3 cycles of adsorption-desorption experiments using 1 mol/L NaCl as the regenerant for the regeneration of MeUrGlu-600Z0.5-2nd packed column. The corresponding flow adsorption parameters are detailed in **Table 3-5**. During the first adsorption cycle, the breakthrough time for the column packed with MeUrGlu-600Z0.5-2nd was 48 min, outperforming the second (24 min) and third adsorption cycles (32 min). During the first regeneration of the phosphate-saturated column with 1 mol/L NaCl, the excess chloride ions introduced into the column displaced the phosphate ions from the N-Q adsorption sites. Studies have shown that N-Q sites bound with chloride ions possess greater ion exchange capacity and stronger adsorption affinity [12]. As a result, when a new round of phosphate ions adsorption cycle begins, the introduced phosphate ions will still be adsorbed onto the activated carbon surface, displacing the chloride ions and maintaining a certain adsorption capacity. The

decrease in breakthrough time (t_b) after the adsorption-desorption cycles suggests that not all phosphate ions adsorbed on the strong N-Q sites were successfully desorbed. On the other hand, the removal efficiency of phosphate before breakthrough point (R_b%) during the three adsorption-desorption cycles was 100%, surpassing the 91.3% reported by Alemu Gizaw et al. [36]. This also highlights the practical value for the reusability of MeUrGlu-600Z0.5-2nd in removing phosphate ions. Additionally, while regenerating the MeUrGlu-600Z0.5-2nd packed column, the collected NaCl solution containing phosphate ions as nutrient can be applied as a soil fertilizer for plant growth [37].

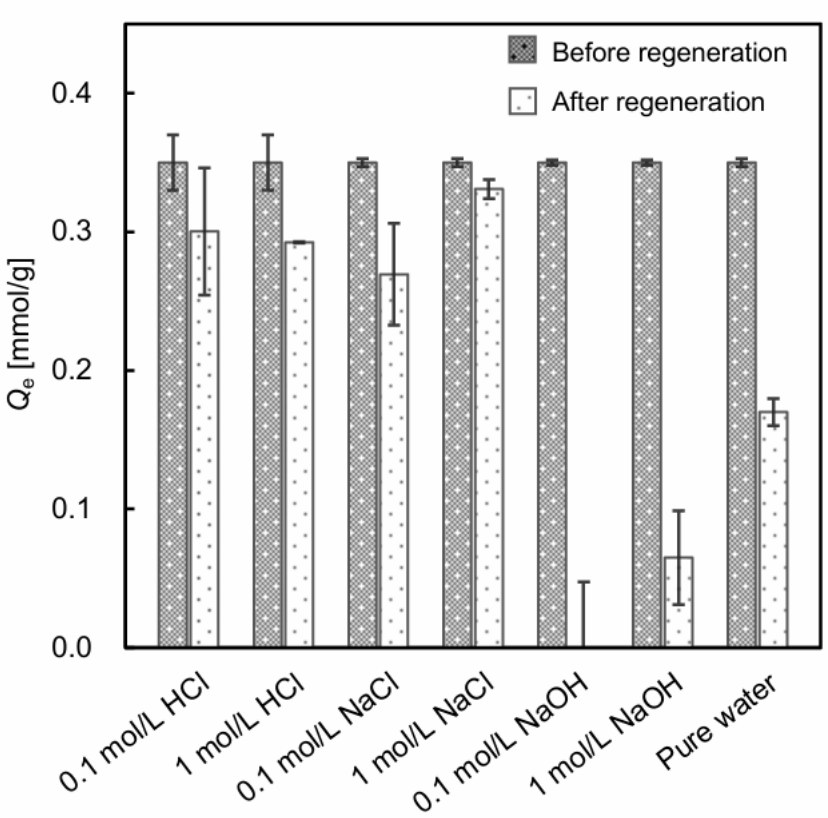

Fig. 3-7. Results of the effect of different regenerants on the regeneration performance of MeUrGlu-600Z0.5-2nd.

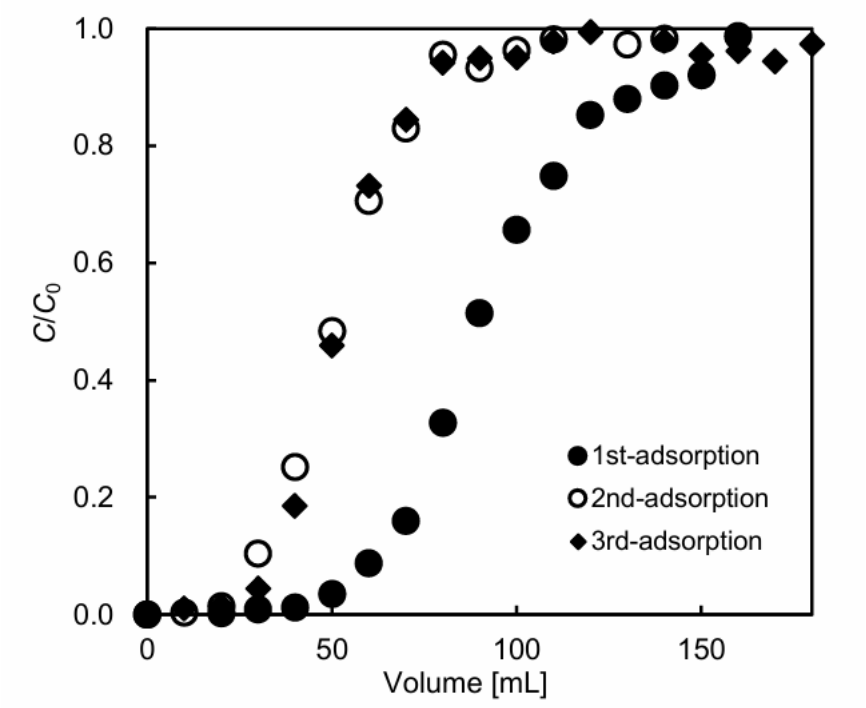

Fig. 3-8. Results of 3 cycles of adsorption-desorption experiments using 1 mol/L NaCl as the regenerant.

Table 3-5 Parameters of continuous flow adsorption experiments.

Cycles	t_b [min]	V_b [mL]	Q_b [mmol/g]	R_b%	t_s [min]	V_s [mL]	Q_s [mmol/g]	R_s%
1st-adsorption	48	60	0.26	100	136	170	0.37	58
2nd-adsorption	24	30	0.13	100	96	120	0.20	48
3rd-adsorption	32	40	0.18	100	104	130	0.23	50

3.4 Conclusion

This study developed the optimal N-Q-containing glucose-derived adsorbent, MeUrGlu-600Z0.5-2nd, for the efficient removal of phosphate ions from aqueous solution. The main conclusions are summarized as follows:

1. MeUrGlu-600Z0.5-2nd demonstrated excellent phosphate ion equilibrium adsorption capacity (Q_e) of 0.42 mmol/g at a phosphate concentration of 3 mmol/L and a solution pH of 4.5.
2. The Langmuir isotherm model can well describe the adsorption process which is a monolayer adsorption, with the maximum adsorption capacity (X_m) calculated to be 0.52 mmol/g.
3. Surface characterization results indicated that introducing effective adsorption sites was more beneficial than simply increasing the specific surface area.
4. In acidic solutions (pH < 4.5), MeUrGlu-600Z0.5-2nd showed a strong equilibrium adsorption capacity (Q_e) of 0.34-0.44 mmol/g, overcoming the limitation of the commercial anion exchange resin HP555, which is ineffective in acidic environments.
5. In the continuous flow adsorption, MeUrGlu-600Z0.5-2nd can be regenerated for at least 3 cycles, and using NaCl as the regenerant was beneficial for the recovery of phosphate ions.

Reference

[1] A. O. Fadiran, S. C. Dlamini, A. Mavuso, A comparative study of the phosphate levels in some surface and ground water bodiesof Swaziland, Bull. Chem. Soc. Ethiop. 22 (2008) 197-206.

[2] E. Priya, S. Kumar, C. Verma, S. Sarkar, P. K. Maji, A comprehensive review on technological advances of adsorption for removing nitrate and phosphate from waste water, J. Water Process Eng. 49 (2022) 103159.

[3] C. Namasivayam, D. Sangeetha, Equilibrium and kinetic studies of adsorption of phosphate onto $ZnCl_2$ activated coir pith carbon, J. Colloid Interface Sci. 280 (2004) 359-365.

[4] P. Cheng, Y. Liu, L. Yang, Q. Ren, X. Wang, Y. Chi, H. Yuan, S. Wang, Y. Ren, Phosphate adsorption using calcium aluminate decahydrate to achieve low phosphate concentrations: Batch and fixed-bed column studie, 11 (2023) 109377.

[5] R. Nazarian, R. J. Desch, S. W. Thiel, Kinetics and equilibrium adsorption of phosphate on lanthanum oxide supported on activated carbon, Colloids Surf. A Physicochem. Eng. Asp. 624 (2021) 126813.

[6] B. Wu, I. M. C. Lo, Surface Functional Group Engineering of CeO_2 Particles for Enhanced Phosphate Adsorption, Environ. Sci. Technol. 54 (2020) 4601-4608.

[7] M. Machida, P. Yoo, Y. Amano, Adsorption of nitrate from aqueous phase onto nitrogen-doped activated carbon fibers (ACFs), SN Appl. Sci. 1 (2019) 323.

[8] Y. Tsuchiya, Y. Yamaya, Y. Amano, M. Machida, Effect of two types of adsorption sites of activated carbon fibers on nitrate ion adsorption, J. Environ. Manage. 289 (2021) 112-484.

[9] M. Machida, Y. Tsuchiya, J. Yuan, Y. Amano, Efficient nitrate adsorbent applicable to wide pH range derived from polyacrylonitrile (PAN) fiber, Results Eng. 11 (2021) 100276.

[10] J. R. Pels, F. Kapteijn, J. A. Moulijn, Q. Zhu, K. M. Thomas, Evolution of nitrogen functionalities in carbonaceous materials during pyrolysis, Carbon, 33 (1995) 1641-1653.

[11] T. Sakamoto, Y. Amano, M. Machida, Phosphate ion adsorption properties of PAN-based activated carbon fiber prepared with Na_2CO_3 activation, J. Water Chem. Technol. 43 (2021) 298-304.

[12] H. Sun, F. S. Cannon, X. He, Enhanced trifluoroacetate removal from groundwater by

quaternary nitrogen-grafted granular activated carbon, Sci. Total Environ. 660 (2019) 577-585.

[13] A. Izza, T. Kojima, Y. Amano, M. Machida, Calcined scallop shells for phosphate adsorption in aqueous solution, J. Environ. Chem. 30 (2020) 119-124.

[14] F. Matsuzawa, Y. Amano, M. Machida, Phosphate ion adsorption characteristics of nitrogen doped carbon-based adsorbent prepared from sucrose, melamine, and urea, 2 (2023) 114-122.

[15] J. C. Olivares, C. P. Alonso, C. B. Díaz, F. U. Nuñez, M. C. Mercado, B. Bilyeu, Modeling of lead (II) biosorption by residue of allspice in a fixed-bed column, Chem. Eng. J. 228 (2013) 21-27.

[16] S. V. Manjunath, M. Kumar, Simultaneous removal of antibiotic and nutrients via Prosopis juliflora activated carbon column: performance evaluation, the effect of operational parameters and breakthrough modeling, Chemosphere 262 (2021) 127820.

[17] A. Manna, N. Naskar, K. Sen, K. Banerjee, A review on adsorption mediated phosphate removal and recovery by biomatrices, J. Am. Chem. Soc. 99 (2022) 100682.

[18] E. R. Raut, M. A. Bedmohata, A. R. Chaudhari, Comparative study of preparation and characterization of activated carbon obtained from sugarcane bagasse and rice husk by using H_3PO_4 and $ZnCl_2$, Mater. Today: Proceedings, 66 (2022) 1875-1884.

[19] V. Pavlenko, S. Khosravi H, S. Żółtowska, A.B. Haruna, M. Zahid, Z. Mansurov, Z. Supiyeva, A. Galal, K.I. Ozoemena, Q. Abbas, T. Jesionowski, A comprehensive review of template-assisted porous carbons: Modern preparation methods and advanced applications, Mater. Sci. Eng. R Rep. 149 (2022) 100682.

[20] J. Yuan, Y. Amano, M. Machida, Surface characterization of mesoporous biomass activated carbon modified by thermal chemical vapor deposition and adsorptive mechanism of nitrate ions in aqueous solution, Colloids Surf. A Physicochem. Eng. Asp. 616 (2021) 126213.

[21] M. S. Shafeeyan, W. Daud, A. Houshmand, A. Shamiri, A review on surface modification of activated carbon for carbon dioxide adsorption, J. Anal. Appl. Pyrol., 89 (2010) 143-151.

[22] G. Yang, H. Chen, H. Qin, Y. Feng, Amination of activated carbon for enhancing phenol

adsorption: Effect of nitrogen-containing functional groups, Appl. Surf. Sci. 293 (2014) 299-305.

[23] Z. Li, L. Zhang, B. S. Amirkhiz, X. Tan, Z. Xu, H, Carbonized Chicken Eggshell Membranes with 3D Architectures as High-Performance Electrode Materials for Supercapacitors, Adv. Energy Mater. 2 (2012) 431-437.

[24] L. L. Ling, W. J. Liu, S. Zhang, H. Jiang, Magnesium Oxide Embedded Nitrogen Self-Doped Biochar Composites: Fast and High-Efficiency Adsorption of Heavy Metals in an Aqueous Solution, Environ. Sci. Technol. 51 (2017) 10081-10089.

[25] B. Chu, Y. Amano, M. Machida, Preparation of bean dreg derived N-doped activated carbon with high adsorption for Cr(VI), Colloids Surf. A physicochem. Eng Asp. 586 (2020) 124262.

[26] S. Wong, N. Ngadi, N. Inuwa, O. Hassan, Recent advances in applications of activated carbon from biowaste for wastewater treatment: A short review, J. Clean Prod. 175 (2018) 361-375.

[27] M. C. Biesinger, Accessing the robustness of adventitious carbon for charge referencing (correction) purposes in XPS analysis: Insights from a multi-user facility data review, Appl. Surf. Sci. 597 (2022) 153681.

[28] Y. Yamada, H. Tanaka, S. Kubo, S. Sato, Unveiling bonding states and roles of edges in nitrogen-doped graphene nanoribbon by X-ray photoelectron spectroscopy, Carbon 185 (2021) 342-367.

[29] N. Diana, Y. Yamada, S. Gohda, H. Ono, S. Kubo, S. Sato, Carbon materials with high pentagon density, J. Mater Sci. 56 (2021) 2912-2943.

[30] C. Peiris, O. Nayanathara, C. M. Navarathna, Y. Jayawardhana, S. Nawalage, G. Burk, A. G. Karunanayake, S. B. Madduri, M. Vithanage, M. N. Kaumal, T. E. Mlsna, E. B. Hassan, S. Abeysundara, F. Ferezi, S. R. Gunatilake, The influence of three acid modifications on the physicochemical characteristics of tea-waste biochar pyrolyzed at different temperatures: a comparative study, RSC Adv. 9 (2019) 17612-17622.

[31] A. Herath, C. Reid, F. Perez, C. U. Pittman, T. E. Mlsna, Biochar-supported polyaniline hybrid for aqueous chromium and nitrate adsorption, J. Environ. Manage. 296 (2021) 113186.

[32] I. Langmuir, The adsorption of gases on plane surface of glass, mica and platinum, J. Am. Chem. Soc. 40 (1918) 1361-1403.

[33] H. Freundlich, Uber die adsorption in losungen, Zeitschrift fur Physikalische Chemie. 57U (1907) 385-470.

[34] Z. Zhang, G. Huang, P. Zhang, J. Shen, S. Wang, Y. Li, Development of iron-based biochar for enhancing nitrate adsorption: Effects of specific surface area, electrostatic force, and functional groups, Sci. Total Environ., 856, 1, 2023, 159037.

[35] A. Ansari, E. T. Nadres, M. Đỗ, D. F. Rodrigues, Investigation of the removal and recovery of nitrate by an amine-enriched composite under different fixed-bed column conditions, Process Saf. Environ. Prot. 150 (2021) 365-372.

[36] A. Gizaw, F. Zewge, Y. Chebude, A. Mekonnen, M. Tesfaye, Simultaneous nitrate and phosphate abatement using calcium silicate hydrate adsorbent: Fixed bed column adsorption study, Surf. Interfaces 30 (2022) 101961.

[37] D. Jiang, B. Chu, Y. Amano, M. Machida, Motoi Machida, Removal and recovery of phosphate from water by Mg-laden biochar: Batch and column studies, Colloids Surf. A Physicochem. Eng. Asp. 558 (2018) 429-437.

Chapter 4 Enhancement of nitrate adsorption from aqueous solutions by glucose-derived nitrogen-doped carbonaceous adsorbent

4.1 Introduction

There is an increasing demand for food as the expansion of population. Since the invention of Haber-Bosch process in 1920, the synthesis of ammonia has accelerated the process of fertilizer production [1]. The adequate supply of fertilizer made a great contribution to the high yield of crops and indirectly brought benefits to the survival of mankind. The use of fertilizers has been extended up-to now. Although chemical fertilizer brings nutrients to crops and satisfies people's demand for food, it will also bring environmental concerns. The major component of almost fertilizers includes nitrogen [2]. Nowadays, the excessive and inappropriate use of fertilizer has caused serious nitrate contamination. In fact, the agricultural and atmospheric systems have low accumulation ability but high transfer ability toward nitrate. The final destination of nitrate is transfer to the surface and groundwater resources through precipitation and surface runoff. Due to its high solubility and stability, nitrate is hard to precipitate and always keeps widespread presence [3]. The regulation of maximum concentration level of the World Health Organization (WHO) for nitrate-nitrogen (NO_3-N) is 10 mg/L in public supply drinking water [4]. High concentration of nitrate in drinking water triggers several health ailments. Brain tumors, hypertension, goiter, stomach cancer, nasopharyngeal and thyroid disorders caused by nitrate are reported in adults [2]. In addition, methemoglobin and other birth defects will occur in infants [5]. High concentration of nitrate not only threatens human health, but also destroys the ecological environment. The presence of nitrate in high concentrations in lakes and reservoirs is one of the main reasons for the eutrophication in surface water, resulting in kinds of environmental problems including algal blooms [6]. Therefore, the development of effective and feasible technologies has become an urgent requirement to meet the current status.

For the remediation of nitrate, several kinds of methods have been established, such as electrodialysis, biological denitrification, reverse osmosis, adsorption and so on. Among these, electrodialysis has been described as a widely used technique in the practical application because it has the advantages of greater accuracy than others. However, this technique requires

detailed design to achieve nitrate removal. Midaoui et al. [7] reported that when the membrane potential was increased from 10 V to 15 V, the nitrate removal efficiency was elevated from 87% to 93%. Apparently, the efficiency of nitrate removal by this method is strongly dependent on the applied external voltage, which consumes extra cost and energy for treating water. Apart from this, the high ion concentration in conventional electrodialysis concentrate will lead to increased transmembrane resistance, hindering the removal efficiency [8]. Moreover, direct degradation of nitrate to molecular nitrogen can be mentioned as an advantage of the biological denitrification [9]. However, this process is complicated to some extent which requires an exact monitoring of carbon/nitrogen ratio and is only applicable for full time operation [10]. The reverse osmosis device is usually operated under high pressure conditions [11]. Besides, the membrane surface of reverse osmosis is easily to get polluted, which reduces the removal efficiency of pollutants [12]. Different from the methods mentioned above, the adsorption method for collecting soluble substances from water has advantages of being simple to operate, requiring no auxiliary equipment and low cost to remove pollutants [13]. This is a promising method that can be used to remove nitrate.

To achieve the purpose of effectively removing target pollutants by adsorption, surface modification of the adsorbent to make it more suitable for the adsorption of a given pollutant is an effective method. In general, there are two types of modification strategies. One is to improve the pore structure of the adsorbent and increase the specific surface area. The other is to improve the surface chemistry of the adsorbent by introducing specific functional groups [14]. According to the relevant literature, for the adsorption of specific ions, the introduction of suitable functional groups is more advantageous than increasing the specific surface area [15]. For nitrate, it is a negative monovalent anion. Thus, the introduction of positively charged adsorption sites on the surface of the adsorbent is more favorable to the adsorption of nitrate. The introduction of nitrogen onto the carbonaceous adsorbent surface will generate Lewis acidity which benefits to nitrate adsorption. The method facilitates the formation of quaternary nitrogen (N-Q). The existence of N-Q will improve the adsorption amount of nitrate by electrostatic forces, because it is always positively charged in a wide range of solution pH [16]. Inspired by the mentioned above, it is possible to design a new type of nitrogen-containing carbonaceous adsorbent with good abilities to capture nitrate from water. Nitrogen-doped

surface modification can be achieved in one way by directly treating nitrogen-containing polymer precursors. Another method involves post-treatment of pristine carbon with certain nitrogen-containing reagents. As reported, Yuan et al. directly treated nitrogen-containing carbon fiber using a thermal chemical vapor deposition method, increasing its nitrate adsorption capacity from 0.09 mmol/g to 0.79 mmol/g [17]. However, this preparation process requires stringent temperature conditions, with high temperatures around 1000°C, which increases operational risks and is not conducive to industrial production. On the other hand, based on the previous research described in chapter 2, an adsorbent with excellent nitrate adsorption properties by post-treating glucose with nitrogen-containing reagents was obtained. This preparation method successfully improved the production process of activated carbon, reducing the required temperature from 1000°C to 550°C [18]. Therefore, post-treatment of the raw materials with a nitrogen-containing reagent is an effective nitrogen-doped surface modification method.

Based on the theoretical analysis and previous research described in chapter 2 and chapter 3, one can conclude that heteroatom-doped carbonaceous adsorbents can serve as a scalable, cost-effective, and excellent adsorbent material for addressing water pollution problems caused by nitrate contamination. In this chapter, in order to achieve the transition from dual nitrogen sources to a single nitrogen source, the interaction between the raw materials in the preparation of glucose-based carbonaceous adsorbents is further explored. The novelty of this chapter lies in further optimizing the preparation conditions of the adsorbent, and the enhancement of its adsorption performance (UrGlu-450Z0.6-2nd). Additionally, an explanation was provided for the formation of the special brown porous foam-like intermediate that emerged during the optimization process and its distinct role. For comparison, glucose precursor without nitrogen-doped surface modification treatment (Glu-450Z0.6-2nd) was also prepared as a reference material, aiming to provide a clearer description of the effectiveness of this modification strategy. A series of batch adsorption experiments and a slightly extended fixed-bed column adsorption experiments were conducted to investigate the effects of various parameters on nitrate adsorption. By combining the characterization results of the adsorbent with the findings from the adsorption studies, the adsorption characteristics and mechanisms of the adsorbent were revealed. The results of the fixed-bed column adsorption demonstrated the excellent

performance of the developed adsorbent in practical application mode. Therefore, the present method of preparing nitrogen-doped adsorbents offers a new approach for addressing water pollution issues caused by nitrate contamination.

4.2 Materials and methods

4.2.1 Preparation of adsorbent

The developed adsorbent was prepared following the steps described below and shown in **Fig. 4-1**. (1) Firstly, for pre-treatment, 20 g of glucose as the carbon source was mixed with a certain mass of urea nitrogen source (10 g, 15 g, 20 g), followed by the addition of a certain mass of zinc chloride (15 g, 20 g, 25 g) as the activator. After thoroughly grinding the mixture in a mortar, the sample was transferred to a stainless steel container and placed in an oven at 110°C overnight. During this pre-treatment process, glucose and urea will undergo activation by $ZnCl_2$ to form a special porous foam-like intermediate, accompanied by volume expansion. (2) Subsequently, for post-treatment, the resulting intermediate was grounded uniformly. Then, 10 g was taken and placed in a horizontal tubular furnace for the first activation step. The activation conditions involved raising up the temperature to Y°C (400, 450, 500°C) within 45 min under a nitrogen gas flow rate of 20 mL/min and maintaining it for 60 min. After the temperature was cooled down to room temperature, the sample was kept under a nitrogen gas flow and slowly removed it from the horizontal tube furnace. The obtained sample was washed 3 times in a 3 mol/L boiling HCl solution, followed by rinsing with boiling distilled water until the filtrate is neutral. The washed sample was then placed in an oven at 100°C for 2 h to dry for the subsequent use. Here, the sample was labeled as UrGlu-YZX-1st, where UrGlu represents urea and glucose, Y stands for the activation temperature (for example, 400°C is denoted as 4.0), Z is the abbreviation for the activator $ZnCl_2$, X indicates the proportion of $ZnCl_2$ to the total mass of urea and glucose, and 1st denotes the first activation process. In the experiments examining the addition of $ZnCl_2$ and urea, a special notation was used for clearer understanding. The actual mass of $ZnCl_2$ and urea added was indicated after the reagent abbreviation. For example, 15 g of $ZnCl_2$ was denoted as Z(15g), and 10 g of urea was denoted as Ur(10g). Subsequently, the sample obtained after the first activation (without washing process) was uniformly ground and then subjected to a second activation process in a horizontal tube furnace.

The activation conditions involved raising up the temperature to Y°C within 45 min under a nitrogen gas flow rate of 20 mL/min and maintaining it for 30 min. After activation, the sample was similarly cooled under a nitrogen flow and slowly removed. At this point, the sample was labeled as UrGlu-YZX-2nd, where 2nd indicates the second activation process. To find the optimal activation conditions, further activation of UrGlu-YZX-2nd will be conducted for the third time, using the same activation conditions as the second time. Similarly, the sample obtained in this process was labeled as UrGlu-YZX-3rd, where 3rd denotes the third activation process. For further comparison, the reference material without nitrogen-doped surface modification was also prepared. It was labeled as Glu-YZX-2nd. The sample which used melamine (Me) as the nitrogen source was denoted as MeGlu-YZX-2nd.

At the same time, in order to find the optimal adsorbent preparation scheme, reagents $MgCl_2$ and Na_2CO_3 were also used to replace $ZnCl_2$ as the activator in the activation step for the preparation of adsorbents. Samples prepared after two activation processes were respectively labeled as UrGlu-YMX-2nd and UrGlu-YNX-2nd, where M represents $MgCl_2$ as the activator and N represents Na_2CO_3.

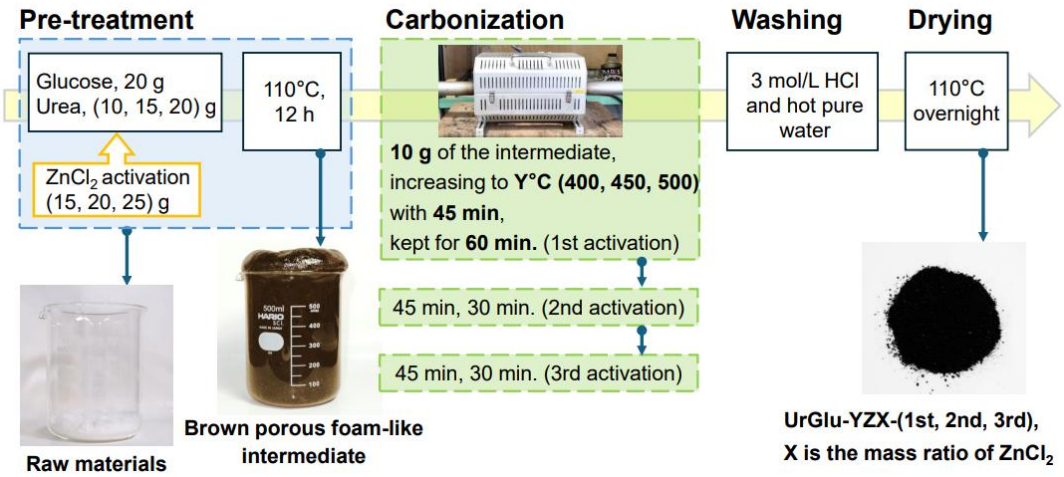

Fig. 4-1. Preparation process of the adsorbent.

4.2.2 Characterization

The prepared samples were characterized through N_2 adsorption-desorption isotherms, elemental analysis, and X-ray photoelectron spectroscopy (XPS). The specific surface area and

pore structure of the samples were tested using a BELSORP-mini II surface analyzer (MicrotracBEL Corporation, Japan), and obtained through N_2 adsorption-desorption method. The specific surface area (S_{BET}, m^2/g), average pore diameter (D_{avg}, nm) and pore volume (V_{total}, cm^3/g) were calculated by Brunauer-Emmer-Teller (BET) method and N_2 adsorption isotherm. The micropore volume (V_{micro}) was obtained by α_s plot. Meanwhile, the mesopore volume (V_{meso}) was calculated from the difference between V_{total} and V_{micro}. The bulk elemental composition of the samples was determined using a PE2400II CHN analyzer (PerkinElmer, Inc., USA). The O content was obtained by subtracting the sum of the C, H, and N contents from the total amount [19]. The configurations of the nitrogen species on the surface of the prepared samples were investigated using X-ray photoelectron spectroscopy (XPS, JPS-9030, JEOL Ltd., Japan).

4.2.3 Batch adsorption

The adsorption studies of the samples were primarily conducted in batch adsorption mode, while a small portion of extended fixed-bed column adsorption experiments were also carried out to investigate their adsorption characteristics under the practical application mode. In batch adsorption studies, the effect of solution pH on the adsorption of nitrate by the prepared adsorbents was investigated. Additionally, adsorption isotherms and kinetics were studied to elucidate the mechanisms governing the adsorption process. The specific operational steps of the adsorption experiments involved weighing 30 mg of dried samples into a 30 mL conical flask. Then, 15 mL of sodium nitrate solution was added to the flask, and the mixture was stirred at room temperature and 200 rpm for at least 12 h to reach adsorption equilibrium. Afterward, the mixture was filtered using filter paper, and the filtrate was retained. The initial concentration of nitrate ions in the solution and the residual nitrate ion concentration in the filtrate were both measured using ion chromatography (model ICS-1100, Nippon Dionex KK, Japan). The adsorption capacity per unit mass of adsorbent at equilibrium was obtained from the following equation:

$$Q_e = \frac{(C_0 - C_e)V}{W} \quad , \tag{4-1}$$

where, Q_e is the equilibrium adsorption amount (mmol/g). C_0 and C_e represent the initial and the equilibrium concentration of nitrate (mmol/L), respectively. V is the solution volume (L) and W expresses the weight of sample (g).

The effect of solution pH on nitrate adsorption was studied in nitrate solutions (C_0 = 200 mg/L) over a pH gradient ranging from 2.0 to 12.0. The pH at the point of zero charge (pH_{pzc}) was determined using the pH drift method [20, 21]. Specifically, nitrate solutions with pH gradients ranging from 2.0 to 12.0 were prepared in advance (C_0 = 200 mg/L). During this process, appropriate amounts of 0.1 mol/L and 1 mol/L HCl or NaOH were used to adjust the solution pH to the desired values, and the final pH of the solution was measured using a portable pH meter (model D-71, Horiba, Japan). Afterwards, a certain number of sets of 30 mg of dried prepared samples were weighed into the 30 mL conical flasks. Then, 15 mL of the nitrate solutions with specified pH values were added separately to each conical flask. The pH_{pzc} was determined as the point where the equilibrium solution pH equals the initial solution pH.

The investigation of adsorption isotherms of the adsorbent was conducted by preparing nitrate solutions with initial concentrations ranging from 10 to 600 mg/L (pH 3.0) at room temperature (25 ± 0.5°C). All other experimental procedures remained consistent with the description above (dosage of 2 g/L). The final conclusion was drawn by determining the nitrate concentration before and after reaching adsorption equilibrium at each initial concentration. In this study, the adsorption isotherms of the adsorbent for nitrate ions at room temperature (25 ± 0.5°C) were fitted and analyzed using the Langmuir and Freundlich adsorption isotherm models to obtain insights from the experimental data.

The investigation of the adsorption kinetics of the adsorbent for nitrate ions was examined by adding 400 mg of the prepared sample into a 200 mL nitrate solution (C_0 = 200 mg/L, pH 3.0). Subsequently, at predefined time intervals (t = 2.5, 5, 7.5, 10, 12.5, 15, 17.5, 20, 25, 30, 40, 50, 60, 70, 80, 90, 100, and 120 min), 1 mL of solution was sequentially collected to measure the nitrate ions concentration in the solution at each designated time point. The experimental data obtained were fitted and analyzed using pseudo-first-order and pseudo-second-order models, respectively.

4.2.4 Fixed-bed column adsorption

The adsorption study of nitrate ions in a fixed-bed column was conducted using a hollow glass column with an inner diameter of 7 mm. The column was filled with 0.8 g of prepared sample between two supporting layers of glass wool. At room temperature, a nitrate solution

(C_0 = 200 mg/L, pH 3.0) was supplied from the bottom to the top of the packed column at a constant rate of 1.25 mL/min using a peristaltic pump (MP-3, Tokyo Rikakikai Co., Ltd., Japan). The effluent at the end of the device was collected at regular intervals (every 8 min, collecting 10 mL of nitrate solution) to determine the concentration of nitrate ions (C_t) at the particular time. The breakthrough curve was expressed as C_t/C_0 as a function of time t. The adsorption capacity (Q) of the sample for nitrate in the fixed bed column was calculated using the following equation:

$$Q = \frac{R}{Wm}\int_0^t (C_0 - C_t)\,\mathrm{d}t \quad , \tag{4-2}$$

where, R is the flow rate (mL/min), W means the molar mass of nitrate (g/mol), m is the weight of adsorbent (g), t represents the flow time (min), C_0 is the nitrate concentration in the influent (mg/L), and C_t is the nitrate concentration in the effluent at time t (mg/L).

4.3 Results and discussion

In the practical production process of adsorbents, achieving the transition from dual nitrogen sources to a single nitrogen source in the preparation of raw materials can bring many benefits, such as cost savings, process simplification, and improved resource utilization. **Fig. 4-2** shows the nitrate adsorption capacity of carbonaceous adsorbents obtained by surface modification of glucose with two different nitrogen reagents. The results indicate that the carbonaceous adsorbent obtained using urea as the nitrogen source exhibits better adsorption capacity, and its intermediate product after pretreatment shows the same volume expansion phenomenon as described in previous sections. Therefore, the preparation method using urea as the nitrogen source will continue to be optimized. A series of key factors in the preparation process of the adsorbent were investigated to explore the optimal preparation scheme. Additionally, the special brown porous foam-like intermediate formed after the pre-treatment was described and reasonably explained. Further studies were conducted using the adsorbent prepared under the optimal condition (UrGlu-450Z0.6-2nd) and the reference adsorbent (Glu-450Z0.6-2nd) to more clearly assess the effectiveness of the nitrogen-doped surface modification method.

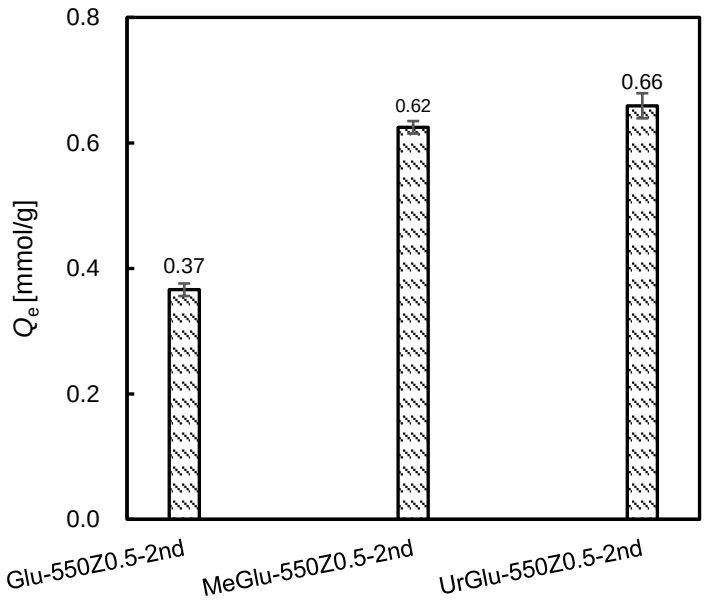

Fig. 4-2. Nitrate adsorption capacity of carbonaceous adsorbents obtained by surface modification of glucose with two different nitrogen reagents. (pH 3.0, C_0 = 200 mg/L, dosage of 2 g/L)

4.3.1 Optimal preparation conditions of the adsorbent and analysis of the brown porous foam-like intermediate

To develop the optimal preparation conditions for the adsorbent, the effects of factors such as activation process, amount of activator $ZnCl_2$, amount of nitrogen-containing reagent urea, activation temperature, and type of activating agent on the adsorption performance of the adsorbent were investigated. **Fig. 4-3** displays the nitrate adsorption capacities (C_0 = 200 mg/L, pH 3.0) of the reference adsorbent and the nitrogen-modified adsorbent under different activation processes. Evidently, the adsorbent using only glucose as the carbon source exhibited lower nitrate adsorption capacity, with the highest Q_e observed in the second activation process being only 0.36 mmol/g (Glu-550Z0.5-2nd). After nitrogen-doped modification, the Q_e of UrGlu-450Z0.6-2nd for nitrate ions significantly increased. Moreover, whether the samples were activated once, twice, or three times, there was little difference in their adsorption capacities, indicating that the composition of the adsorbent remained relatively stable during the thermal decomposition process. The proportion of unreacted raw materials was high in the sample obtained after the first activation, and the Q_e of the sample after the third activation did

not show significant improvement. Therefore, considering factors such as raw material utilization and energy conservation, the second activation process was optimal.

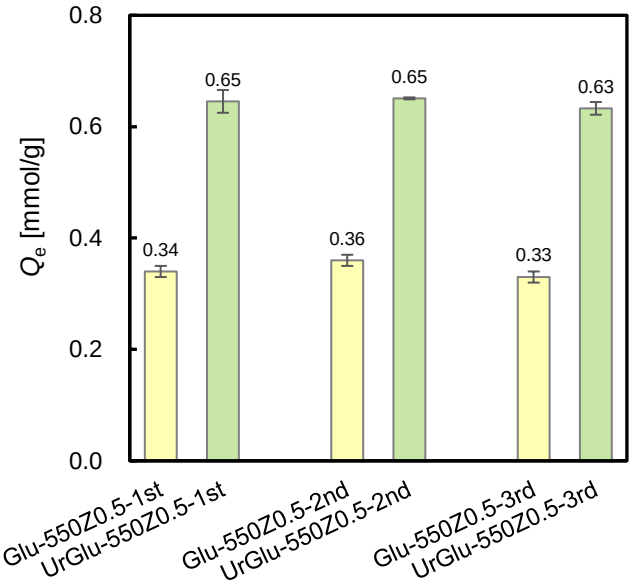

Fig. 4-3. Effect of different activation processes on nitrate adsorption. (pH 3.0, C_0 = 200 mg/L, dosage of 2 g/L)

The influence of the amount of activator $ZnCl_2$ and nitrogen-containing reagent urea on the Q_e (C_0 = 200 mg/L, pH 3.0) of the adsorbent can be seen in **Fig. 4-4 (a)** and **(b)**. One can be concluded that the addition of $ZnCl_2$ has little effect on the Q_e. In the process of increasing the mass of $ZnCl_2$ from 15 g to 25 g, there was only a slight difference of 0.02-0.03 mmol/g in Q_e. Simultaneously, after undergoing pre-treatment at 110°C, all intermediates exhibited a porous foam-like structure accompanied by volume expansion. From the results regarding the influence of urea on Q_e, it can be observed that the Q_e exhibited a trend of initially increasing and then decreasing with the increasing usage of urea. However, when the amount of urea continued to increase to 25 g, Q_e decreased from 0.73 mmol/g to 0.64 mmol/g. It is worth noting that at this point, the intermediates after pre-treatment did not exhibit a porous foam-like structure. This indicates that the specific macroscopic changes in the appearance of these intermediates to some extent affect the final Q_e of the adsorbent. To explain the special

phenomenon, it is necessary to start from the composition of the raw material reagents. When only glucose was used as the raw material (without $ZnCl_2$ activation) for pre-treatment at 110°C, a flowable brown viscous liquid was obtained. However, when $ZnCl_2$ activator was added to the glucose, the product after pre-treatment changes from a viscous liquid to a black hard solid. This is due to the strong dehydrating action exhibited by $ZnCl_2$ during the pre-treatment process. However, at this point, there was no appearance of the brown porous foam-like intermediate, and Q_e was only 0.36 mmol/g. However, it is worth noting that when an appropriate amount of nitrogen-containing reagent urea was added, this special intermediate structure appeared. Simultaneously, the adsorption capacity of nitrate ions by the adsorbent also pleasantly increased, with Q_e rising to 0.73 mmol/g. Moreover, when the urea content was too high, the intermediate did not exhibit a porous foam-like structure but instead became a hard solid. The adsorption capacity also significantly decreased (Q_e was 0.64 mmol/g) at the same time. The results indicated that urea was the primary factor influencing the formation of the porous foam-like intermediate in the reactant system, and this particular intermediate structure directly affected the Q_e of the adsorbent. Therefore, it could be explained that this particular phenomenon may be attributed to the self-decomposition of urea, as well as the interaction between urea and glucose, which likely acted similarly to the initial stages of the classic Maillard reaction, such as the following reaction formula:

$$NH_2CONH_2 \rightarrow NH_3 + HNCO \quad (4\text{-}3)$$

$$HNCO + H_2O \rightarrow NH_3 + CO_2 \quad (4\text{-}4)$$

$$C_6H_{12}O_6 + NH_3 \rightarrow Glucosamine + H_2O \quad (4\text{-}5)$$

Therefore, the glucose, presenting as a viscous liquid at 110°C, in which bubbles were formed due to the release of gases resulting from the partial decomposition of urea and the reaction of glucose with ammonia. Subsequently, under the activation of $ZnCl_2$ at 100°C, it underwent sugar-blowing [22], drying, and shaping, ultimately forming the brown porous foam-like intermediate that we observed. However, an excess amount of urea in the reactant system leads to an increase in viscosity, and at this point, the rate of gas generation exceeds their diffusion and escape rate within the system, preventing the formation of the stable foam structure, thus restricted the volume expansion. In summary, the pre-treatment process ensures a more uniform distribution of nitrogen within the carbon source, which facilitates the subsequent fixation of

nitrogen onto the carbon framework during the post-treatment process, subsequently enhances the adsorption capacity of the adsorbent for nitrate ions.

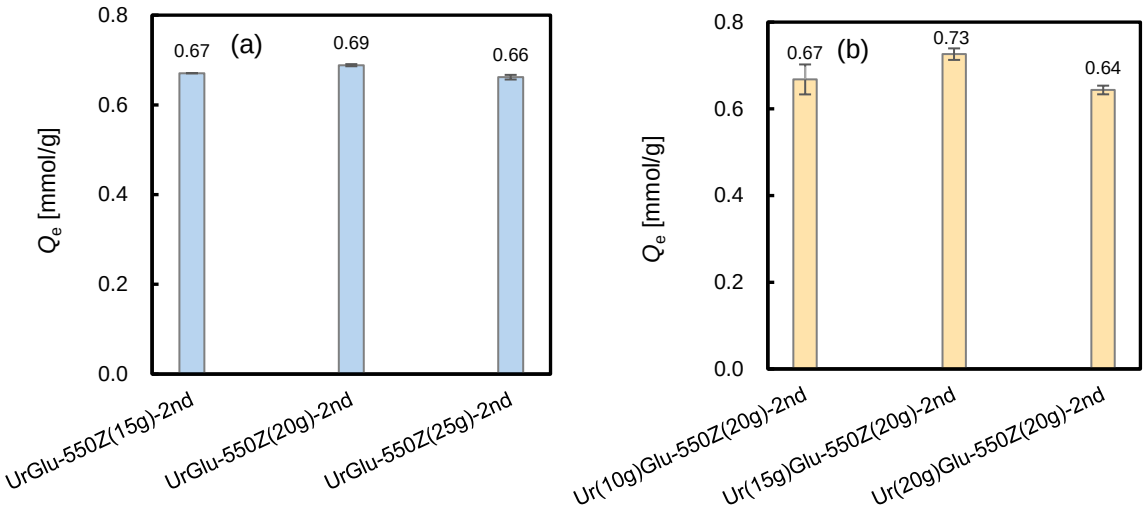

Fig. 4-4. Effect of different amounts of (a) $ZnCl_2$ and (b) urea on nitrate adsorption. (pH 3.0, C_0 = 200 mg/L, dosage of 2 g/L)

The experiment also investigated the effects of different activation temperatures (400, 450, 500°C) and various activating agents ($ZnCl_2$, $MgCl_2$, Na_2CO_3) on the adsorption capacity of the adsorbent. **Fig. 4-5 (a)** and **(b)** show the adsorption performance of the adsorbents prepared under different conditions in nitrate solutions at pH 3.0 and pH 5.0, respectively. The results showed that when the temperature increased from 450°C to 550°C, Q_e exhibited a decreasing trend, with Q_e dropping from 0.78 mmol/g to 0.73 mmol/g at pH 3.0 and from 0.76 mmol/g to 0.64 mmol/g at pH 5.0. There was no significant difference in Q_e between 400°C and 450°C. However, considering that the sample at 450°C had a more balanced Q_e in nitrate solutions at both pH 5.0 and pH 3.0, the optimal activation temperature for the post-treatment was chosen to be 450°C. $MgCl_2$ and Na_2CO_3 are also commonly used as activating agents in the preparation of carbon materials. Therefore, for comparison, they were also adapted in this part of the experiment. As shown in **Fig. 4-5 (b)**, compared to $MgCl_2$ and Na_2CO_3, the adsorbent activated with $ZnCl_2$ exhibited the most effective nitrate adsorption performance. At pH 3.0, the Q_e of Urglu-4.5M0.6-2nd and Urglu-4.5N0.6-2nd decreased by 24% and 88%, respectively,

compared to Urglu-450Z0.6-2nd. Under pH 5.0 conditions, the decrease was 43% and 91%, respectively. It can be inferred that $ZnCl_2$, as the activating agent, played a decisive role in successfully introducing nitrogen functional groups onto the carbon surface during the activation process after pre-treatment.

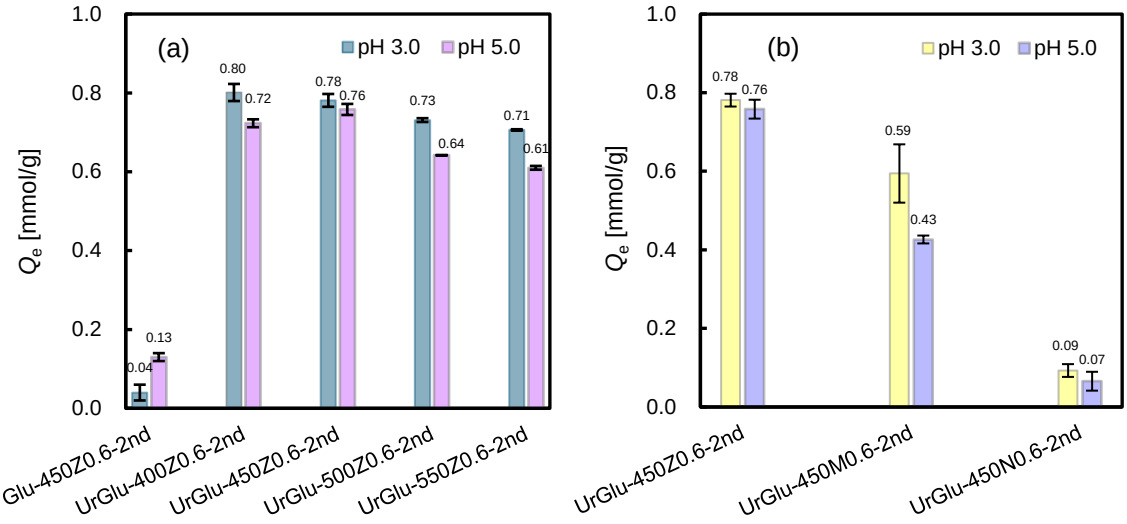

Fig. 4-5. Effect of different (a) activation temperatures and (b) activators on nitrate adsorption. (C_0 = 200 mg/L, dosage of 2 g/L)

In summary, the appearance of the special brown porous foam-like intermediate during the pre-treatment process can aid in a more uniform distribution of nitrogen within the carbon source. Consequently, this facilitates the subsequent fixation of nitrogen onto the carbon framework in the post-treatment. The adsorbent UrGlu-450Z0.6-2nd, obtained under the optimal preparation conditions, exhibited a Q_e of 0.78 mmol/g in nitrate solution at pH 3.0 and 0.76 mmol/g at pH 5.0. UrGlu-450Z0.6-2nd showed a significant improvement in Q_e compared to the adsorbents reported in chapter 2 at pH 5.0 (0.69 mmol/g) [18]. The adsorbent UrGlu-450Z0.6-2nd prepared under the optimal conditions and the reference sample Glu-450Z0.6-2nd were used as the main research subjects in the subsequent sections.

4.3.2 Characterization

The structural characteristics and surface chemistry of Glu-450Z0.6-2nd and UrGlu-

450Z0.6-2nd were determined and analyzed. The results of their specific surface area and porous structure are listed in **Table 4-1**. Glu-450Z0.6-2nd had a Brunauer-Emmett-Teller (BET) surface area (S_{BET}) of 1675 m^2/g, which sharply dropped to 6.13 m^2/g (UrGlu-450Z0.6-2nd) upon modification by the nitrogen-doped surface modification method using $ZnCl_2$ as the activator. With the S_{BET} of UrGlu-450Z0.6-2nd decreasing by 273 times, both V_{total} and V_{micro} decreased by 74 times as well. It can be inferred that during the surface modification process, nitrogen deposition blocked the micro and mesopores on the carbon surface, restricting the entry and adsorption of N_2, consequently reducing the S_{BET} and V_{micro} obtained from the BET analysis. The V_{meso} of modified UrGlu-450Z0.6-2nd also decreased from 0.076 cm^3/g to 0.004 cm^3/g. Although the V_{meso} decreased by 0.072 cm^3/g, based on the percentage of V_{meso} to V_{total}, it did not decrease. The mesopore volume percentage in Glu-450Z0.6-2nd was 10%, while in UrGlu-450Z0.6-2nd it was 40%. At the same time, with the increase in the percentage of V_{meso}, the D_{avg} increased from the original 0.78 nm to 6.81 nm. This was also due to the disappearance of the majority of micropores in the reference material and the well-preserved mesoporous structure in the modified material. The structure of mesopores (2-20 nm) can provide sufficient pathways for internal reaction spaces between pollutants and adsorbents, allowing nitrate ions to move rapidly to adsorption sites, thereby accelerating the adsorption process [23]. Therefore, excellent adsorption rates of UrGlu-450Z0.6-2nd can be expected during the adsorption process of nitrate ions. In general, the Q_e of carbonaceous materials is positively correlated with their S_{BET}. However, based on the Q_e listed in **Table 4-1**, despite the S_{BET} of UrGlu-450Z0.6-2nd became 273 times smaller than that of Glu-450Z0.6-2nd, its adsorption capacity was 8.8 times higher than that of UrGlu-450Z0.6-2nd. This indicates that during the surface modification of carbon materials, while micropores are being blocked, effective active sites are introduced. Introducing effective active sites is more beneficial for enhancing the adsorption performance of carbonaceous materials than attempting to increase the S_{BET} of the adsorbent.

Table 4-1 The specific surface area and porous structure of carbonaceous adsorbents.

Sample	Q_e (mmol/g)	S_{BET} (m^2/g)	V_{total} (cm^3/g)	V_{micro} (cm^3/g)	$V_{meso}\times10$ (cm^3/g)	D_{avg} (nm)
Glu-450Z0.6-2nd	0.09	1675	0.74	0.74	0.76	1.78
UrGlu-450Z0.6-2nd	0.79	6.13	0.01	0.01	0.04	6.81

Table 4-2 represents the surface bulk elemental content and nitrogen distribution of Glu-450Z0.6-2nd and UrGlu-450Z0.6-2nd. Clearly, the chemical composition of Glu-450Z0.6-2nd indicated a low nitrogen content. After surface modification with nitrogen-doped, the nitrogen content of UrGlu-450Z0.6-2nd significantly increased from 1.18% to 17.0%. At the same time, the nitrogen modification process was accompanied by the decomposition of hydrogen and oxygen elements. The hydrogen content had decreased by 0.06%, and that of oxygen content decreased by 1.6%. This indicates that during the modification process, while the beneficial nitrogen-containing functional groups were introduced, some unfavorable functional groups containing hydrogen and oxygen were also decomposed. For example, carboxyl and hydroxyl groups may decompose into CO_2 and H_2O, leading to a decrease in the content of hydrogen and oxygen elements in the sample. Therefore, there was also a slight decrease in the carbon content. It is worth noting that acidic oxygen-containing functional groups such as carboxyl and hydroxyl groups typically dissociate in aqueous solutions, generating negative charges. These negative charges then form a negatively charged layer on the carbon surface, which repels nitrate anions that also carry negative charges. Additionally, such acidic oxygen-containing functional groups also exhibit strong hydrophilicity, resulting in the formation of a hydration layer. It will further weaken the accessibility and affinity of the carbon material surface [24]. Therefore, acidic oxygen-containing functional groups on the surface of carbon materials inhibit the adsorption of nitrate anions through charge repulsion and competitive adsorption. The decrease in the content of acidic oxygen-containing functional groups in carbonaceous materials after modification with nitrogen-containing reagents is beneficial for enhancing the adsorption performance of the adsorbent towards nitrate ions.

To further demonstrate the success of nitrogen-doped and the detailed atomic environment of nitrogen on the surface of carbon materials, XPS measurements were conducted. The original

XPS spectra of the N1s signal for the two types of adsorbents are shown in **Fig. 4-6**. Through peak deconvolution, four types of nitrogen-containing functional groups can be identified in the sample: pyridinic-N (N-6, 398.7 ± 0.3 eV), pyrrolic-N (N-5, 400.4 ± 0.3 eV), quaternary-N (N-Q, 401.3 ± 0.3 eV), and pyridine-N-oxide (N-X, 402.0-403.0 eV) [25]. By comparing the two spectra in **Fig. 4-6**, it is evident that the N1s feedback intensity of UrGlu-450Z0.6-2nd was much higher than that of Glu-450Z0.6-2nd. Additionally, it can be easily observed that the peak of N-Q for UrGlu-450Z0.6-2nd has significantly increased. Combining the bulk elemental analysis of the adsorbents with the XPS N1s analysis results, the relative content of each nitrogen configuration can be obtained, as shown in **Table 4-2**. By comparing the relative content of each nitrogen functional group in the table, it can be observed that the content of the four nitrogen functional groups on the surface of the modified adsorbent has indeed increased. Specifically, the content of N-6, N-5, N-Q, and N-X has increased by 10.0, 12.3, 343.0, and 172.7 times, respectively. Although N-6 and N-5 dominated in both samples, their presence creates a slight negative charge due to their ability to provide electrons and form conjugated systems with the carbon ring, which can repel anions [26]. Therefore, they did not contribute to the adsorption of nitrate anions on the carbonaceous adsorbent. Furthermore, since N-X exists in various oxidation states depending on different chemical environments, and most of these forms of nitrogen atoms exhibit neutral or negative charges, they also cannot participate in the adsorption process of nitrate ions. It is worth noting that the content of N-Q has the biggest increase among the four nitrogen functional groups. It is considered to be quaternary nitrogen doped within the graphene plane, connected to three carbon atoms, and typically carrying a positive charge. Therefore, this particular and stable nitrogen-doped form is bound to be beneficial for enhancing the adsorption of nitrate anions on the surface of carbon materials. This also provides strong theoretical support for the previous hypothesis that explains why there is a qualitative leap in Q_e despite the dramatic decrease in the S_{BET} of carbon materials. It is convinced that introducing effective functional groups suitable for the adsorption of target pollutants is more advantageous than attempting to increase the specific surface area of carbonaceous materials.

Table 4-2 Bulk elemental composition and configuration of nitrogen species of carbonaceous adsorbents.

Sample	Bulk elemental composition (wt%)				Configuration of nitrogen species (wt%)			
	C	H	N	O*	N-6	N-5	N-Q	N-X
Glu-450Z0.6-2nd	78.2	2.43	1.18	18.2	0.43	0.74	0.01	0.00
UrGlu-450Z0.6-2nd	64.0	2.37	17.0	16.6	4.31	9.07	3.43	0.19

*By balance

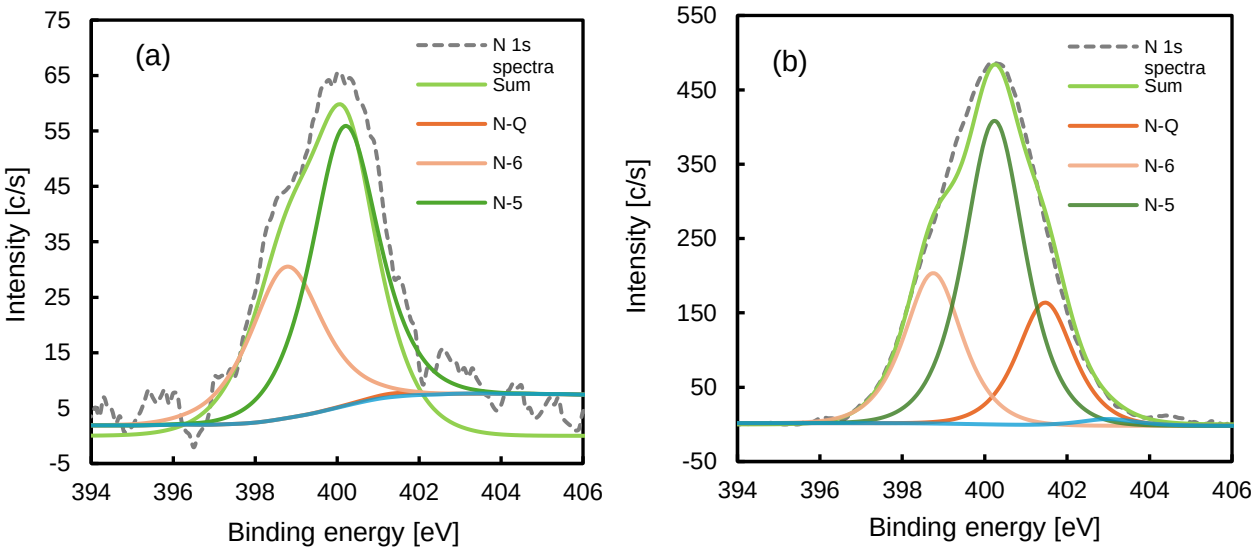

Fig. 4-6. XPS N1s spectra of (a) Glu-450Z0.6-2nd and (b) UrGlu-450Z0.6-2nd.

4.3.3 Effect of solution pH

Different solution pH values can cause ionization and changes in the surface charge of the adsorbent, thereby affecting the nitrate adsorption process. Therefore, specific experiments were designed to investigate the adsorption performances of the adsorbent in nitrate solutions with an initial concentration of 200 mg/L over a pH range of 2.0-12.0 (dosage of 2 g/L, room temperature, 25 ± 0.5°C). **Fig. 4-7** shows the results of the zero point of charge of the adsorbent and the effect of solution pH on the adsorption capacity. The specific zero point of charge value of the adsorbent reflects the protonation/deprotonation behavior of surface functional groups

under certain pH conditions. Through the pH drift method, it was found that Glu-450Z0.6-2nd and UrGlu-450Z0.6-2nd have the same pH_{pzc} of 3.0, as shown in **Fig. 4-7 (a)**. From the figure, it can also be observed that even the initial pH of the solution was 10.0, the final pH of the solution always decreased to around 3.0. This may be because the adsorbent surface may still contain acidic functional groups that are easily protonated, such as hydroxyl and carboxyl groups. These groups are easily protonated under low pH conditions, resulting in a positively charged surface. As the pH increases, these acidic groups gradually lose protons, causing the surface to become negatively charged. Therefore, it can be inferred that the adsorbent exhibited the highest nitrate adsorption capacity under specific acidic conditions.

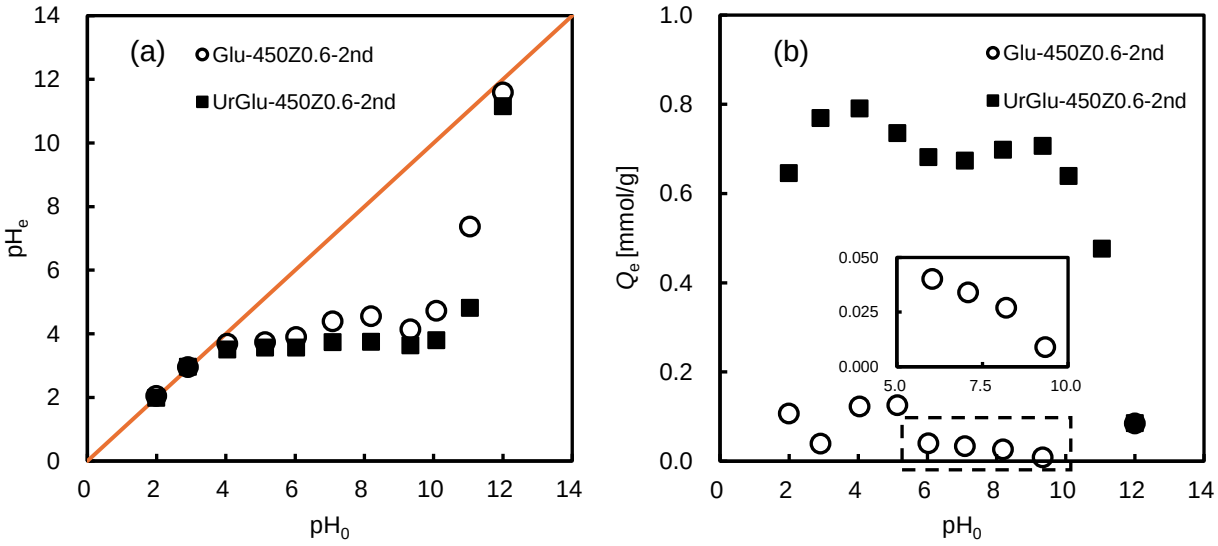

Fig. 4-7. (a) The pH of the point of zero charge (pH_{pzc}) and (b) effect of solution pH on the adsorption of nitrate. (C_0 = 200 mg/L, dosage of 2 g/L)

According to the results listed in **Fig. 4-7 (b)**, it was clear that the Q_e of UrGlu-450Z0.6-2nd was much higher than that of Glu-450Z0.6-2nd at all solution pH levels. Regarding the Q_e of UrGlu-450Z0.6-2nd, at the extremely low initial solution pH (pH < 2.0), its adsorption capacity was only 0.65 mmol/g. This could be due to the presence of a large amount of chloride ions in the solution, which may hinder the adsorption of nitrate ions. Subsequently, as the solution pH increased to around 4.0, its Q_e showed an increasing trend. This could be attributed to the decrease in the concentration of competing ions in the solution at this pH. Additionally, in this situation, the solution pH was lower than the pH_{pzc}, making the functional groups on the adsorbent surface more prone to protonation, thereby increasing the Q_e of UrGlu-450Z0.6-2nd.

It exhibited a peak Q_e at pH 4.0, reaching 0.79 mmol/g. Hereafter, as the pH continued to rise to around 10.0, Q_e was surprisingly maintained a relatively stable level. On the one hand, even though the solution pH has surpassed the pH_{pzc}, the functional groups on the adsorbent surface are more prone to deprotonation. On the other hand, another widely present C-π sites on the carbon material surface can contribute to the adsorption of nitrate ions by attracting protons and converting from negative to positive charge. Therefore, the adsorption capacity of the C-π sites largely depends on the pH of the solution. In alkaline solutions, the weakening of its ability to attract protons leads to a decrease in Q_e. The same conclusion was also reported in chapter 2 of this thesis [27]. However, as shown in **Fig. 4-7 (b)**, under the combined influence of these two factors, the Q_e value of UrGlu-450Z0.6-2nd did not undergo a sharp decrease as the solution pH gradually increased; instead, it remained relatively stable. This result undoubtedly validated the conclusions drawn from the physical characterization of the adsorbent, revealing that the introduction of N-Q through nitrogen-doped surface modification methods is an effective nitrate adsorption site. It can maintain the Q_e of the adsorbent for nitrate ions within a certain pH range. Finally, when the solution pH exceeded 10.0, Q_e values experienced a sharp decline, reaching as low as 0.1 mmol/g. This could be explained by the fact that when the solution pH was too high, the concentration of hydroxyl ions in the solution became excessive, leading to a preference for hydroxyl ions to occupy the adsorption sites on the adsorbent surface. Consequently, this resulted in a sharp decrease in Q_e. Considering the zero point of charge depicted in **Fig. 4-7 (a)**, it can be observed that after the initial pH of the solution (pH_0) exceeded 10.0, the corresponding equilibrium pH (pH_e) also shifted from its previous relatively stable trend to a sharp increase. This indicates that the excessive concentration of hydroxyl ions in the solution weakened the deprotonation capacity of the functional groups on the adsorbent surface. To further validate the significance of N-Q in the adsorption process of nitrate ions, experiments were conducted on adsorbents that had not undergone nitrogen-doped to investigate the effect of solution pH on the adsorption capacity of nitrate ions. From **Fig. 4-7 (b)**, it can be observed that Glu-450Z0.6-2nd, due to its extremely low adsorption capacity, exhibited less obvious changes in Q_e with variations in solution pH. Its optimal adsorption capacity at pH 5.13 was only 0.13 mmol/g, which may cause bias into the conclusions. Therefore, we will introduce the optimized sample Glu-550Z0.5-2nd into this section of the discussion to more intuitively

elucidate the mechanism of the adsorbent. The bulk elemental composition and XPS N1s analysis results of Glu-550Z0.5-2nd can be found in **Table 4-3**. **Fig. 4-8** shows the results of pH_{pzc} and the influence of solution pH on Glu-550Z0.5-2nd, it can be observed that the Q_e of Glu-550Z0.5-2nd exhibited a continuous decrease trend over the pH range of 2.0-12.0. According to **Table 4-3**, it was evident that the surface content of N-Q in Glu-550Z0.5-2nd was extremely low, only 1/52 of UrGlu-450Z0.6-2nd content. Therefore, in the absence of effective N-Q adsorption sites, the Q_e of the adsorbent cannot maintain relative stability. This result further illustrated the effectiveness of nitrogen-doped surface modification and the dominant role of N-Q active adsorption sites in the adsorption process.

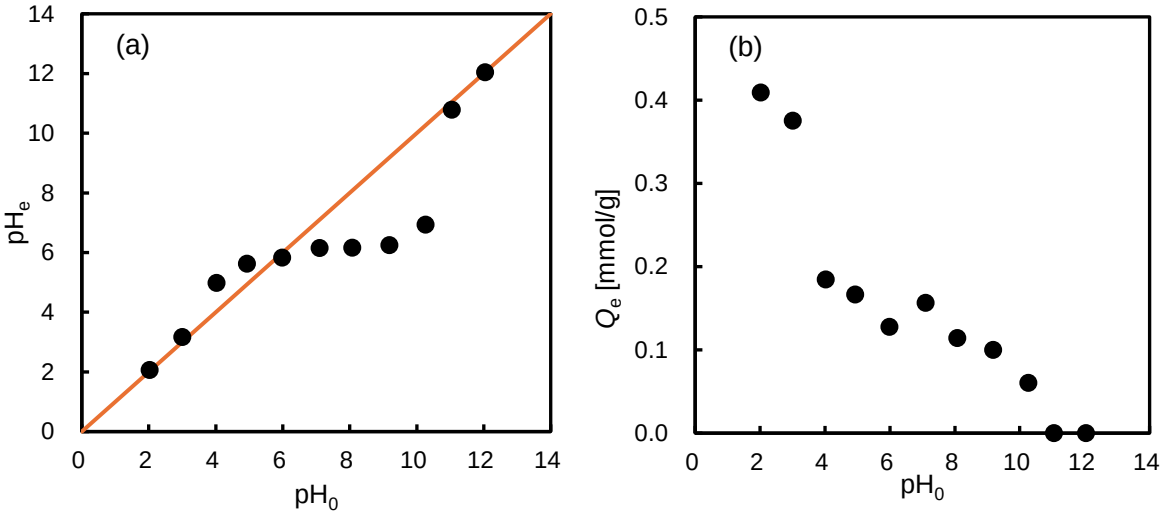

Fig. 4-8. (a) The pH of the point of zero charge (pH_{pzc}) and (b) effect of solution pH on the adsorption of nitrate by Glu-550Z0.5-2nd. (C_0 = 200 mg/L, dosage of 2 g/L)

Table 4-3 Bulk elemental composition and XPS N1s analysis of Glu-550Z0.5-2nd.

Sample	Elemental analysis [wt%]				XPS (N1s) analysis [wt%]			
	C	H	N	O	N-6	N-5	N-Q	N-X
Glu-5.5Z0.5-2nd	85.0	1.87	1.08	12.1	0.56	0.42	0.08	0.01

4.3.4 Adsorption isotherms

The study of adsorption isotherms plays a significant role in both scientific research and industrial application. Adsorption isotherms provide information about the interactions between adsorbent and adsorbate when the adsorption process reaches equilibrium at a specific temperature. After fitting experimental data using the Langmuir [28] and Freundlich [29] isotherm models, the obtained parameters can assist in describing the adsorption equilibrium process, determining adsorption capacity, and understanding adsorption mechanisms. Nitrate adsorption on Glu-450Z0.6-2nd and UrGlu-450Z0.6-2nd was conducted in nitrate solutions with the equilibrium concentration range from 0.1 to 10.0 mmol/L at the solution pH of 3.0 (dosage of 2 g/L, room temperature, 25 ± 0.5°C). As shown in **Fig. 4-9**, the experimental results indicated a significant increase in the Q_e of UrGlu-450Z0.6-2nd with the increasing equilibrium concentration (C_e) of nitrate ions. After that, as C_e continued to increase, the rate of increase in Q_e slowed down. The Q_e of Glu-450Z0.6-2nd shows a slight upward trend with the increase in C_e. This is because when the amount of adsorbent is constant, effective adsorption sites are abundant in low concentration nitrate solutions, leading to a rapid increase in Q_e. In relatively high concentration ranges of the solution, empty adsorption sites are quickly occupied. At this point, the high mass transfer driven by the high concentration solution propels the nitrate ions into the deep and narrow pores. Consequently, the rate of increase in Q_e slows down.

The parameters obtained by fitting the experimental data using the Langmuir and Freundlich isotherm models are listed in **Table 4-4**. The results indicated that the coefficient of determination (R^2) of the Langmuir isotherm model for UrGlu-450Z0.6-2nd was 0.991, which was higher compared to the Freundlich isotherm model (0.965). Moreover, the corresponding sum squares due to error (*SSE*) and mean square error (*MSE*) obtained from fitting the Langmuir isotherm model were smaller compared to those of the Freundlich isotherm model. Thus, the Langmuir isotherm model can effectively describe the adsorption process, suggesting that nitrate adsorption on UrGlu-450Z0.6-2nd could occur in a monolayer adsorption. The maximum adsorption capacity (X_m) predicted by the Langmuir isotherm mode of UrGlu-450Z0.6-2nd was 1.18 mmol/g, which exceeded the experimental Q_e (1.11 mmol/g) at the initial nitrate concentration of 500 mg/L. This indicates that the adsorbent did not reach saturation at this concentration of the nitrate solution. The X_m of Glu-450Z0.6-2nd was 0.30 mmol/g, which

was not significantly different from the experimental Q_e (0.29 mmol/g) at the initial nitrate concentration of 500 mg/L. This indicates that Glu-450Z0.6-2nd was already saturated at this point, and the nitrogen-modified adsorbent exhibited a certain enhancement in adsorption potential. Additionally, the K_e value of UrGlu-450Z0.6-2nd was 1.54 L/mmol, which is 6.16 times higher than that of Glu-450Z0.6-2nd. This reveals that the nitrogen-doped modified adsorbent, due to the introduction of effective functional groups, significantly improved the affinity between the adsorbent and the adsorbate, thereby enhancing the adsorption capacity of the adsorbent for nitrate ions.

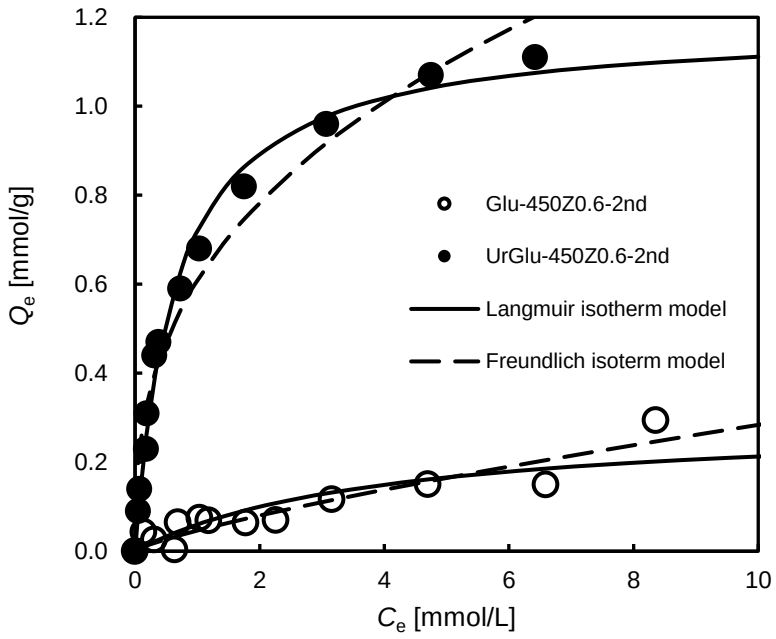

Fig. 4-9. Adsorption isotherms of nitrate on Glu-450Z0.6-2nd and UrGlu-450Z0.6-2nd by Langmuir and Freundlich isotherm models. (pH 3.0, room temperature, 25 ± 0.5℃)

4.3.5 Adsorption kinetics

The study of adsorption kinetics allows for the assessment of adsorption efficiency, thereby aiding in better control of the adsorption process. Furthermore, fitting the experimental data using pseudo-first-order and pseudo-second-order kinetic models enables further description of the adsorption process and facilitates analysis of the adsorption mechanism. **Fig. 4-10** displays the experimental data of Glu-450Z0.6-2nd and UrGlu-450Z0.6-2nd, along with

the fitting curves of the two kinetic models for their adsorption processes. From the figure, it is evident that there was a significant difference in the adsorption behavior of the two adsorbents over time. The Q_e of UrGlu-450Z0.6-2nd sharply increased within the first 5 min of adsorption, followed by a gradual slowing of the upward trend after 5 min. After 15 min, the Q_e gradually approached equilibrium, and thereafter, the change in Q_e remained constant over time. Within the first 5 min of adsorption, the adsorbent surface contained numerous N-Q active adsorption sites, facilitating rapid nitrate ion adsorption. However, in time nitrate ions occupied part of the active sites, and they are also subjected to electrostatic repulsion from the adsorbed nitrate ions, resulting in a slower increase in Q_e. UrGlu-450Z0.6-2nd achieved a nitrate adsorption capacity of 0.72 mmol/g within just 5 min and reached adsorption equilibrium within 15 min (C_0 was 200 mg/L, dosage of 2 g/L), making it an adsorbent with excellent adsorption rate. According to Shen et al., the kinetic study of polypyrrole-modified plastic-carbon reported a Q_e of 0.73 mmol/g for nitrate ions after 350 min (C_0 was 30 mg/L, dosage of 10 g/L) [30]. Zhang et al. studied the equilibrium time for nitrate ions adsorption using modified straw, which was approximately 2 h (C_0 was 100 mg/L, dosage of 1 g/L) [31]. Thus, the adsorbents developed in this study exhibit highly attractive adsorption efficiency.

Table 4-5 displays the corresponding kinetic parameters obtained by fitting using the two models. By analyzing **Table 4-5**, the R^2, *SSE*, *MSE* can be used to evaluate the fitting accuracy of the models to the data. As a result, the pseudo-second-order kinetic model yielded the closest R^2 value to 1 (0.993), with lower *SSE* and *MSE* values (0.42×10^{-2}, 0.02×10^{-2}), indicating that the pseudo-second-order kinetic model could more reasonably describe the adsorption of nitrate on UrGlu-450Z0.6-2nd. The rate of this adsorption process was directly proportional to the concentration of the adsorbate and the number of adsorption sites. Simultaneously, it can be inferred that the Q_e and k_2 predicted by the pseudo-second-order kinetic model are closest to the intrinsic properties of the adsorbent. It is noteworthy that the theoretical saturation adsorption capacity predicted by the pseudo-second-order kinetic model was 0.82 mmol/g, whereas in **Section 4.3.4** of the adsorption isotherm study, the X_m of UrGlu-450Z0.6-2nd obtained from the Langmuir adsorption isotherm fitting was 1.18 mmol/g. Therefore, it can be inferred that the increasing concentration of nitrate ions in the solution provides a higher mass transfer driving force, allowing pollutant ions to move and be adsorbed towards deeper

Table 4-4 Langmuir and Freundlich isotherm parameters for nitrate adsorption on Glu-450Z0.6-2nd and UrGlu-450Z0.6-2nd.

Sample	Langmuir isotherm model					Freundlich isotherm model				
	X_m (mmol/g)	K_e (L/mmol)	R^2	*SSE*	*MSE*	*1/n*	K_F ((mmol/g)(L/mmol)$^{1/n}$)	R^2	*SSE*	*MSE*
Glu-450Z0.6-2nd	0.30	0.25	0.773	0.02	0.03	0.79	0.05	0.881	0.01	0.13
UrGlu-450Z0.6-2nd	1.18	1.54	0.991	0.02	0.03	0.37	0.61	0.965	0.06	0.07

Table 4-5 Kinetic parameters for nitrate adsorption on Glu-450Z0.6-2nd and UrGlu-450Z0.6-2nd.

Sample	Pseudo-first-order model					Pseudo-second-order model				
	Q_e (mmol/g)	k_1 (min^{-1})	R^2	SSE ×10^{-2}	MSE ×10^{-2}	Q_e (mmol/g)	k_2 (g/mmol min)	R^2	SSE ×10^{-2}	MSE ×10^{-2}
Glu-450Z0.6-2nd	0.09	0.06	0.773	2.43	0.13	0.10	0.96	0.315	2.37	0.13
UrGlu-450Z0.6-2nd	0.79	0.50	0.991	0.49	0.03	0.82	1.39	0.993	0.42	0.02

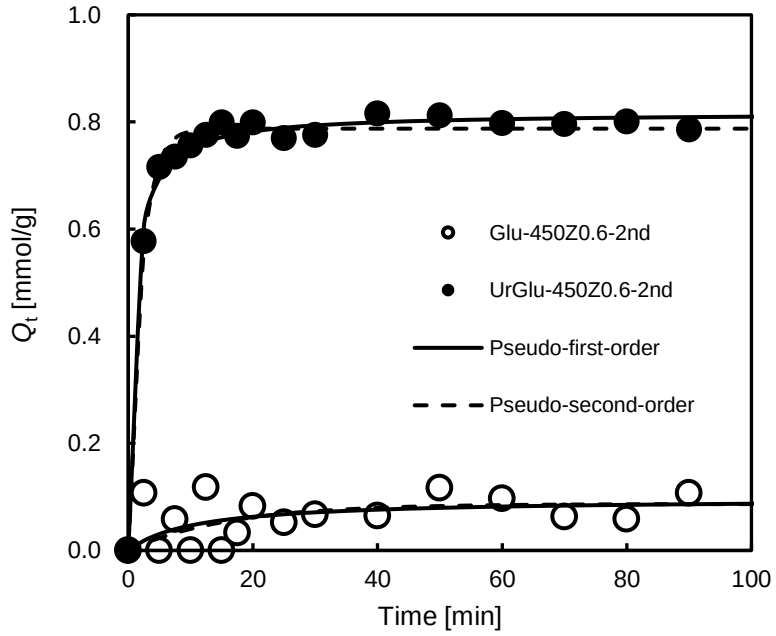

Fig. 4-10. Adsorption kinetics of nitrate on Glu-450Z0.6-2nd and UrGlu-450Z0.6-2nd fitted by Pseudo-first-order and Pseudo-second-order kinetic models. (C_0 = 200 mg/L, pH 3.0)

adsorption sites on the surface of the adsorbent. Through the modified adsorbent, it is evident that the adsorption rate constant k_2 increased from 0.96 g/mmol min to 1.39 g/mmol min. This confirms that the introduction of effective active sites N-Q in UrGlu-450Z0.6-2nd makes it more conducive to the adsorption of nitrate ions, despite the decrease in the adsorbent's S_{BET} by several orders of magnitude. The above conclusions further indicate that N-Q is an effective type of nitrate adsorption site.

4.3.6 Fixed-bed column adsorption

The preliminary investigation into the adsorption performance of Glu-450Z0.6-2nd and UrGlu-450Z0.6-2nd for nitrate ions under fixed-bed column mode was conducted. The fixed-bed column adsorption approached closely resembles the actual operational conditions in industrial applications. Through this mode of study, the performance of adsorbents in practical applications can be more accurately reflected. Additionally, the conclusions drawn from this study can provide guidance on the feasibility and effectiveness of adsorbents in large-scale applications. The experiment was conducted in a nitrate solution with a concentration of 200 mg/L and a pH of 3.0. The breakthrough curves of nitrate ions adsorbed by the two adsorbents

in fixed-bed column adsorption are depicted in **Fig. 4-11**. The breakthrough curves are typically represented by plotting C_t/C_0 (the ratio of the concentration of nitrate in the effluent at time t to the initial nitrate concentration) versus time t. When assessing the effectiveness of breakthrough curves, the definition of the breakthrough point is an important parameter. If the breakthrough point occurs later as time progresses, it indicates that the material is more effective in purifying pollutants. Clearly, the breakthrough point for Glu-450Z0.6-2nd occurred at the beginning of the adsorption process, while UrGlu-450Z0.6-2nd continued to exhibit an excellent adsorption characteristic under the fixed-bed column adsorption mode. Combining the corresponding parameters listed in **Table 4-6**, the breakthrough times (t_b) for the adsorbents increased from 8 min to 136 min after nitrogen-doped modification, extending by 17 times. Additionally, the corresponding adsorption capacity (Q_b) of Glu-450Z0.6-2nd before the breakthrough point increased from 0.08 mmol/g to 0.70 mmol/g, amplifying by 8.8 times. Before the breakthrough point, the removal efficiency (R_b%) of nitrate ions for both adsorbents were 100%. This is because there were sufficient adsorption sites available to adsorb nitrate ions effectively. As the adsorption time progressed, the effective adsorption sites were gradually occupied by nitrate ions, and the adsorbents tended toward saturation. When their adsorption processes reached saturation points, the adsorption capacities (Q_s) of Glu-450Z0.6-2nd and UrGlu-450Z0.6-2nd were 0.14 mmol/g and 0.77 mmol/g, respectively. Hence, it can be observed that the adsorbent UrGlu-450Z0.6-2nd still exhibited an excellent performance under this simulated industrial application fixed-bed column adsorption mode. Therefore, promising application prospects can be anticipated for it in the field of water purification.

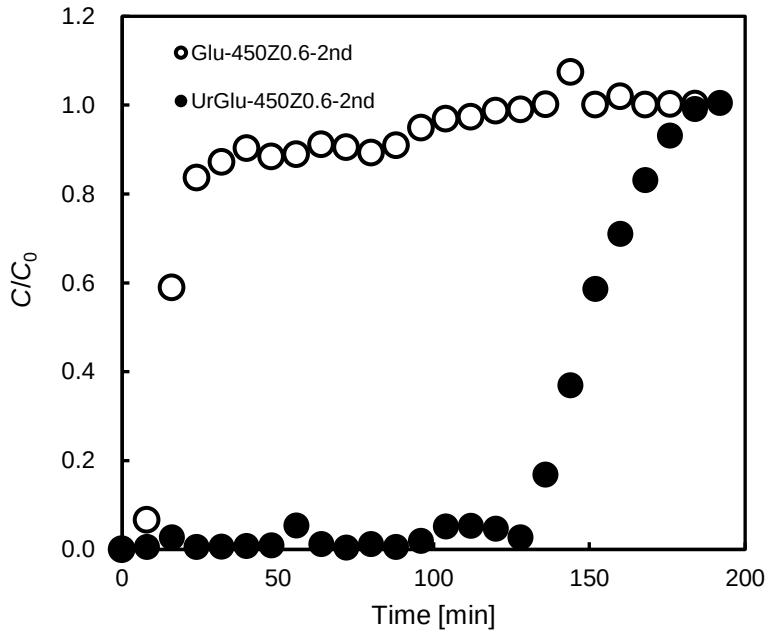

Fig. 4-11. Breakthrough curve of nitrate adsorption on Glu-450Z0.6-2nd and UrGlu-450Z0.6-2nd packed column. (C_0 = 200 mg/L, pH 3.0, m = 0.8 g, R = 1.25 mL/min)

Table 4-6 Parameters of fixed-bed column adsorption experiments.

Sample	t_b (min)	V_b (mL)	Q_b (mmol/g)	R_b%	t_s (min)	V_s (mL)	Q_s (mmol/g)	R_s%
Glu-450Z0.6-2nd	8	10	0.08	100	136	170	0.14	20
UrGlu-450Z0.6-2nd	136	170	0.70	100	192	240	0.77	80

4.3.7 Comparison of the adsorption capacity and N-Q amount with the previously developed adsorbents

The comparison of the preparation temperature of the previously developed adsorbent and the relationship between the adsorption capacity and N-Q amount of then was listed in **Table 4-7**. The results indicate that in the previous preparation methods involving the introduction of N-Q, a preparation temperature of over 800°C was typically required to shift the thermal equilibrium from pyridinic nitrogen (N-6) on carbon to N-Q. However, in the experimental system of this chapter, we found that a sufficient amount of N-Q could be directly generated at a processing temperature below 500°C. The preparation process of UrGlu-4.5Z0.6-2nd not only

significantly reduced the required preparation temperature but also exhibited a considerable adsorption capacity. This finding is beneficial for expanding its scope in practical industrial applications.

Table 4-7 Comparison of the Q_e and N-Q content with the previously developed adsorbents.

Sample	Preparation temperatures at each stage (°C)	N-Q content (wt.%)	Q_e at pH 3.0 (mmol/g)	Reference
PYR-7Z4-9.5HT10	700, 950	2.90	0.60	[16]
KF-8ST10-8AN20-9.5HT30-8ST30	800, 800, 950, 800	1.86	0.74	[17]
Py-7.0Z4-9.5HT10	700, 950	1.91	1.02	[26]
BAP6-8AN20-9.5HT30-8ST30	800, 950, 800	2.12	0.46	[32]
UrGlu-450Z0.6-2nd	450, 450	3.43	0.78	This chapter

4.3.8 Evaluation of the preparation cost of UrGlu-450Z0.6-2nd

The preparation cost of UrGlu-450Z0.6-2nd mainly includes the cost of reagent purchase and energy consumption. The primary raw materials required for the preparation of UrGlu-450Z0.6-2nd include glucose, urea, and zinc chloride. According to the adsorbent preparation process described in this chapter, 20 g of glucose, 15 g of urea, and 20 g of $ZnCl_2$ undergone pre-treatment process to obtain the brown porous foam-like intermediate, which can be used for three rounds of carbonization process. Therefore, based on the market prices of the reagents, the calculated raw material cost for producing each gram of adsorbent is approximately \$0.67 (glucose: \$31.32/500 g, urea: \$10.90/500 g, zinc chloride: \$19.82/500 g). The tubular furnace used in the laboratory has a power of 1.5 kW, so the electricity consumption for a single preparation of UrGlu-450Z0.6-2nd is 4.5 kWh. According to investigations, the electricity price in the laboratory is relatively high, making it unsuitable for accurately assessing the electricity cost in an industrial setting. Considering that the energy required for adsorbent preparation can be supplemented by additional energy from the carbonization of coal and wood in industrial

production, UrGlu-450Z0.6-2nd can regarded as a low-cost adsorbent with promising application potential.

4.4 Conclusion

This study successfully optimized a nitrogen-doped carbonaceous adsorbent, UrGlu-450Z0.6-2nd, which efficiently utilizes a single nitrogen source, and investigated its capacity for nitrate ions pollution remediation. The special brown porous foam-like intermediate facilitates the uniform distribution of nitrogen within the reactant system during the modification process, as well as the subsequent fixation of nitrogen on the carbon framework. In addition to being optimized for using a single nitrogen source, the adsorbent also reduced the required preparation temperature by 100°C and exhibited an increased adsorption capacity in nitrate solutions with a pH greater than 5.0 (compare with chapter 2). Adsorption studies results indicate that UrGlu-450Z0.6-2nd maintained high adsorption capacities for nitrate ions within a wide solution pH range of 2.0-10.0, which attributed to the positive role of N-Q adsorption sites. The Langmuir adsorption isotherm model and pseudo-second-order kinetic model can well describe the adsorption process of nitrate by UrGlu-450Z0.6-2nd, indicating that the adsorption occurred as monolayer adsorption on a homogeneous surface with the adsorbent having a limited and uniformly distributed number of adsorption sites. The Langmuir adsorption isotherm model predicted the maximum adsorption capacity (X_m) of 1.18 mmol/g for nitrate ions by UrGlu-450Z0.6-2nd, which is a favorable result. Furthermore, the adsorption performance of modified UrGlu-450Z0.6-2nd showed significant improvement under the fixed-bed column adsorption mode, which simulated practical application conditions. This further demonstrated the effectiveness of the nitrogen-doped surface modification method and the promising application prospects of UrGlu-450Z0.6-2nd in the field of water purification.

Reference

[1] J. Humphreys, R. Lan, S. Tao, Development and recent progress on ammonia synthesis catalysts for Haber-Bosch process, Adv. Energy Sustainability Res. 2 (2021) 2000043.

[2] S. Singh, J. Singh, A. G. Anil, V. Kumar, P. C. Ramamurthy, Nitrates in the environment: A critical review of their distribution, sensing techniques, ecological effects and remediation, Chemosphere 287 (2022) 131996.

[3] Y. Zhu, X. Li, Y. Si, X. Zhang, P. Sang, Y. Fu, Regulating dissolution chemistry of nitrates in carbonate electrolyte for high-stable lithium metal batteries, J. Energy Chem. 73 (2022) 422-428.

[4] M. H. Ward, R. R. Jones, J. D. Brender, T. M. de Kok, P. J. Weyer, B. T. Nolan, C. M. Villanueva, S. G. van Breda, Drinking water nitrate and human health: An updated review, Int J Environ Res Public Health. 215 (2018) 1557.

[5] S. F. Johnson, Methemoglobinemia: Infants at risk, Current Problems in Pediatric and Adolescent Health Care, 49 (2019) 57-67.

[6] K M. Moloantoa, Z. P. Khetsha, E. Heerden, J. C. Castillo, E. D. Cason, Nitrate water contamination from industrial activities and complete denitrification as a remediation option, Water 14 (2022) 799.

[7] A. E. Midaoui, F. Elhannouni, M. Taky, L. Chay, M. A M. Sahli, L. Echihabi, M. Hafsi, Optimization of nitrate removal operation from ground water by electrodialysis. Separ. Purif. Technol. 29 (2002) 235-244.

[8] T. Kikhavani, S. N. Ashrafizadeh, B. Van der Bruggen, Nitrate selectivity and rransport properties of a novel anion exchange membrane in electrodialysis, Electrochimica Acta 144 (2014) 341-351.

[9] L. Amor, M. Eiroa, C. Kennes, M. C. Veiga, Phenol biodegradation and its effect on the nitrification process, Water Res. 39 (2005) 2915-2920.

[10] S. W. How, C. X. Ting, J. Y. Yap, Effect of carbon-to-nitrogen ratio on high-rate nitrate removal in an upflow sludge blanket reactor for polluted raw water pre-treatment application, Sustain. Environ. Res. 31:16 (2021).

[11] A. A. Ahuchaogu, O. J. Chukwu, A. I. Obike, C. E. Igara, I. C. Nnorom, J. B. O. Echeme, Reverse osmosis technology, its applications and nano-enabled membrane, Int. J. Adv. Res.

Chem. Sci. 5 (2018) 20-26.

[12] M. A. Ahmed, S. Amin, A. A. Mohamed, Fouling in reverse osmosis membranes: monitoring, characterization, mitigation strategies and future directions, Heliyon 9 (2023) e14908.

[13] N. A. A. Qasem, R. H. Mohammed, D. U. Lawal, Removal of heavy metal ions from wastewater: a comprehensive and critical review. npj Clean Water 4:36 (2021).

[14] M. Machida, Y. Amano, F. Imazeki, Water purification with activated carbons (ACs): A short review-Influence of the textural and surface properties of ACs on the adsorptive removal of pollutants-, Tanso 270 (2015) 241-249.

[15] S. Wong, N. Ngadi, N. Inuwa, O. Hassan, Recent advances in applications of activated carbon from biowaste for wastewater treatment: A short review, J. Clean. Prod. 175 (2018) 361-375.

[16] K. Kino, T. Sakamoto, J. Yuan, Y. Amano, M. Machida, Quaternary nitrogen functionalized carbonaceous adsorbents to remove nitrate from aqueous phase, Catalysis Today. 388-389 (2022) 269-273.

[17] J. Yuan, Y. Amano, M. Machida, Surface modified mechanism of activated carbon fibers by thermal chemical vapor deposition and nitrate adsorption characteristics in aqueous solution, Colloids Surf. A Physicochem. Eng. Asp. 580 (2019) 123-710.

[18] J. Wang, Y. Amano, M. Machida, Nitrate removal from aqueous solution by glucose-based carbonaceous adsorbent: Batch and fixed-bed column adsorption studies, Colloids Surf. A: Physicochem. Eng. Asp. 686 (2024) 133296.

[19] M. Machida, Y. Tsuchiya, J.H. Yuan, Y. Amano, Efficient nitrate adsorbent applicable to wide pH range derived from polyacrylonitrile (PAN) fiber, Results Eng. 11 (2021) 100-276.

[20] M. V. Lopez-Ramon, F. Stoeckli, C. Moreno-Castilla, F. Carrasco-Marin, On the characterization of acidic and basic surface sites on carbons by various techniques, Carbon 37 (1999) 1215-1221.

[21] A. Herath, C. Reid, F. Perez, C. U. Pittman Jr., T. E. Mlsna, Biochar-supported polyaniline hybrid for aqueous chromium and nitrate adsorption, J. Environ. Manage. 296 (2021) 113186.

[22] J. Chung, N. Sharma, M. Kim, K. Yun, Activated carbon derived from sucrose and melamine as low-cost adsorbent with fast adsorption rate for removal of methylene blue in wastewaters, J. Water Process Eng. 47 (2022) 102763.

[23] J. Liang, C. Wang, S. Lu, Glucose-derived nitrogen-doped hierarchical hollow nest-like carbon nanostructures from a novel template-free method as an outstanding electrode material for supercapacitors, J. Mater. Chem. A 3 (2015) 24453-24462.

[24] D. Jiang, B. Chu, Y. Amano, M. Machida, Removal and recovery of phosphate from water by Mg-laden biochar: Batch and column studies, Colloids Surf. A: Physicochem. Eng. Asp. 558 (2018) 429-437.

[25] J.R. Pels, F. Kapteijn, J.A. Moulijn, Q. Zhu, K.M. Thomas, Evolution of nitrogen functionalities in carbonaceous materials during pyrolysis, Carbon 33 (1995) 1641-1653.

[26] Y. Tsuchiya, Y. Yamaya, Y. Amano, M. Machida, Effect of two types of adsorption sites of activated carbon fibers on nitrate ion adsorption, J. Environ. Manag. 289 (2021) 112-484.

[27] J. Wang, F. Matsuzawa, N. Sato, Y. Amano, M. Machida, Preparation of nitrogen-doped glucose-derived activated carbon and its application for the efficient removal of phosphate ions from aqueous solution, Bull. Chem. Soc. Jpn. 96 (2023) 1088-1098.

[28] I. Langmuir, The adsorption of gases on plane surfaces of glass, mica and platinum. J. Am. Chem. Soc. 40 (1918) 1361-1403.

[29] H. M. F. Freundlich, Over the adsorption in solution. J. Phys. Chem. 57 (1906) 1100-1107.

[30] Y. Shen, N. Chen, Z. Feng, C. Feng, Y. Deng, Treatment of nitrate containing wastewater by adsorption process using polypyrrole-modified plastic-carbon: Characteristic and mechanism, Chemosphere 297 (2022) 134107.

[31] L. Zhang, W. Fu, S. Qiu, M. Li, M. Feng, M. Yuan, C. Guo, K. Zhang, F. Wang, W. Han, One-pot high-speed shear preparation of modified straw: An efficient, convenient, nontoxic, and green method with high adsorption capacity for nitrate removal from aqueous solution, J. Environ. Chem. Eng. 11 (2023) 111459.

[32] J. Yuan, Y. Amano, M. Machida, Surface characterization of mesoporous biomass activated carbon modified by thermal chemical vapor deposition and adsorptive mechanism of nitrate ions in aqueous solution, Colloids Surf. A Physicochem. Eng. Asp. 616 (2021) 126213.

Chapter 5 Conclusions and outlooks

5.1 Conclusions

This study aims to address water pollution caused by nitrate and phosphate ions by preparing effective carbonaceous adsorbents using glucose as a precursor through nitrogen-doped surface modification methods. The nitrogen-doped surface modification method effectively introduced active functional groups that facilitate the adsorption of anionic pollutants, significantly enhancing the adsorption performance of the carbonaceous adsorbent. Through continuous optimization of the preparation process of the carbonaceous adsorbent, along with characterization results and adsorption studies, the following main conclusions were drawn.

In chapter 2, a novel glucose-based carbonaceous adsorbent (MeUrGlu-550Z0.5-1.0-2nd) with efficient nitrate ions adsorption capacity was successfully developed. It exhibited good adsorption performance in terms of both batch adsorption and fixed-bed column adsorption. In the batch adsorption experiments, the results indicated that in case of low initial NO_3^- concentration, quaternary nitrogen (N-Q) became a strong adsorption site that kept the Q_e without significant decrease. As the pH of the solution increased, the ability of C-π sites to accommodate protons weakened, resulting in a decrease in adsorption amount. The isotherm data and kinetic data were fitted well to the Langmuir model and pseudo-second-order model, respectively, and the maximum adsorption capacity calculated by Langmuir model was 1.58 mmol/g. The results of fixed-bed column adsorption studies well demonstrated the potential of the adsorbent in industrial applications. Effective removal of nitrate could be achieved even in solutions containing high concentrations of coexisting ions. The saturated columns could be regenerated by 1 mol/L HCl and reused for at least 5 adsorption-desorption cycles. Therefore, MeUrGlu-550Z0.5-1.0-2nd could be a promising adsorbent for the practical nitrate removal in the future.

In chapter 3, the optimal N-Q-containing glucose-derived adsorbent MeUrGlu-600Z0.5-2nd was achieved for the efficient removal of phosphate ions from aqueous solution. MeUrGlu-600Z0.5-2nd exhibited an excellent phosphate ions equilibrium adsorption amount (Q_e) of 0.42 mmol/g at a phosphate concentration of 3 mmol/L and solution pH of 4.5. The Langmuir

isotherm model can well describe the adsorption process which is a monolayer adsorption, and the maximum adsorption amount (X_m) obtained by Langmuir model was 0.52 mmol/g. Based on the results of surface characterization, the introducing of effective adsorption sites was more advantageous than increasing the specific surface area. In acidic solutions (pH < 4.5), MeUrGlu-600Z0.5-2nd exhibited good equilibrium adsorption capacity (Q_e) of 0.34-0.44 mmol/g, overcoming the limitation of commercial anion exchange resin HP555 which cannot be used effectively in acidic environment. In the continuous flow adsorption mode, MeUrGlu-600Z0.5-2nd can be regenerated for at least 3 cycles, and using NaCl as the regenerant was beneficial for the recovery of phosphate ions.

In chapter 4, a highly efficient nitrogen-doped carbonaceous adsorbent (UrGlu-450Z0.6-2nd) was successfully optimized for nitrate pollution remediation by efficiently utilizing a single nitrogen source. The special brown porous foam-like intermediate facilitates the uniform distribution of nitrogen within the reactant system during the modification process, as well as the subsequent fixation of nitrogen on the carbon framework. In addition to being optimized for using a single nitrogen source, the adsorbent also reduced the required preparation temperature by 100°C and exhibited an increased adsorption capacity in nitrate solutions with a pH greater than 5.0 (compare with chapter 2). Adsorption studies results indicate that UrGlu-450Z0.6-2nd maintained high adsorption capacities for nitrate ions within a wide solution pH range of 2.0-10.0, which attributed to the positive role of N-Q adsorption sites. The Langmuir adsorption isotherm model and pseudo-second-order kinetic model can well describe the adsorption process of nitrate by UrGlu-450Z0.6-2nd, indicating that the adsorption occurred as monolayer adsorption on a homogeneous surface with the adsorbent having a limited and uniformly distributed number of adsorption sites. The Langmuir adsorption isotherm model predicted the maximum adsorption capacity (X_m) of 1.18 mmol/g for nitrate ions by UrGlu-450Z0.6-2nd, which is a favorable result. Furthermore, the adsorption performance of modified UrGlu-450Z0.6-2nd showed significant improvement under the fixed-bed column adsorption mode, which simulated practical application conditions. This further demonstrated the effectiveness of the nitrogen-doped surface modification method and the promising application prospects of UrGlu-450Z0.6-2nd in the field of water purification.

5.2 Outlooks

Through the research presented in chapters 2 to 4, it can be concluded that the developed glucose-based carbon adsorbent can effectively remove nitrate and phosphate ions from aqueous solutions. However, due to time and condition limitations, further research and outlooks were suggested to develop more efficient carbonaceous adsorbents.

1. Although the preparation process of the adsorbent was verified through three parallel experiments, the adsorption capacity of the adsorbent obtained under the same preparation conditions still showed some differences. Excluding operational errors, equipment errors, and external environmental factors, this may be due to various random factors during the carbonization process. These factors can lead to the formation of different types and quantities of functional groups in different batches of the adsorbent, resulting in fluctuations in adsorption capacity. If the reaction process between raw materials during carbonization can be better controlled, it will improve the stability of the adsorbent's performance in batch production.

2. Selective adsorption, which prioritizes the adsorption of a specific pollutant among multiple contaminants, significantly improves removal efficiency and extends the service life of the adsorbent. To further enhance the selective adsorption capacity of glucose-based adsorbents, future studies could explore to achieve selective adsorption of pollutant ions.

3. Based on the research in chapters 2 to 4, although the developed carbonaceous adsorbents can be regenerated by eluting with regeneration agents, a worthwhile future research topic would be to find better and more appropriate methods to treat these elution solutions containing pollutant ions. For example, whether it can be converted into a recyclable solution could also be worthwhile research in the future.

Publication

Journal

1. **Jing Wang**, Fumiya Matsuzawa, Natsuho Sato, Yoshimasa Amano, Motoi Machida, Preparation of nitrogen-doped glucose-derived activated carbon and its application for the efficient removal of phosphate ions from aqueous solution, **Bulletin of the Chemical Society of Japan** 96 (2023) 1088-1098.
2. **Jing Wang**, Yoshimasa Amano, Motoi Machida, Nitrate removal from aqueous solution by glucose-based carbonaceous adsorbent: Batch and fixed-bed column adsorption studies, **Colloids and Surfaces A: Physicochemical and Engineering Aspects** 686 (2024) 133296.
3. **Jing Wang**, Yoshimasa Amano, Motoi Machida, Enhancement of nitrate adsorption from aqueous solutions by glucose-derived nitrogen-doped carbonaceous adsorbent, **Journal of Analytical and Applied Pyrolysis** (Major revision).

Conference

1. **Jing Wang**, Yoshimasa Amano, Motoi Machida, Effect of nitrogen-containing adsorbent for nitrate/nitrite adsorption in aqueous solution, WET2022, 2A-1-b (Poster, online, 2022. 07).